Nitrogen line spectroscopy in O-stars

III. The earliest O-stars [*],[**]

J.G. Rivero González[1], J. Puls[1], P. Massey[2][***], and F. Najarro[3]

[1] Universitätssternwarte München, Scheinerstr. 1, 81679 München, Germany, e-mail: `jorge@usm.uni-muenchen.de`
[2] Lowell Observatory, 1400 West Mars Hill Road, Flagstaff, AZ 86001, USA
[3] Centro de Astrobiología, (CSIC-INTA), Ctra. Torrejón a Ajalvir km 4, 28850 Torrejón de Ardoz, Spain

ABSTRACT

Context. The classification scheme proposed by Walborn et al. (2002, AJ, 123, 2754), based primarily on the relative strengths of the N IVλ4058 and N IIIλ4640 emission lines, has been used in a variety of studies to spectroscopically classify early O-type stars. Owing to the lack of a solid theoretical basis, this scheme has not yet been universally accepted though.

Aims. We provide first theoretical predictions for the N IVλ4058/N IIIλ4640 emission line ratio in dependence of various parameters, and confront these predictions with results from the analysis of a sample of early-type LMC/SMC O-stars.

Methods. Stellar and wind parameters of our sample stars are determined by line profile fitting of hydrogen, helium and nitrogen lines, exploiting the helium and nitrogen ionization balance. Corresponding synthetic spectra are calculated by means of the NLTE atmosphere/spectrum synthesis code FASTWIND.

Results. Though there is a monotonic relationship between the N IV/N III emission line ratio and the effective temperature, all other parameters being equal, theoretical predictions indicate additional dependencies on surface gravity, mass-loss, metallicity, and, particularly, *nitrogen abundance*. For a given line ratio (i.e., spectral type), more enriched objects should be typically hotter. These basic predictions are confirmed by results from the alternative model atmosphere code CMFGEN.

The effective temperatures for the earliest O-stars, inferred from the nitrogen ionization balance, are partly considerably hotter than indicated by previous studies. Consistent with earlier results, effective temperatures increase from supergiants to dwarfs for all spectral types in the LMC. The relation between *observed* N IVλ4058/N IIIλ4640 emission line ratio and effective temperature, for a given luminosity class, turned out to be quite monotonic for our sample stars, and to be fairly consistent with our model predictions. The scatter within a spectral sub-type is mainly produced by abundance effects.

Conclusions. Our findings suggest that the Walborn et al. (2002) classification scheme is able to provide a meaningful relation between spectral type and effective temperature, as long as it is possible to discriminate for the luminosity class. In terms of spectral morphology, this might be difficult to achieve in low-Z environments such as the SMC, owing to rather low wind-strengths. According to our predictions, the major bias of the classification scheme is due to nitrogen content, and the *overall* spectral type-$T_{\rm eff}$ relation for low-metallicity (e.g., SMC) O-stars might be non-monotonic around O3.5/O4.

Key words. stars: early-type - stars: fundamental parameters - stars: atmospheres - line: formation

1. Introduction

Though important for the evolution of the early Universe and the present cosmos, massive stars are not as thoroughly understood as desirable to safely infer or predict their interaction with their surroundings, e.g., their input of (ionizing) radiation, wind-energy and momentum, and nuclear processed material.

Particularly uncertain is the situation for the earliest O-stars (earlier than O4, see below), both with respect to their physical parameters, and the relation between their spectroscopic definition and these parameters. Since the earliest O-type stars include the most massive stars in the Universe, i.e., the top end of the stellar initial mass function, such a lack of knowledge is intolerable. As pointed out by Massey et al. (2005), already a 10% uncertainty in the effective temperature, $T_{\rm eff}$ (which is still possible for the hottest stars to present date), results in a factor of two or more uncertainty in the Lyman flux, affecting our understanding of the ionization balance of H II regions and, e.g., the porosity of the interstellar medium (e.g., Oey & Kennicutt 1997, Oey 2006).

This large uncertainty is produced because the standard approach to derive $T_{\rm eff}$, exploiting the He I/He II ionization equilibrium, fails in the earliest O-star regime. This is the result of rather insensitive He II lines to changes in $T_{\rm eff}$, and quite weak strategic He I lines, with their equivalent widths falling below 200 mÅ, about the limit achievable with normal photo-

graphic emulsions in the 1970s. The apparent absence of He I was used by Walborn (1971) to extend previous classification criteria to the O3 spectral type, which then displayed a degeneracy with respect to effective temperature. This degeneracy was partially broken by Kudritzki (1980) and Simon et al. (1983) who used better photographic data to detect He I in the spectra of some O3 stars, but even today with modern CCDs and high S/N the detection of He I is not always achievable. To circumvent this problem Walborn et al. (2002) suggested to use the N IVλ4058/N IIIλ4640[1] (hereafter N IV/N III) emission line ratio as the primary classification criterion for the earliest spectral types, instead of the He I/He II absorption line ratio. By means of this criterion, the former O3 class was split into three different types O2, O3, and O3.5, being O2 the degenerate one instead.

This scheme has been used in a variety of studies during the past years to classify spectra of early O-stars in the Large and Small Magellanic Clouds (LMC and SMC) (e.g., Walborn et al. 2004, Massey et al. 2004, 2005, 2009, Evans et al. 2006) and in the Milky-Way, e.g., Sota et al. (2011). However, these additional sub-types are not (yet) universally accepted. In particular Massey et al. (2004, 2005) criticized that relying on the relative strengths of the optical nitrogen emission lines lacks a solid theoretical basis, since the (photospheric) line emission is the result of complex NLTE processes.

To provide more insight into this and related matter, we started a series of publications dealing with nitrogen spectroscopy in O-type stars. In the first paper of this series (Rivero González et al. 2011, hereafter Paper I), we concentrated on the formation of the emission at N III$\lambda\lambda$4634 − 4640 − 4642. In the follow-up paper (Rivero González et al. 2012, hereafter Paper II), we investigated the N IVλ4058 emission line formation, and applied our accumulated knowledge to derive nitrogen abundances for an LMC O-star sample.

The primary goal of the present paper is a quantitative study of the atmospheric parameters of the earliest O-stars, by means of nitrogen line spectroscopy and building on the results from our previous work within this series. Particularly, we concentrate on testing the Walborn et al. (2002) classification scheme on its capability of providing a reasonable relation between spectral types and effective temperatures. To this end, we investigate the theoretical N IV/N III emission line ratio, and the impact of different parameters on this ratio. Subsequently, our predictions are confronted with corresponding observational results, derived from an analysis of an early O-type sample of LMC/SMC stars.

This paper is organized as follows. In Sect. 2, we describe the tools used within this work, the atmospheric code FASTWIND and a suitable model grid. Open questions from our previous studies regarding the formation of the N III and N IV emission lines are addressed in Sect. 3. Section 4 presents first theoretical predictions on the N IV/N III emission line ratio. In Sect. 5, we compare our results and predictions with corresponding ones from the alternative atmospheric code CMFGEN (Hillier & Miller 1998). The stellar sample and the observations used within this study as well as the procedure to determine stellar/wind parameters together with nitrogen abundances are presented in Sect. 6. Finally, we provide a discussion of our results in Sect. 7, and summarize our findings and conclusions in Sect. 8.

Table 1. Model-grid used within this work: coverage of fundamental parameters. For $T_{\rm eff}$ and $\log g$ coverage, see also asterisks in Fig. 6.

Parameter	Range	Typical step size
$T_{\rm eff}$ (kK)	35.0 - 55.0	1.0
$\log g$ (cgs)	3.2, 3.5 - 4.2, 4.5	0.1
$\log Q^a$ /series	−14.00/A, −13.50/B, −13.15/C	0.35
	−12.80/D, −12.45/E, −12.10/F	
$Y_{\rm He}$	0.08, 0.10 - 0.20	0.05
Galactic		
Z	$Z_\odot$	-
[N]	7.64, 7.78 - 8.98	0.2
LMC		
Z	$0.5Z_\odot$	-
[N]	6.90, 6.98 - 8.58	0.2
SMC		
Z	$0.2Z_\odot$	-
[N]	6.50, 6.78 - 8.38	0.2

$^{(a)}$ in units of $M_\odot{\rm yr}^{-1}/({\rm km\,s}^{-1}R_\odot)^{1.5}$.

Notes. Other model parameters adopted as follows: wind terminal velocity, v_∞, as a function of the photospheric escape velocity, $v_{\rm esc}$ (see Kudritzki & Puls 2000); stellar radius, R_*, as a function of spectral type and luminosity class, corresponding to prototypical values; velocity field exponent, $\beta = 0.8$; and micro-turbulence, $v_{\rm mic} = 10\ {\rm km\,s}^{-1}$. Nitrogen baselines abundances (first entry in [N] range) have been drawn from Hunter et al. (2007).

2. Code and model grid

All calculations within this work were performed by means of the NLTE atmosphere/spectrum synthesis code FASTWIND (Santolaya-Rey et al. 1997, Puls et al. 2005), using the recently updated version v10.1 (see Paper II). Most results presented here (except for the fine-tuned fits in Sect. 6) are based on a model-grid, with H, He, and N as 'explicit' elements. Corresponding model atoms have been described in Puls et al. (2005) (H/He) and Papers I/II (N), and Table 1 provides the coverage of important grid parameters. Details of the basic grid were already provided in Paper II, and only its 'hot' range ($T_{\rm eff} \geq 35$kK) was used for our current analysis. This subgrid has been extended to cover a broader range in background metallicity, $Z = 1, 0.5, 0.2\ Z_\odot$, associated with the Milky Way (MW), Large Magellanic Cloud (LMC), and Small Magellanic Cloud (SMC), respectively. Moreover, we increased the sampling with respect to $\log g$, and also the coverage of the wind-strength parameter (or optical depth invariant), $Q = \dot{M}/(v_\infty R_*)^{1.5}$, towards larger values, resulting in 6 model series of different wind-strength (from series 'A' with $\log Q$ = -14.00 to series 'F' with $\log Q$ = -12.10, for details see Table 1). Finally, the sampling in helium content, $Y_{\rm He} = N_{\rm He}/N_{\rm H}$, and nitrogen abundance, $[{\rm N}] = \log_{10}(N_{\rm N}/N_{\rm H}) + 12$, has been improved, for studying the reaction of important nitrogen lines on extreme changes in [N] (Sects. 3.3 and 4.2.3), and for better constraining abundances in our analysis of LMC/SMC stars (Sect. 6). The current grid accounts for a total of 104,000 models.

The major potential of such a model-grid (besides theoretical investigations) is the possibility of obtaining rather precise estimates of stellar parameters within a reasonable amount of time (few minutes). With the advent of large stellar surveys, such as the VLT-FLAMES Tarantula survey (VTFS, Evans et al. 2011) or the IACOB project (Simón-Díaz et al. 2011), this will turn

---

[1] The individual components NIII$\lambda\lambda$4640.64-4641.85 become blended for a projected rotational velocity $v \sin i \geq 40\ {\rm km\,s}^{-1}$.
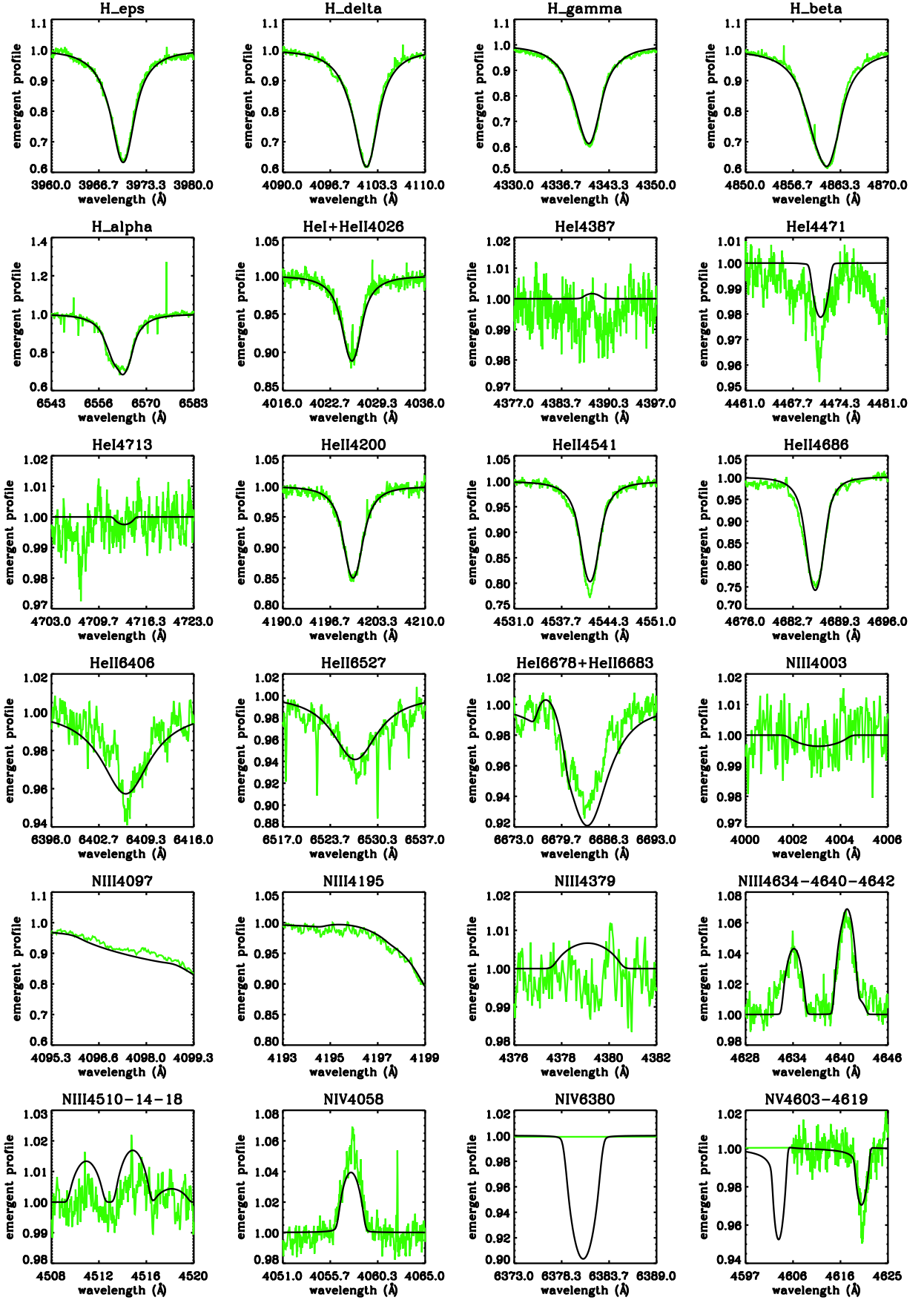
Fig. 1. High resolution optical spectrum of the Galactic O3 V((f*)) star HD 64568 (green), compared with the best-fitting synthetic H/He/N spectrum from our grid (black, convolved with $v \sin i = 100 \, \text{km s}^{-1}$, see Markova et al. 2011). N IVλ6380 and N Vλ4603 not observed. Grid parameters: $T_{\text{eff}} = 48 \, \text{kK}$, $\log g = 4.0$, $\log Q = -12.8$ (series 'D'), Y_{He}=0.1, [N] = 8.38. Fine tuning of the parameters can improve the fit.

3

out to become a very useful tool. As an example for the present quality of our models, we show in Fig. 1 the comparison of a high resolution (resolving power $R = 48,000$), high S/N (≥ 150) spectrum of the Galactic O3 V((f*)) star HD 64568 (for details, see Markova et al. 2011) with the best fitting synthetic spectrum from our grid models. Obviously, the grid resolution is sufficient to achieve quite a fair representation of the observed spectrum, both with respect to H/He and N (note that lines from N III, N IV, and N V are present in parallel). Further analyses of Galactic objects will be performed in a forthcoming paper.

3. N III/N IV emission lines – parameter-dependence

Our previous studies on the formation of N III$\lambda\lambda 4634 - 4640 - 4642$ and N IV$\lambda 4058$ prompted a number of questions, which are investigated in the following. First we concentrate on the N III triplet emission in low-Z environments, to discriminate the counteracting effects of line blocking (less blocking – more emission) and mass-loss (less mass-loss – less emission) under these conditions. Subsequently, we study the impact of Z and [N] on N IV$\lambda 4058$.[2]

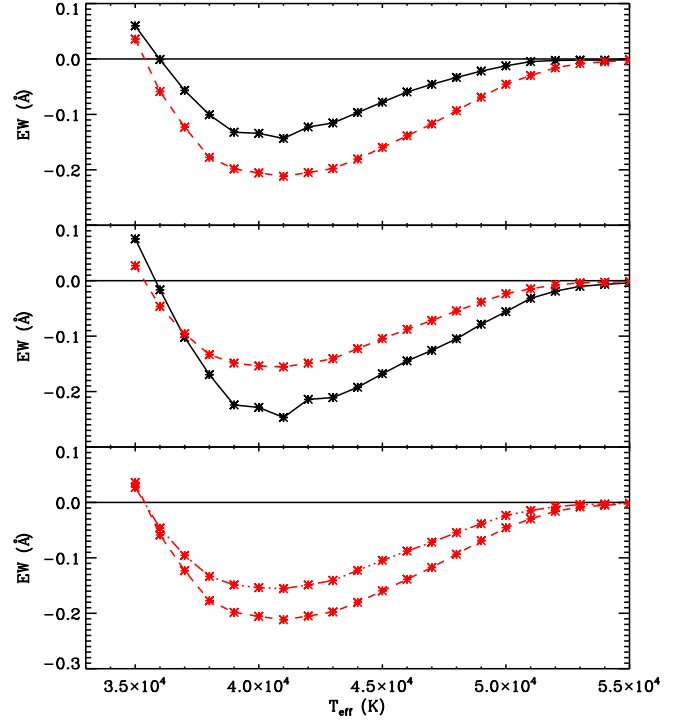### 3.1. N III emission line formation: EUV line-blocking vs. wind-strength

In Paper I we argued that, for Galactic conditions, the canonical explanation for the presence of emission at N III$\lambda\lambda 4634 - 4640 - 4642$ (related to dielectronic recombination, Mihalas & Hummer 1973) no longer or only partly applies if one accounts for the presence of line-blocking/blanketing and winds. The key role is now played by the stellar wind, as long as the wind-strength is large enough to enable a significantly accelerating velocity field already in the photospheric formation region of the resonance line(s) connected to the upper level of the involved transition. Furthermore, our study implied that particularly the efficiency of the 'two electron' drain (depopulating the lower level, see Paper I) is strongly dependent on the degree of EUV line-blocking, i.e., on Z. For a given wind-strength and nitrogen abundance, the emission should become stronger in low-Z environments, because of less blocking (see Fig 16 in Paper I). Nevertheless, this comparison might be unrealistic, since less blocking goes hand in hand with a lower wind-strength, which might (over-) compensate the discussed effect. Moreover, one might need to consider a lower nitrogen content, owing to a lower baseline abundance.

Here we investigate the combined effect. First, we compare the behavior of the N III emission lines for two different Z environments (MW and SMC), applying a consistent scaling of $\log Q$, via $\dot{M} \propto (Z/Z_\odot)^{0.72}$ (clumping corrected, Mokiem et al. 2007b) and $v_\infty \propto (Z/Z_\odot)^{0.13}$ (Leitherer et al. 1992). For the SMC with $Z/Z_\odot = 0.2$, this yields a reduction of $\log Q$ by -0.37 dex compared to the Galactic case, and corresponds well to the step size of $\Delta \log Q = 0.35$ used within our model grid. Thus, Galactic models from, e.g., series 'E' need to be compared with SMC models from series 'D'.

In Fig. 2 (upper panel), we compare the equivalent widths of N III$\lambda\lambda 4640.64$, 4641.85[3], in the following abbreviated by N III$\lambda 4640$, as a function of T_{eff}, for MW series 'E' (black/solid) and SMC series 'D' models (red/dashed). All models have the same gravity, $\log g = 4.0$, and the same nitrogen content,

Fig. 2. Equivalent width of N III$\lambda 4640$ as a function of T_{eff}, for MW and SMC models at $\log g = 4.0$ and mass-loss rates scaled according to Z (see text). Solid/black and dashed(-dotted)/red curves refer to MW series 'E' and SMC series 'D' models, respectively ($\Delta \log Q = -0.35$ dex). Upper panel: [N] = 7.78 for both Galactic and SMC models. Middle panel: comparison accounting for the theoretically expected maximum [N] enrichment, drawn from tailored evolutionary calculations by Brott et al. (2011a): MW models with [N] = 8.18 and SMC models with [N] = 7.58. Lower panel: SMC series 'D' models, with [N] = 7.58 (dashed-dotted) and [N] = 7.78 (dashed). The line emission increases with increasing [N].

[N] = 7.78 dex (almost solar, Asplund et al. 2005, 2009). As usual, we define equivalent widths (hereafter EWs) to be positive for absorption and to be negative for emission lines. The result of this comparison is similar to our findings from Paper I. Even when we account for consistently scaled mass-loss rates, the low-Z models result in more emission. Thus, lower mass-loss rates associated with low-Z environments do not compensate the increase in emission strength due to a lower degree of line-blocking.

So far, we neglected the fact that a lower Z also implies a difference in the [N] baseline abundance, which needs to be considered in a final comparison. In the middle panel of Fig. 2, we compare the same series of models as in the upper one, accounting now for more consistent abundances (MW: black/solid, SMC: red/dashed). Here we used [N] values in agreement with the theoretically expected maximum enrichment as provided by Brott et al. (2011a), for MW and SMC models of 40 $M_\odot$ and initial rotation velocities of 270 km s^{-1}. This roughly corresponds to models with [N] = 8.2 and 7.6 for the MW and SMC, respectively. [4]

---

[2] For a detailed description of the formation process of N III and N IV emission lines, we refer to Paper I and Paper II, respectively.

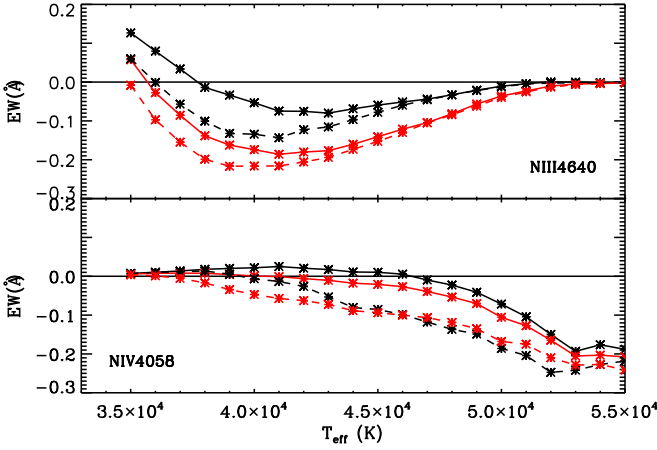[3] The blue component of the triplet shows a similar behavior.

[4] Unfortunately, there are only few abundances studies in the O-star regime to confirm these assumptions, and most of them are biased towards late O-types (reviewed by, e.g. Herrero 2003, Herrero & Lennon

Fig. 3. Equivalent width of N $\text{\sc{iii}}\lambda4640$ (upper panel) and N $\text{\sc{iv}}\lambda4058$ (lower panel) as a function of T_{eff}, for MW (black) and SMC (red) models, at $\log g$=4.0 and [N]=7.78 dex. Solid lines: series 'A' (thin winds), dashed lines: series 'E' (prototypical for Galactic supergiants).

Fig. 4. Equivalent width of N $\text{\sc{iv}}\lambda4058$ as a function of T_{eff} for models with [N] = 7.78 (black) and [N] = 9.0 (red). All models correspond to $\log g$=4.0 and $Z = Z_{\odot}$, with mass-loss rates according to series 'A' (solid) and 'E' (dashed). See text.
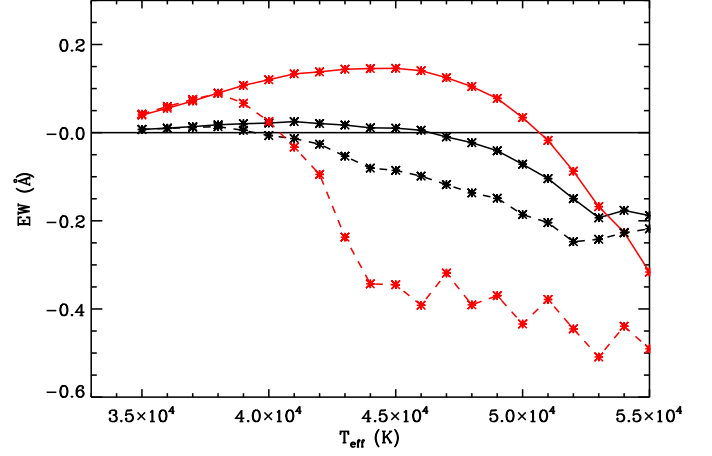
It turns out that with the inclusion of more realistic abundance conditions, the increase of emission strength due to less blocking becomes strongly suppressed, and now the MW models display stronger emission that the SMC ones. This might explain the relatively low number of "f" objects among the SMC O-stars (see Sect. 7.6).

For convenience, the lower panel of Fig. 2 displays a direct comparison of SMC models with expected maximum enrichment ([N] = 7.58, dashed-dotted) and a solar nitrogen content ([N] = 7.78, dashed). Obviously, the emission strength of N $\text{\sc{iii}}\lambda4640$ increases with increasing nitrogen content (see also Fig. 15 in Paper I).

3.2. N $\text{\sc{iv}}\lambda4058$ – dependence on background abundance

Though we studied the response of the N $\text{\sc{iii}}$ triplet on different background abundances already in Paper I, a similar analysis for N $\text{\sc{iv}}\lambda4058$ is still missing. This is now done in Fig. 3, by means of our model-grid. We display models with thin winds (series 'A'; solid) and with wind-strengths typical for Galactic supergiants (series 'E'; dashed), and compare the impact of MW (black) and SMC (red) background abundances. All models have the same gravity, $\log g$= 4.0, and the same [N] = 7.78. To enable a better comparison, we show the effects for both N $\text{\sc{iii}}\lambda4640$ (upper panel) and N $\text{\sc{iv}}\lambda4058$ (lower panel). We clearly see that N $\text{\sc{iii}}\lambda4640$ is much more influenced by Z than N $\text{\sc{iv}}\lambda4058$, irrespective of wind-strength and T_{eff}. For LMC background abundances, $Z = 0.5$ (not displayed), the effect on N $\text{\sc{iv}}\lambda4058$ becomes almost negligible.

With respect to the formation of this line, all 'A' and also the 'cooler' 'E' models (with $T_{\text{eff}} \leq 45$ kK) behave as discussed in paper II. A lower background Z induces a more depopulated ground state, owing to somewhat higher ionizing fluxes around

the N $\text{\sc{iv}}$ edge at $\lambda = 160$ Å. Consequently, the drain of the lower level of the $\lambda4058$ transition, 3p, via the 'two electron' transitions becomes enhanced, and more emission is produced at lower Z. For 'E' models with $T_{\text{eff}} \geq 45$ kK the situation changes, and now the higher Z (MW) models produce slightly more emission: At higher T_{eff} and $\dot{M}$, the resonance line towards 3p (at $\lambda = 247$ Å) leaves detailed balance and 3p becomes pumped, stronger at low Z because of higher EUV fluxes. Thus, less emission at N $\text{\sc{iv}}\lambda4058$ is produced, compared to a Galactic environment.

Overall, however, background abundances have a weak effect on N $\text{\sc{iv}}\lambda4058$, much weaker than wind-strength effects (e.g., red solid vs. red dashed). This is related to the much higher sensitivity of the N $\text{\sc{iv}}$ continuum on mass-loss rate. Accordingly, also the helium content has a certain impact on the N $\text{\sc{iv}}$ emission strength, since this parameter controls the overall flux level of the He $\text{\sc{ii}}$ continuum including the N $\text{\sc{iv}}$ edge. In particular, an increase of Y_{He} decreases the N $\text{\sc{iv}}$ emission strength. [5]

As already discussed above and in Paper I, N $\text{\sc{iii}}\lambda4640$ reacts much stronger on different background abundances (e.g., upper panel of Fig. 3, black vs. red), and in a similar way for all mass-loss rates. Because of this different behavior, the (theoretical) N $\text{\sc{iv}}\lambda4058$/N $\text{\sc{iii}}\lambda4640$ emission line ratio, studied in Sect. 4, is affected by metallicity.

Interestingly, the reaction of N $\text{\sc{iii}}\lambda4640$ on $\dot{M}$ becomes negligible for models with $T_{\text{eff}} \geq 46$ kK. At these temperatures, N $\text{\sc{iii}}$ has become a real trace ion, and the (weak) line emission is formed in quite deep layers, hardly affected by mass loss and velocity field (see also Fig. 10 in Paper I). In this case, the relative overpopulation is caused by recombination cascades and depopulation of the lower level by 'two electron' drain (particularly for low Z conditions), whilst dielectronic recombination remains unimportant.

3.3. N $\text{\sc{iv}}\lambda4058$ – dependence on nitrogen abundance

Figure 4 displays the reaction of N $\text{\sc{iv}}\lambda4058$ on variations of [N] and $\log Q$ for MW models. As in Fig. 3, solid and dashed lines

2004, Morel 2009). Heap et al. (2006), following previous work by Bouret et al. (2003), found most of their 18 SMC sample stars to be enriched, and more than half of the sample displayed [N] > 7.5. Regarding Galactic objects, Martins et al. (2012b) (see also Martins et al. 2012a) recently found a typical enrichment by 0.4-0.6 dex above the Galactic baseline abundance, corresponding to [N] ≈ 8.0-8.2.

---

[5] A similar behavior is found for the N $\text{\sc{iii}}$ triplet emission, for $T_{\text{eff}} \leq 40$ kK.
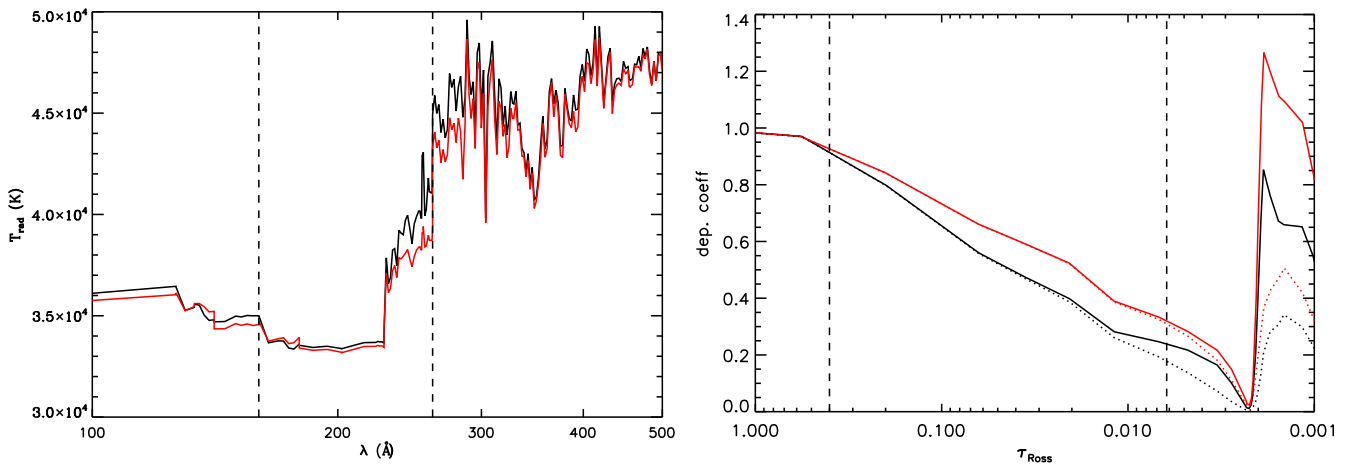
Fig. 5. Radiation temperatures and NLTE departure coefficients for two MW-models at T_{eff}= 45 kK, log g= 4.0, *and a low density wind* (series 'A'), with solar (black) and strongly enhanced nitrogen ([N] = 9.0, red). Left panel: Enhanced nitrogen leads to lower N IV (and N III) continuum-fluxes, here expressed as radiation temperatures. Corresponding edges at 160 Å and 261 Å indicated by vertical lines. Right panel: The lower fluxes give rise to less depopulated N IV ground- (solid) and $2p^2$ (dotted) states, where the latter are the lower levels of the important two-electron transitions draining N IV 3p. Consequently, there is more absorption/less emission at N IVλ4058 when [N] becomes increased. Formation region of N IVλ4058 indicated by dashed lines.

correspond to model series 'A' and 'E', respectively. We compare models with [N] = 7.78 (black) and highly enhanced nitrogen, [N] = 9.0 (red), selected to demonstrate extreme effects.

First, we concentrate on the influence of [N] for model series 'E' (supergiant mass-loss rates, dashed). These models behave as expected. As for the N III triplet (e.g., Fig. 2, lower panel), we obtain more emission when we increase the nitrogen content. This is mostly because the formation zone, due to the increased number of absorbers/emitters, is shifted outwards into the transition region photosphere/wind where the relative overpopulation becomes very large or even inverted (cf. Fig. 4 in Paper II). Small inaccuracies in the population ratio (e.g., due to inappropriate gridding) can lead to sizeable effects in line-strength when close to inversion, and this is the reason for the non-monotonicity in EW encountered for the high [N] 'E'-models.

Somewhat unexpectedly, however, we found the opposite reaction for low-$\dot{M}$ models (solid). For large nitrogen content (red), we either obtain more absorption or less emission than solar-[N] models (black), for almost the whole temperature range. Furthermore, the turning point from absorption to emission occurs at hotter T_{eff} (by 5 kK) than for the solar-[N] models, whilst for the 'E' series this turning point remains rather unaffected by nitrogen content. The underlying mechanism is again related to a diminished drain of the lower level when [N] becomes increased. Here, a higher [N] is responsible for a lower N IV continuum-flux (Fig. 5, left), leading to less depopulated ground- and $2p^2$ states (Fig. 5, right), and thus to a higher population of 3p, i.e., to more absorption/less emission at N IVλ4058. Note that this process is similar to the effect produced by a higher Z (Sect. 3.2).

These findings imply an important consequence. According to our predictions, in a certain T_{eff} range N IVλ4058 might switch, for growing [N], from emission to absorption, provided the wind-strength is not too high! The other way round (and exploiting the results from the complete grid): If N IVλ4058 is observed in absorption at 44 kK $\leq T_{eff} \leq$ 50 kK (for Galactic stars), this would be an indication of strong nitrogen enrichment (and mass-loss rates below 'D' corresponding to log Q < −12.8). The lower limit in T_{eff} corresponds to the absorption/emission turn-

ing point for 'D' models (at higher T_{eff} and similar or higher $\dot{M}$, only emission lines are predicted, independent of [N]), whilst the upper one refers to the same point for model series 'A'.

4. Predictions on the N IV/N III emission line ratio

4.1. Overview

The complete Walborn et al. (2002) classification scheme proposed for 'normal' O-stars,[6] which also covers the O4 type, is summarized in Table 2. Walborn et al. suggested to use the N IV/N III emission line ratio as the primary classification criterion for the earliest spectral types, instead of the He I/He II absorption line ratio. This scheme has been used in a variety of studies during the past years to classify spectra of early O-stars (e.g., Walborn et al. 2004, Massey et al. 2004, 2005, 2009, Evans et al. 2006, Sota et al. 2011), though there are still some controversial issues. (i) The classification criteria are not quantitative and involve secondary statements regarding the strength of He Iλ4471, see Table 2. (ii) Massey et al. (2005, hereafter Mas05) have criticized that relying on the strength of the nitrogen emission lines lacks a theoretical basis, i.e., it is not clear whether T_{eff} is the only parameter that differentiates the newly defined spectral types. Indeed, our previous and present work implies that the emission strength of N IVλ4058 (and also that of N IIIλ4640, at least until $T_{eff} \approx$ 46 kK) crucially depends on $\dot{M}$. Based on their analysis of early LMC and SMC stars, Mas05 pointed out that for stars with similar T_{eff} and log g the N IV/N III ratio could vary by the full range defined for the scheme (but see Sect. 6.4). Furthermore, they suggested that any spectroscopic classification should be able to constrain T_{eff} without knowledge of other important parameters such as log g or $\dot{M}$. (iii) Already Walborn et al. (2002) pointed out that even though there were no indications of any correlation between the newly defined spectral types and the corresponding host galaxy, effects of Z on the emission line ratio might need to be considered, accounting for

---

[6] Crowther & Walborn (2011) have updated the classification scheme for O2-3.5 If*/WN5-7 stars using the morphology of H$_\beta$.

Table 2. Classification scheme for spectral types O2-O4 using the emission line ratio N IVλ4058/ N IIIλ4640 and the strength of He Iλ4471, as defined by Walborn et al. (2002).

Spectral type	Criteria
	Supergiants
O2 If*	N IV $\gg$ N III, no or very weak He I
O3 If*	N IV > N III, very weak or no He I
O3.5 If*	N IV $\sim$ N III, very weak He I
O4 If+	N IV < N III, weak He I
	Giants
O2 III(f*)	N IV $\gg$ N III, no or very weak He I
O3 III(f*)	N IV > N III, very weak or no He I
O3.5 III(f*)	N IV $\sim$ N III, very weak He I
O4 III(f+)	N IV < N III, weak He I
	Dwarfs
O2 V((f*))	N IV $\gg$ N III, no He I
O3 V((f*))	N IV > or $\sim$ N III, very weak He I
O3.5 V((f+))	N IV < N III, very weak He I
O4 V((f+))	no N IV, weak He I

Notes. Luminosity classes defined as follows. Supergiants (I): He IIλ4686 in emission; giants (III): He IIλ4686 in weak absorption/P-Cygni profile; dwarfs (V): He IIλ4686 in strong absorption. Note that the f+ designation recently became obsolete since the Si IV emission at $\lambda\lambda$4089 − 4116 has been established as a common feature in normal O-type spectra (Sota et al. 2011).

the results from Crowther (2000) for WR-stars. Using synthetic WN models, Crowther had found that earlier spectral types are predicted at lower metallicity, following the Smith et al. (1996) classification scheme for WN stars. Since both nitrogen emission lines seem to react differently on variations of Z (Sect. 3.2), it is clear that such a dependence cannot be ruled out.

In the following, we will address these and other problems, first by means of theoretical predictions for the N IV/N III emission line ratio, and later on by a comparison with observed spectra.

4.2. Basic considerations

We took advantage of the large model-grid described in Sect. 2, and analyzed the influence of various parameters (Z, log Q, [N]) by studying the iso-contours of specific emission line ratios in the $T_{\rm eff}$-log g plane (Figs. 6 to 8). Here and in the following, we always used models with $Y_{\rm He} = 0.1$.

To discriminate the specific spectral types by nitrogen lines alone, one has basically to account for five different, qualitatively defined ranges with respect to the line strengths of N IVλ4058 vs. N IIIλ4640 (see Table 2). Note that the ranges for luminosity classes I/III are somewhat shifted relative to class V. To allow for a quantitative description, we investigated the behavior of three extreme values, namely N IV/N III = 0.1 (lower limit for O4 I/III and O3.5 V), N IV/N III = 1 (O3.5 I/III and O3 V) and N IV/N III = 10 (representative for O2 I/III/V).

Before going into the details of our analysis, we compare in Fig. 6 the N IV/N III emission line ratios expressed in terms of EW (left) and line-strength (right, quantified in terms of emission peak height), to ensure that different definitions[7] would not lead to different conclusions. Except for small subtleties, there is no significant change in the run of the iso-contours,

---

[7] Note that line ratios for He I/He II are partly defined using EWs.

regardless whether EWs or line-strengths are used to derive the line ratio. The encountered subtle differences are mostly caused by the considerable wind-strength (model series 'E') used in Fig. 6: Particularly for N IVλ4058, enhanced EWs owing to extended wings are produced, whilst the peak heights remain unaffected. We have also convinced ourselves that a convolution of the theoretical spectra with typical rotational speeds, $v \sin i = 100$ km s^{-1}, and/or a degrading to a resolving power of 6000 have a rather low impact (but see Markova et al. 2011): Generally, the iso-contours are shifted to somewhat lower $T_{\rm eff}$, by roughly 500 to 1000 K in extreme cases of high wind-strength and high [N]. In the following we concentrate on the ratio of line-strengths alone, as originally defined by Walborn et al. (2002).

The inspection of the different iso-contours displayed in the $T_{\rm eff}$-log g plane, Figs. 6 to 8, allows us to infer an important characteristics for the emission line ratio. As it is true for the He I/He II line ratio (e.g., Mas05), also the N IV/N III line ratio is a sensitive function of surface gravity. The hotter the temperature, the larger the log g-value necessary to preserve a specific ratio (ionization vs. recombination). This trend seems to have vanished for the cooler models ($T_{\rm eff} \leq 40$ kK) at high log g in Fig. 6, but here the influence of gravity is counteracted by the rather strong wind (see Sect. 4.2.2).

4.2.1. Impact of background metallicity

Figure 6 shows the dependence of the line ratio on $T_{\rm eff}$ and log g for a fixed wind-strength, log $Q = -12.45$, and [N] = 7.78, for iso-contours corresponding to N IV/N III = 0.1, 1 and 10. To study the influence of Z, we display the predicted behavior for MW (red), LMC (green), and SMC (blue) O-stars.

Even a first inspection indicates the potential of this line ratio as a temperature diagnostics. For a fixed surface gravity, e.g., log $g = 4.0$, we find difference on the order of 3 kK (for MW models) to 8 kK (for SMC models) between iso-contours at N IV/N III = 0.1 and 1, roughly corresponding to O4 (lower limit) vs. O3.5 I/III or O3 V. For low-$\dot{M}$ models this spread becomes somewhat smaller, 6 kK for SMC stars, whilst for Galactic objects the N IV/N III = 0.1 iso-contour is no longer present since N IV turns into weak absorption (Fig. 3). The difference between the N IV/N III = 1 and 10 iso-contours (O3.5 I/III or O3 V vs. O2) is on the order of 4-5 kK for all metallicities, decreasing to 2.5-3 kK for low $\dot{M}$.

The specific differences of the emission line ratios as a function of Z can be easily explained in terms of our conclusions from Sect. 3.2 and by remembering the basic features displayed in Fig. 3. First, N IIIλ4640 is strongly affected by Z (more emission at lower Z, irrespective of temperature), in contrast to N IVλ4058. The latter line is increasing in strength over almost the complete range in $T_{\rm eff}$, whilst the former is increasing until a certain maximum located at ≈ 40 kK, and decreasing thereafter. Taken together, this implies that *lower* $T_{\rm eff}$ are required to produce similar line ratios for low-metallicity objects at cooler temperatures, compared to Galactic objects (lower $T_{\rm eff}$ means less N III emission, to compensate for the basically larger emission due to lower Z). Beyond 40 kK, on the other hand, *higher* $T_{\rm eff}$ are required instead to reduce the increased N III emission. This explains why the SMC/LMC iso-contours at N IV/N III = 0.1 are located at cooler $T_{\rm eff}$ than their Galactic counterpart, whilst the corresponding N IV/N III = 1 and 10 iso-contours are on the hotter side. Because the Z effect is largest for SMC objects, also the $T_{\rm eff}$ differences between the N IV/N III = 0.1 and 1 levels are largest in this situation.
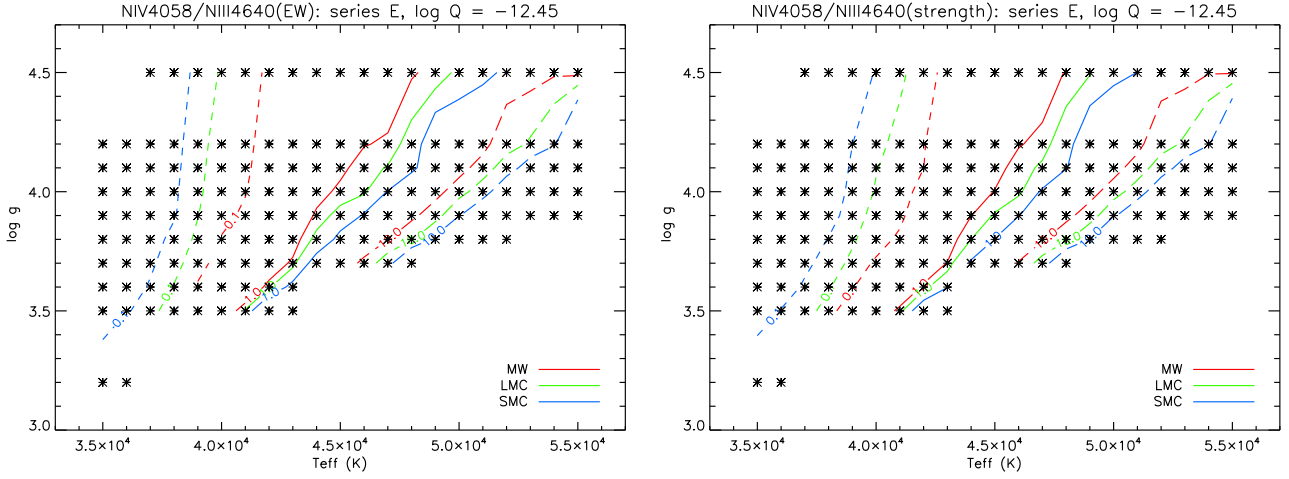
Fig. 6. N IVλ4058/N IIIλ4640 for Galactic (red), LMC (green) and SMC (blue) O-stars. Displayed are iso-contours of the emission line ratio in the $T_{\rm eff}$-log g plane (model series 'E', [N] = 7.78), for values of N IV/N III = 0.1 (dashed), 1 (solid) and 10 (long-dashed). The asterisks indicate the position of the grid-models used. Left panel: emission line ratio calculated using EWs; right panel: emission line ratio calculated using line-strengths.

Finally, let us mention that the influence associated with Z (around 2-3 kK for a given line ratio) is comparable with the typical spread present in early spectral types, and thus in agreement with the non-detection of any correlation between the new spectral types and the host galaxy (see above).

4.2.2. Impact of wind-strength

To test the influence of log Q on the emission line ratio, in Fig. 7 we compare the iso-contours corresponding to N IV/N III = 1 (O3.5 I/III or O3 V) for different wind-strengths, from thin (series 'A') to dense winds (series 'F'). All models have LMC background abundances and [N] = 7.78. Since lower metallicities counteract the impact of wind-strength, corresponding iso-contours for SMC conditions vary to a lesser degree, whilst the variations are larger for Galactic conditions, in both cases by few hundreds of Kelvin.

Generally, the impact of wind-density on the N IV/N III emission line ratio is quite strong, particularly for larger surface gravities. From Fig. 7 it is evident that for a fixed log g cooler $T_{\rm eff}$ are required to produce similar line ratios at higher wind densities. Basically, we can combine the reaction into three groups, namely 'A' to 'C' models, 'D' models, and models with winds stronger than 'D'. The first group consists of low-$\dot{M}$ models with line ratios which are almost insensitive to wind-strength. Models belonging to the 'D' series display a slight reaction, since the wind begins to affect the line emission (either from both lines or, for hotter stars, only from N IVλ4058, see Fig. 3), and in a different way, so that the line ratio becomes modified. From the 'E' series on, we found larger differences, e.g., at log g = 4.0, of roughly 2 and 4.5 kK for 'E' and 'F' models compared to low-$\dot{M}$ ones.

In conclusion, objects with the same $T_{\rm eff}$ and log g but substantially different wind-strengths are predicted to display significantly different line ratios. Consequently, the assigned spectral types would be no longer monotonic in $T_{\rm eff}$ if there would be a large scatter in wind-strength. One has to note, however, that a certain $T_{\rm eff}$-log g pair also implies a certain luminosity class, and that the wind densities per luminosity class are only mildly varying. Thus, the monotonicity of a spectral type-$T_{\rm eff}$ relation might still be warranted for a *specified* luminosity class, as long as the corresponding luminosity class indicators (for the earliest
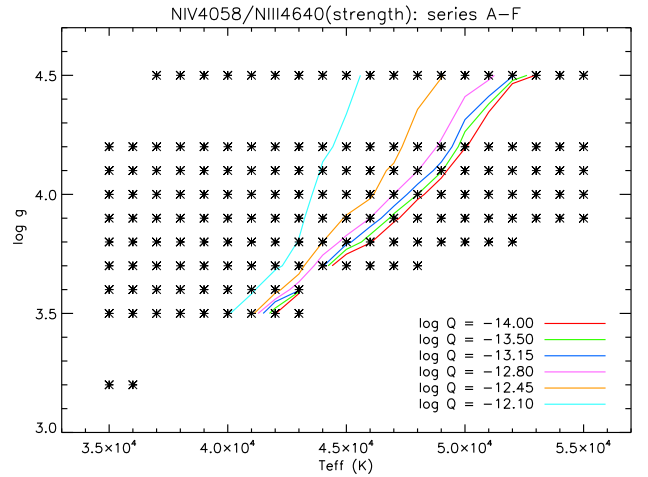

Fig. 7. Dependence of N IVλ4058/N IIIλ4640 on wind-strength (series 'A'-'F'), for LMC models with [N] = 7.78. The iso-contours correspond to a nitrogen emission line ratio of unity.

O-stars, He IIλ4686) allow for a reliable classification (but see Sect. 8).

4.2.3. Impact of nitrogen abundance

After investigating the impact of background metallicity and wind-strength, we now concentrate on the influence of nitrogen content. At first glance, this is somewhat surprising. Abundance should have a marginal or only small effect on line *ratios*, since it should cancel out as long as the lines are not too strong and the ionization equilibrium is not disturbed. This statement, however, is only true if the lines form in a 'typical' way, i.e., are simple absorption lines (e.g., He Iλ4471/He IIλ4541 used for the classification of not too early O-stars). In the case considered here, however, the lines are formed by complex and *different* NLTE processes, and different abundances might have a different impact on the formation of both lines (see Sect. 3.3), so that the ratio might become affected. Moreover, the variation of [N] in early type stars can be much larger than, e.g., the variation of

8
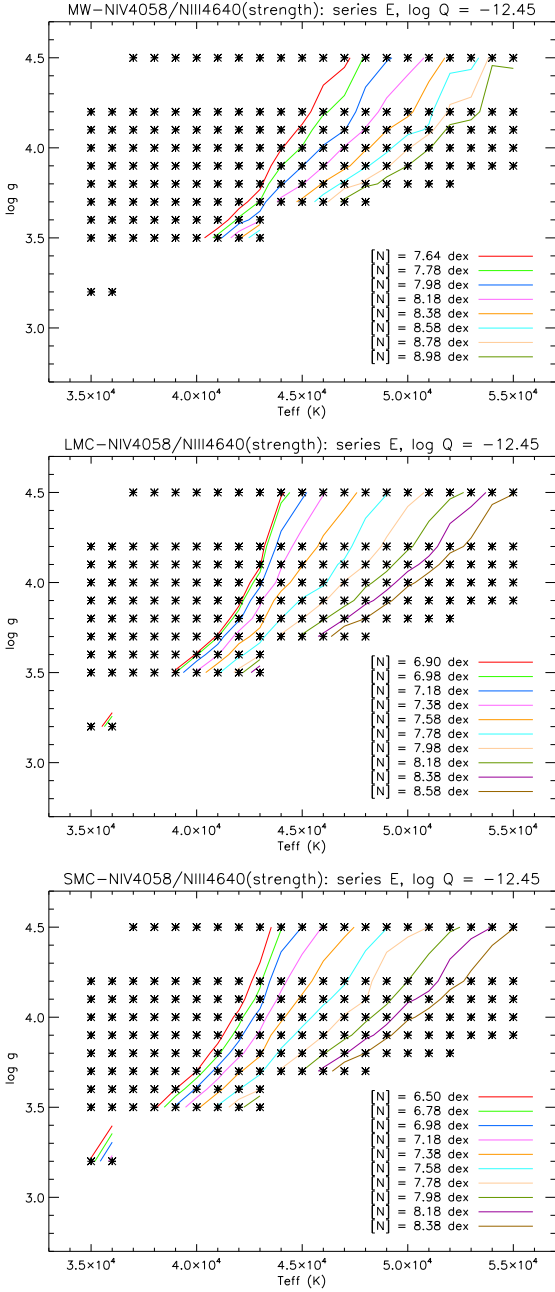
Fig. 8. Dependence of N ɪᴠλ4058/N ɪɪɪλ4640 on nitrogen abundance, for three different background metallicities: Galactic (upper panel), LMC (middle panel), and SMC (lower panel). All models have $\log Q = -12.45$ (series 'E'). The iso-contours correspond to a nitrogen emission line ratio of unity.

Y_{He}, which amplifies the effect. Thus, it is mandatory to test for the impact of nitrogen content on the N ɪᴠ/N ɪɪɪ emission line ratio.

For this purpose, we display in Fig. 8 the response of the line ratio on different nitrogen abundances as present in our model-grid, for each Z (Galactic, LMC, and SMC background abundances). To allow for a fair comparison, all models belong to series 'E'. Again, we display only contours with N ɪᴠ/N ɪɪɪ = 1, as a representative value. Note that for each Z, the range of nitrogen content is different, from the corresponding baseline abundance to enrichments of roughly 1.3, 1.6, and 1.9 dex for MW, LMC, and SMC objects, respectively (see legend and Table 1).

Table 3. Stellar and wind parameters of models used to compare synthetic nitrogen line profiles from ꜰᴀꜱᴛᴡɪɴᴅ and ᴄᴍꜰɢᴇɴ. The grid is a subset of the grid presented by Lenorzer et al. (2004). For details, see Paper I. Even entries provide those parameters from our ꜰᴀꜱᴛᴡɪɴᴅ grid models which reproduce best the H/He spectra from ᴄᴍꜰɢᴇɴ.

Model	code	T_{eff} (K)	R_* ($R_\odot$)	$\log g$ (cgs)	$\log Q$
d2v	ᴄᴍꜰɢᴇɴ	46100	11.4	4.01	-12.43
E4740	ꜰᴀꜱᴛᴡɪɴᴅ	47000		4.00	-12.45
d4v	ᴄᴍꜰɢᴇɴ	41010	10.0	4.01	-12.75
D4140	ꜰᴀꜱᴛᴡɪɴᴅ	41000		4.00	-12.80
s2a	ᴄᴍꜰɢᴇɴ	44700	19.6	3.79	-11.99
F4540	ꜰᴀꜱᴛᴡɪɴᴅ	45000		3.80	-12.15
s4a	ᴄᴍꜰɢᴇɴ	38700	21.8	3.57	-12.15
F3935	ꜰᴀꜱᴛᴡɪɴᴅ	39000		3.50	-12.15

Notes. All models were calculated with $v_{\text{mic}}= 10$ km s^{-1}, and with four different nitrogen abundances, [N] = 7.78, 7.98, 8.38, 8.78. Wind strength parameter, Q, calculated in units of $M_\odot \, yr^{-1}$, $R_\odot$ and km s^{-1}.

Generally, an enhancement of [N] at fixed $\log g$ shifts the iso-contours towards higher temperatures. We checked that this shift indeed is related to the different [N]-dependencies of the specific formation mechanisms of N ɪᴠλ4058 and N ɪɪɪλ4640 rather than to a modified ionization equilibrium, which remains quite unaffected from variations in [N]. Moreover, the shift is quite similar for all Z, producing an increase of roughly 1 kK for a change of +0.2 dex in nitrogen abundance (at $\log g$= 4.0; lower ΔT_{eff} are found at lower $\log g$). This is an interesting result because objects with considerable differences in [N] would display, for the same line ratio, i.e., spectral type, large differences in T_{eff}. If we, e.g., consider LMC models at $\log g$ = 4.0, a line ratio of unity (corresponding to an O3 dwarf) would be obtained at temperatures differing by 6 kK if either [N] is at the baseline abundance (red, $T_{\text{eff}} \approx 42.5$ kK) or if [N] = 8.18 (dark green, $T_{\text{eff}} \approx 48.5$ kK), corresponding to a typical enrichment of LMC stars (paper II)! Such a difference is much larger than the typical spread of temperature per spectral type, and we conclude that the present classification scheme for the earliest O-stars might be strongly biased by nitrogen abundance. Only if the nitrogen content/enrichment would be rather similar for a given position in the T_{eff}-$\log g$ plane[8], this bias would not contaminate a spectral-type-T_{eff} relation, similar to our argumentation regarding the bias by wind-strength from above.

5. Comparison with results from ᴄᴍꜰɢᴇɴ

In Paper I we compared our results for N ɪɪɪ lines with those from the alternative code ᴄᴍꜰɢᴇɴ, for a grid of models comprising dwarfs and supergiants in the T_{eff} range between 30 and 45 kK, and with 'old' solar abundances according to Grevesse & Sauval (1998). In the following, we examine the consistency also with respect to N ɪᴠ and N ᴠ, concentrating on the hotter models (d4v, d2v, s4a, s2a, see Table 3), but allowing for different nitrogen abundances to check the predictions from the previous sections.

ᴄᴍꜰɢᴇɴ models were computed with a modified photospheric structure following the approach from Santolaya-Rey et al.

---

[8] If, e.g., nitrogen would be enriched by rotational mixing alone and the initial rotational speeds were similar.
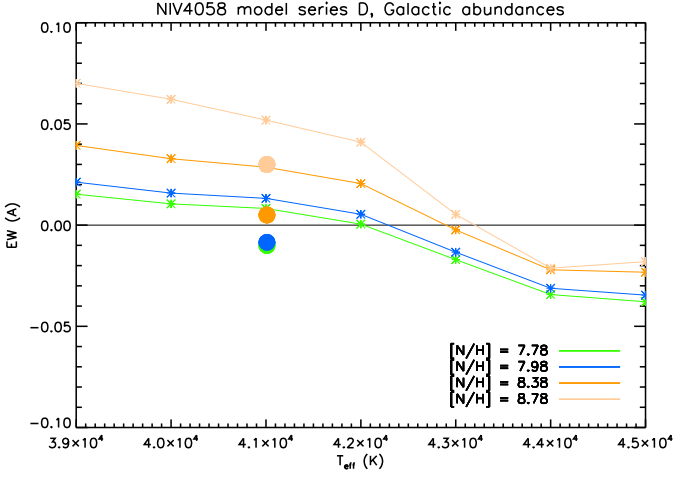
Fig. 9. N IVλ4058, switching from emission to absorption with increasing abundance. Model series 'D' ($\log Q = -12.8$), $\log g = 4.0$, compared to results from CMFGEN, model d4v (at $T_{eff} \approx 41$ kK, filled circles).
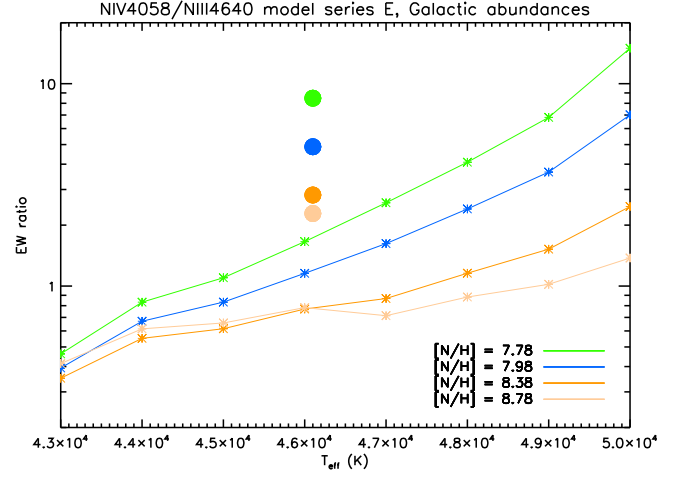
Fig. 10. Equivalent width ratio N IVλ4058/N IIIλ4640, as a function of nitrogen abundance. Model series 'E' ($\log Q = -12.45$), $\log g = 4.0$, compared to results from CMFGEN, model d2v (at $T_{eff} \approx 46$ kK, filled circles).

(1997), smoothly connected to a beta velocity law. In our approach, the Rosseland mean from the original formulation was replaced by the more appropriate flux-weighted mean. Several comparisons using 'exact' photospheric structures from TLUSTY (Hubeny & Lanz 1995) showed excellent agreement with our method (see also Najarro et al. 2011). A turbulent velocity of $10\,\mathrm{km\,s^{-1}}$ was assumed when computing both the level populations and line profiles. Our models account for the presence of H, He, C, N, O, Si, P, S, Fe, and Ni, totaling 3965 full levels (1319 super-levels) and $\approx 70{,}000$ lines.

First, we examine the potential switch of N IVλ4058 from emission to absorption when increasing the abundance. From Fig. 4, this effect should occur at lower wind-strengths and not too high T_{eff}, i.e., potentially for model d4v. Indeed, the predicted effect is clearly present in the corresponding CMFGEN models, where λ4058 is in emission for [N] = 7.78 and 7.98, and in absorption for [N] = 8.38 and 8.78 (filled circles in Fig. 9). The total variation in equivalent width as a function of [N] compares very well to results from FASTWIND, which appear at somewhat higher $T_{eff} = 42.5$ kK, as shown by the solid lines (based on our FASTWIND grid for $\log g = 4.0$ and model series 'D'). Thus we conclude that the predicted effect is more or less code independent.

In Fig. 10 we compare the influence of the nitrogen abundance on the emission line ratio N IV/N III (calculated from EWs), by means of model d2v. Again, CMFGEN (filled circles) predicts a similar effect as FASTWIND, i.e., the EW ratio increases with [N]. The actual values of these ratios, however, are quite different from those calculated by FASTWIND. Similar ratios are only reached at higher T_{eff}, because, as discussed below, FASTWIND predicts stronger N III and weaker N IV emission lines for hot objects. Nevertheless, the '[N]-effect' is clearly visible in the CMFGEN models, not only for model d2v but also for the others. Thus, the position of a certain emission line ratio in the T_{eff}-$\log g$ plane depends on the actual nitrogen abundance. As already discussed, this can lead to an ambiguity of the spectral-type-T_{eff} relation. We come back to this problem in Sect. 7.

In Appendix A we provide a detailed comparison of strategic H/He/N lines predicted by CMFGEN and FASTWIND, for all models from Table 3, and for different [N]. FASTWIND spectra have been taken from our grid, to show that the provided resolution in parameter space is sufficient in most cases.

Let us first concentrate on the H/He spectra (upper panels of Figs. A.1, A.4, A.5 and A.8), which turn out to remain unaffected by typical variations in [N]. In most cases, there is an excellent agreement between the H/He spectra from CMFGEN and the closest or almost closest FASTWIND grid-model, even for the He I singlet lines (but see Najarro et al. 2006). The Stark-wings of the Balmer lines are well reproduced at a similar gravity. The largest discrepancies occur for model d2v where He I$\lambda\lambda$4471,4713 result in a better fit at $T_{eff} = 47$ kK instead at the nominal value of 46 kK, and for model s4a where $\log g = 3.5$ produces better consistency than a model at $\log g = 3.6$ which would lie closer to the nominal value of $\log g = 3.57$. Finally, H_α (FASTWIND) shows less emission for model s2a, mostly because the closest grid model has a lower wind-strength of $\log Q = -12.15$ than the nominal value, $\log Q = -11.99$. Figure A.1 illustrates how the H/He spectrum changes when T_{eff} is modified by ± 1000 K. In the considered temperature range, the major reaction occurs in He I, predominantly in the singlet lines ($\lambda\lambda$4387, 6678).

The lower panels of Figs. A.1, A.4, A.5 and A.8 display important nitrogen lines for the four investigated models, at [N] = 8.78 (ten times solar), whilst Figs. A.2, A.3, A.6 and A.7 display these lines for [N] = 7.78 (solar).

N III lines have been already compared in Paper I, for [N] = 7.92 (and $v_{mic} = 15\,\mathrm{km\,s^{-1}}$), and these findings remain valid also at higher nitrogen abundance.

For the dwarf models d4v and d2v, the emission lines at $\lambda\lambda$4634−4640−4642 are stronger than predicted by CMFGEN, and indeed stronger than displayed in Paper I, where the disagreement was less obvious. This discrepancy could be tracked down to a different value of v_{mic} used in the present models. A lower value (10 vs. 15 $\mathrm{km\,s^{-1}}$) results in narrower resonance zones, and can lead to higher emission peaks.[9] Moreover, differences in the occupation numbers - when close to inversion in certain regions - become more pronounced, due to less averaging. For models s4a and s2a we note similar discrepancies, though at a tolerable level.

---

[9] A similar influence of v_{turb} has been seen, e.g., in synthetic spectra of Br_α when in emission due to *photospheric* processes (Najarro et al. 2011).

As discussed in paper I, the N III absorption line at $\lambda4097$ is slightly stronger in FASTWIND models at hot temperatures. Note that for d2v the profiles become identical when comparing with a model that reproduces the CMFGEN He I lines, i.e., for T_{eff} = 47 kK instead of 46 kK.

The quartet lines[10] at $\lambda\lambda4510 - 4514 - 4518$ behave quite interestingly. Among the low [N] models, these lines are in absorption only at d4v, whilst for the other models (higher T_{eff} and/or higher $\dot{M}$) they appear in emission. In a certain parameter range (models d2v and s4a) and in analogy to N IV$\lambda4058$, these lines switch, for increasing [N], from emission to absorption. Regarding these major trends, CMFGEN and FASTWIND behave similarly, and the lines agree quite well for the dwarf models. For the supergiant models, on the other hand, FASTWIND predicts more emission/less absorption than CMFGEN, in particular for s2a. Thus, and due to their complex behavior, the quartet lines need to be treated with care when analyzing *early* O-stars.

N III$\lambda4003$ and $\lambda4195$ (in the blue wing of He II$\lambda4200$ and additionally blended by Si III at hotter temperatures) show a mostly reasonable agreement. N III$\lambda4195$ matches almost perfectly when predicted to be in emission, and [N] is low. The biggest discrepancy for $\lambda4003$ is found in the low [N] model of s4a, where CMFGEN predicts much more absorption.

N IV and N V lines have not been compared so far. N IV$\lambda4058$ from FASTWIND shows always less emission than produced by CMFGEN, though for models s2a and for the low [N] model s4a the agreement becomes satisfactory.

In combination with more emission from the N III triplet at hotter temperatures, this leads to a lower N IV/N III EW/line-strength ratio in FASTWIND (see Fig. 10), i.e., effective temperatures deduced from this line-ratio *alone* would be higher compared to CMFGEN results. This general trend is independent of abundance.

N IV$\lambda3480$ is in good agreement for most models, except for d4v where FASTWIND predicts more absorption. In contrast, N IV$\lambda6380$ shows considerable differences, and for almost all models (except for the high [N] model of d4v) our grid predicts much more absorption. Since this line provided no difficulties when comparing with observations (neither in Paper II nor in the present investigation), we suggest that it might suffer from certain problems in CMFGEN. We are currently working on this problem, which we think is connected to the desaturation of the N IV resonance line around 247 Å at the base of the wind.

Finally, the N V doublet $\lambda\lambda4603-4619$ compares very well in most cases, and only for the low [N] models of s2a and s4a we find more absorption by FASTWIND.

Summarizing the major discrepancies, we note that in the early O-type domain FASTWIND produces more emission in the N III triplet, less emission at N IV$\lambda4058$, and mostly much more absorption at N IV$\lambda6380$, compared to CMFGEN. We now ask how such discrepancies might affect an abundance/T_{eff} analysis, and how one might proceed to diminish the impact of corresponding uncertainties.

Since the H/He lines are in very good agreement, the stellar parameters should be constrained quite well, as long as He I remains visible. For the hottest stars with no or negligible He I, the situation might become more difficult, since T_{eff} needs to be constrained mostly from the nitrogen lines, and we would deduce lower T_{eff} from CMFGEN if concentrating on the N III triplet and N IV$\lambda4058$ alone (see above). In turn, this would lead to rather different abundances. Fortunately, however, there is also

N V which is very sensitive on T_{eff} (see below and Figs. A.1, A.3 and A.4), and seems to be quite code-independent[11]. In conclusion, T_{eff} for 'cooler' objects should be mostly determined from the He I/He II ionization balance. Potential discrepancies regarding N III$\lambda\lambda4634 - 4640 - 4642$ and N IV$\lambda4058$ because of 'erroneous' predictions can be easily identified then. For the hottest objects, on the other hand, N V should obtain a strong weight when determining T_{eff}. As long as either N IV$\lambda6380$ or N IV$\lambda3480$ are observed, these lines might be used as abundance indicators, whilst any inconsistency of N IV$\lambda4058$ will tell about the quality of that line.

In Fig. 11 we now 'analyze' synthetic spectra from CMFGEN by means of our FASTWIND grid, to check the overall consistency when accounting for *all* important lines. This is done for the high [N] model of d4v, which is a prototypical case, and by means of EW iso-contours in the T_{eff}-[N] plane (for the appropriate model series 'D' with $\log Q$ = -12.8, and a gravity of $\log g$= 4.0). Equivalent width for all analyzed lines have been measured from the CMFGEN spectra. These EWs are displayed as iso-contours with respect to our FASTWIND grid and should cross, in the ideal case of a perfect consistency between both codes, at one point corresponding to the model parameters, i.e., T_{eff} = 41 kK and [N] = 8.78. Because of the various discrepancies discussed above, this is not the case, but at least almost all iso-contours are close to each other in quite a confined region, marked by a black box. In particular, five out of eight lines cross around the point T_{eff} = 41.5 kK / [N] = 8.55. At the original (CMFGEN) values, T_{eff} = 41 kK and [N] = 8.78, on the other hand, there is only N V$\lambda4603$ and N III$\lambda4003$. Thus, a FASTWIND analysis of this model spectrum would yield lower nitrogen abundances, by roughly 0.2 dex (more on this below).

Figure 11 displays a number of interesting aspects. Most iso-contours have a parabola-like shape with a minimum at low [N], where the 'left' branch with negative slope relates to increasing ionization fractions (the same EW at higher T_{eff} implies a lower abundance), and the 'right' branch with positive slope to decreasing fractions. Because the right branch applies for lines from lower ionization stages (N III), and the left branch for lines from higher ones (N IV, N V), these different slopes allow to constrain the actual parameter region quite well, even though both codes produce different line-strengths when compared at the same location in parameter space.

The only feature which is quite outside the enclosed region is the N III triplet, which is *significantly* different in both codes (and stronger in FASTWIND, thus formed at lower T_{eff} when compared to the CMFGEN EWs).

At the comparatively 'cool' temperature of model d4v, N V$\lambda\lambda4603-4619$ becomes almost independent of abundance (almost vertical left branch), and thus a very sensitive temperature indicator. Indeed, it perfectly fits at the actual T_{eff} (which is also true for the He I/He II lines, see Fig. A.1). Interestingly as well, the iso-contours for N IV$\lambda6380$ and N IV$\lambda3480$ occupy an almost identical region, i.e., give very similar results, though being members of different spin systems (singlet and triplet system, respectively). Insofar, the information provided by both lines is similar, and the observation/analysis of either of these lines should be sufficient, which is fortunate since the 3500 Å region is scarcely observed.

Overall, when 'analyzing' [N] from the CMFGEN spectrum and accounting for the rather fixed T_{eff} and $\log g$ values from H/He and N V, we would derive a lower or roughly similar nitrogen

---

[10] Preferentially used by Martins et al. (2012a) to derive nitrogen abundances in magnetic O-stars of late and intermediate spectral type.

[11] And not affected by X-rays from wind embedded shocks under typical conditions, see Paper II.
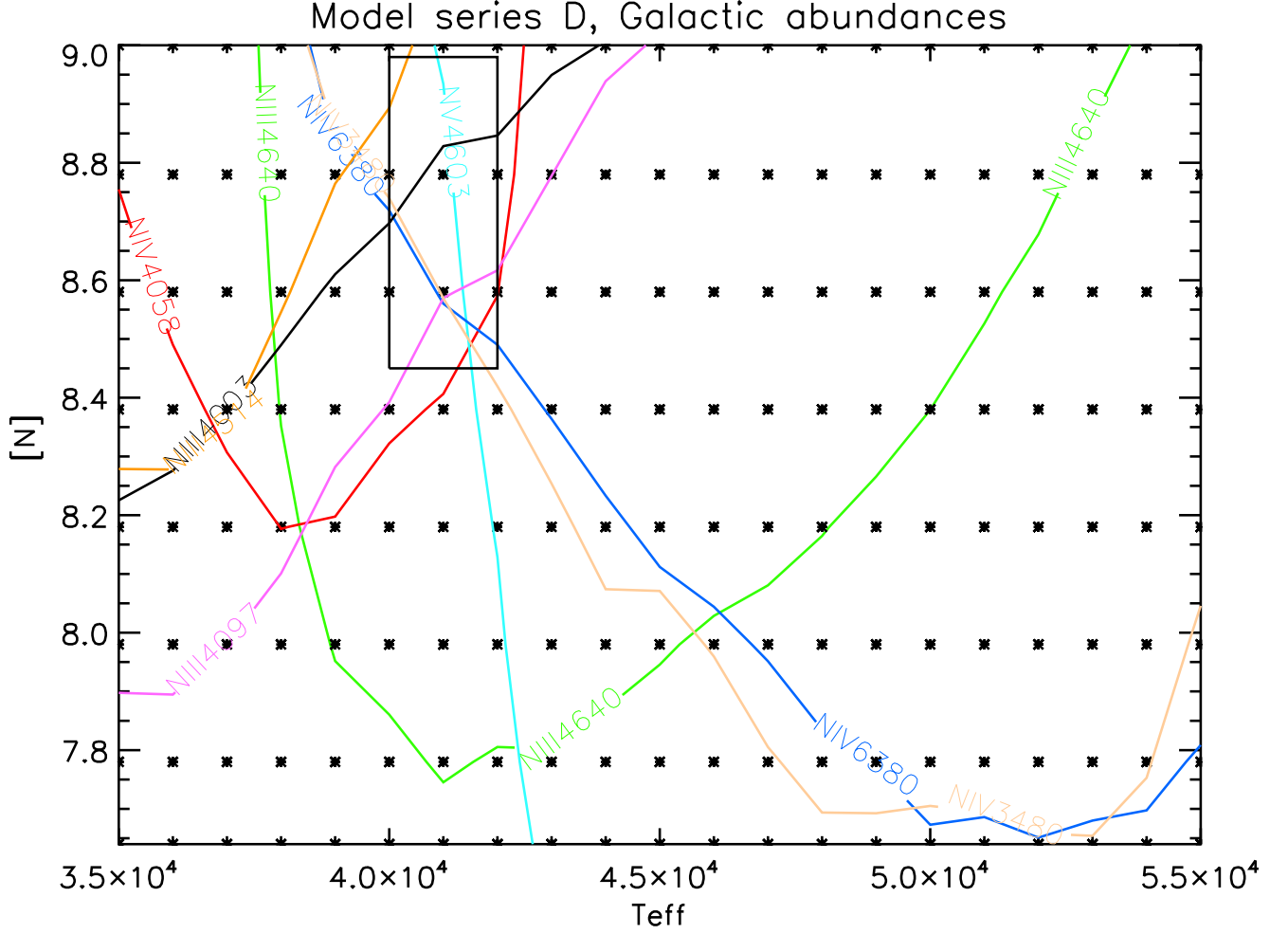
Fig. 11. Nitrogen abundance 'analysis' of CMFGEN model d4v with [N] = 8.78. EW iso-contours for important nitrogen lines are displayed in the T_{eff}-[N] plane of our FASTWIND model grid (series 'D', log Q = −12.8, log g= 4.0). The displayed iso-contours refer to EWs measured from the CMFGEN spectra of model d4v. In the ideal case, i.e., if CMFGEN and FASTWIND produce identical results, all iso-contours would cross at a single point located at T_{eff}= 41kK and [N] = 8.78. The black box marks the smallest region in parameter space where almost all lines (except for N IIIλ4640) are predicted at the measured value. In particular, five out of eight lines cross around the point T_{eff} = 41.5 kK / [N] = 8.55, i.e., at a lower abundance (by roughly 0.2 dex) than present in the original CMFGEN model.

abundance from most lines, compared to the actual value used by CMFGEN, except for the N III quartet lines which would imply a somewhat higher abundance. These results are also valid for the other models from Table 3. We thus conclude that in those cases where T_{eff} can be additionally constrained, FASTWIND analyses of early O-type stars will yield mostly lower nitrogen abundances than analyses performed by means of CMFGEN.[12]

6. Analysis of a sample of LMC/SMC early-type O-stars

So far, we mainly provided theoretical predictions on the N IV/ N III emission line ratio as used by Walborn et al. (2002) to classify the earliest O-stars, and concentrated on the impact of various parameters. For testing our predictions, we need to confront these results with the analysis of a significant stellar sample. The

LMC sample analyzed in Paper II contained only a few early-type objects (BI237, BI253, N11-026, N11-031, and N11-060). These stars, biased towards O2, did not cover all spectral types and luminosity classes within the classification scheme. To allow for a larger sample, we added the earliest stars from the analyses of LMC/SMC objects by Massey et al. (2004, 2005, 2009, hereafter Mas04, Mas05, and Mas09).

6.1. The stellar sample

In particular, we selected objects with spectral types earlier than O5. Table 4 gives a complete list of all early O-type stars considered in the following, along with their spectral type and galaxy membership. The final sample consists of seventeen stars, fourteen from the LMC and three from the SMC. Thirteen objects have been drawn from Mas04 and Mas05, plus one object from Mas09 (the only early-type star of that sample). Two of the objects analyzed in Paper II (BI237 and BI253) were also studied

---

[12] At the present stage of knowledge, we do not know which code does a 'better' job in reproducing reality.

Table 4. Sample stars used within this study, along with galaxy membership and spectral type.

Star	Cross-IDs	Galaxy	Spectral Type
AV 177	-	SMC	O4 V((f))[a]
AV 435	-	SMC	O3 V((f*))[a]
NGC 346-355	NGC 346 W3	SMC	ON2 III(f*)[b]
LH 81:W28-5	-	LMC	O4 V((f+))[a]
LH 81:W28-23	-	LMC	O3.5 V((f+))[a]
LH 90:ST 2-22	-	LMC	O3.5 III(f+)[a]
LH 101:W3-24	ST 5-27	LMC	O3.5 V((f+))[a]
LH 101:W3-19	ST 5-31	LMC	O2 If*[a]
R136-018	-	LMC	O3 III(f*)[a]
R136-040	R136a-535	LMC	O2-3.5 V[a]
Sk–65° 47	LH 43-18	LMC	O4 If[a]
Sk–67° 22	BAT 99-12	LMC	O2 If*/WN5[c]
BI237	-	LMC	O2 V((f*))[d]
BI253	-	LMC	O2 V((f*))[d]
N11-026	-	LMC	O2 III(f*)[d]
N11-031	P3061/LH10-3061	LMC	ON2 III(f*)[d]
N11-060	P3058/LH10-3058	LMC	O3 V((f*))[d]

[a] Mas05; [b] Walborn et al. (2004); [c] Crowther & Walborn (2011); [d] Mokiem et al. (2007a) and references therein

Notes. The horizontal line separates stars analyzed within this work (drawn from Mas04/05/09) from stars previously analyzed in Paper II. Identifications are as follows: "AV" from Azzopardi & Vigneau (1982); "BAT" from Breysacher et al. (1999); "BI" from Brunet et al. (1975); "LH" from Lucke (1972) except "LH10-3058" that is from Walborn et al. (2002, 2004); "N11" from Evans et al. (2006); "NGC" from Massey et al. (1989); "P" from Parker et al. (1992); "R136" from Massey & Hunter (1998); "R136a" from Malumuth & Heap (1994); "Sk" from Sanduleak (1970).

by Mas05. For these objects, as well as for the remaining sample members (N11-026, N11-031, and N11-060), we refer to our analysis from Paper II.

From the original subsample of early-type stars studied by Mas04 and Mas05, we selected representative objects. Owing to various reasons, eight stars have been discarded. (i) Three dwarfs (R136-033, R136-040 and R136-055) did not show any trace of either N III$\lambda\lambda$4634 − 4640 − 4642 or N IVλ4058 in their spectra, and Massey and co-workers could not classify them according to the Walborn et al. (2002) scheme. Therefore, we analyzed only one prototypical example for these stars, R136-040. (ii) From the four early giants compiled in Mas05, we discarded two of them, R136-047 (O2 III(f*)) and LH 64-16 (O2N III(f*)). The FOS data used for the R136 stars, see Sect. 6.2, suffered from an intermittent behavior of some of the FOS diodes (Massey & Hunter 1998), which could result in the appearance of spurious features contaminating the spectra. Owing to a rather bad quality of the spectra, we were not able to obtain a satisfactory fit for R136-047, and we decided to discard it from the analysis. This problem was not met for the remaining R136 stars used within this work (R136-018 and R136-040). The other giant discarded, LH 64-16, shows similar severe discrepancies as we had found in Paper II for another star of this class, N11-031. Owing to extreme difficulties to fit either N III/N IV or N IV/N V lines, we excluded it from the present analysis. (iii) Regarding supergiants, we selected three out of seven stars. For typical conditions ($\dot{M}$ ≥ $10^{-5} M_\odot$yr^{-1}, $v_\infty \sim$ 3000 km s^{-1}, and $R_* \sim$ 15 $R_\odot$), the corresponding wind-strength, log Q ≥ −12, is well outside of our model-grid (Table 1), and we concentrated on representative ob-

jects since analyzing all of them would have been extremely time-consuming, even with a fast code such as FASTWIND.

In summary, our sample comprises 9 dwarfs, 5 giants, and 3 supergiants. The source of the corresponding spectral types for each object is listed in Table 4.

6.2. Observational data

Spectra for the 12 early O-stars from Massey et al. were taken in three ranges, the UV, the blue and the red visual band. Only optical data were used within this work.

(i) For the bulk of the stars, these data were obtained at the Cerro Tololo Inter-American Observatory (CTIO) 4m Blanco telescope with the RC spectrograph, during January 1999 (P.I. P. Massey). The blue and red spectra cover the ranges 3750-4900 Å and 5400-7800 Å, respectively. The spectral resolution was 1.4 Å for the blue and 2.8 Å for the red band, with a S/N between 200 to 560 per resolution element, corresponding to about 4 pixels, in the blue (measured at 4500 Å), and a typical S/N of about 150 per resolution element in the red.

For LH 101:W3-24, additional spectra for the H$_\alpha$ region were taken by means of the Hubble Space Telescope (HST) using STIS/CCD (as part of programme GO-9412, P.I. P. Massey), to amend the ground-based observations which were heavily contaminated by strong nebulosity. These data cover 6300-6850 Å, with a spectral resolution of 0.84 Å and S/N of 50.

(ii) For the R136 stars, we used two different data sets obtained with the HST. One was taken with the G400 FOS/RD configuration under GO-6417 (P.I. P. Massey), with a resulting wavelength coverage from 3250 to 4820 Å, 3 Å resolution and a S/N of 60 at 4400 Å. Additional observations were taken with STIS/CCD under GO-7739 (P.I. P. Massey). Blue observations covered the wavelength range 4310-4590 Å, at a S/N of 100 for a spectral resolution of 0.4 Å. Observations centered around H$_\alpha$ were made with the same setup as for LH 101:W3-24 described above. Since the STIS spectra have better S/N and resolution, we used them preferentially for our analysis. Because of their limited wavelength coverage, excluding the spectral region that comprises the most important nitrogen lines, we nevertheless had to consider the FOS data, see Figs. B.1 and B.5.

(iii) Spectra for NGC 346-355 were collected with the Clay 6.5m (Magellan II) telescope at the Las Campanas Observatory, using the Boller & Chivens Spectrograph (P.I. P. Massey). The coverage was 3410-5040 Å with a S/N of 600 at 4500 Å in the blue, and from 5315 to 6950 Å in the red, achieving a S/N of 400 at 6500 Å. For both ranges, the spectral resolution was 2.4 Å.

All spectra were reduced with IRAF,[13] and we performed additional re-normalizations for different wavelength ranges within this work.

As outlined in Sect. 6.1, our present sample includes two objects (BI237 and BI253) which have been studied both in Paper II and by Mas05. The UVES spectra used in the former analysis have a considerably higher resolving power, 40,000, compared to a resolving power of 3,000 as provided by the RC spectrograph used by Mas05. After comparing both data sets amongst each other and with our fits from Paper II, it turned out that the nitrogen lines are quite similar, whilst the cores of the hydrogen (except for H$_\alpha$) and He II lines are somewhat deeper in

---

[13] IRAF is distributed by the National Optical Astronomy Observatories, which are operated by the Association of Universities for Research in Astronomy, Inc., under cooperative agreement with the National Science Foundation.

the UVES data, more than expected from the higher resolution. Because of the high quality of the UVES data, we kept the parameters as derived in Paper II, though a re-analysis based on the Mas05 data would have provided rather similar values.

6.3. Analysis

Stellar and wind parameters were derived following the methodology outlined in Paper II, and are listed in Table 5. Comments on individual objects and corresponding H/He/N line fits are provided in Appendix B.

In brief, we proceeded as follows. In accordance with Paper II and the investigations by Massey and collaborators, we assumed unclumped mass-loss throughout the analysis.[14] First, we determined $v \sin i$ for each object using the Fourier method (Gray 1976).[15] Subsequently, we roughly constrained the stellar/wind parameters as well as the helium and nitrogen abundances by means of our model-grids for LMC and SMC background metallicities. For deriving T_{eff}, we used both the helium and nitrogen ionization balance when possible, i.e., when nitrogen lines from at least two ionization stages were visible For the cooler objects of our sample ($T_{\mathrm{eff}} \leq 44$ kK), we mainly relied on the helium ionization balance, and used nitrogen as a consistency check. For hotter objects, where He IIλ4541 begins to loose its sensitivity to T_{eff}, we gave larger weight to the nitrogen balance, as long as a reasonable fit to the He I/He II lines could be maintained. Note that any T_{eff}/[N] degeneracy (as present, e.g., for the line-strength *ratio* of N IV/N III) is broken by the absolute strengths of the lines, and the fact that we have usually more than two lines at our disposal, which react quite differently on changes in T_{eff} and [N] (cf. Fig. 11). Thus, as long as lines from at least two nitrogen ionization stages are available, T_{eff} and [N] can be determined in parallel from fitting these lines (as long as the other stellar/wind parameters can be inferred from independent diagnostics). If nitrogen lines were not available (too weak), we either relied on He I/He II alone (LH 101:W3-24 and AV 177), or, when even He I was no longer visible, we settled for a lower limit on T_{eff} (R136-040). We refer to Appendix B for a detailed discussion on the specific diagnostics used (see also Table 5), and on particular problems for individual stars.

Gravities were inferred from the wings of the Balmer lines, and log Q from fitting H$_\alpha$ and He IIλ4686, with nitrogen lines serving as a consistency check for both quantities. Because of the rather low resolution and the mostly high $v \sin i$ values, we were able to constrain the 'macro-turbulence', v_{mac}, for only two objects (LH 81:W28-5 and LH 90:ST 2-22). For the remaining ones, our fits were acceptable without any need for extra-broadening.

At this point, we adopted terminal velocities as derived by Massey et al. from UV lines, updating $\dot{M}$ to preserve Q if necessary. For the bulk of the stars, we kept the velocity field exponent used within our model-grid, $\beta = 0.8$, because of reasons of consistency, since also Massey et al. used this value. Only for LH 81:W28-23 we adopted $\beta = 1.0$, to better reproduce He IIλ4686 (see Fig. B.2). For those objects with H$_\alpha$ and He IIλ4686 in emission (LH 101:W3-19, Sk–67° 22, and Sk–65° 47), it would have been also possible to derive β from the profile shape. Because of the quite good fit-quality for both lines

already with $\beta = 0.8$ (see Figs. B.7, B.8, and B.9), we had no real reason to change this value though.

Final parameters were derived from a grid of much higher resolution around the initial constraints. Stellar radii were calculated from M_V as provided by Mas04/05/09 and synthetic fluxes, with a corresponding final update of $\dot{M}$. Following our experience for the earliest O-stars from Paper II, we used a micro-turbulent velocity, $v_{\mathrm{mic}} = 10$ km s^{-1}, for all objects considered here.

Errors on stellar/wind parameters are adopted following Paper II. In brief, we estimate an uncertainty of ± 1 kK in T_{eff} (for those objects with a unique solution, see Table 5), ± 0.1 dex in log g, and ± 0.05 dex in log R_*, adopting a typical error of ± 0.25 mag in M_V (see Eq. 8 in Repolust et al. 2004). Together with the errors for T_{eff}, this adds up to an uncertainty of ± 0.11 dex for log $L/L_\odot$. Larger errors, plus/minus a factor of two, are present for $\dot{M}$, when H$_\alpha$ is in absorption.[16] For objects with mass-loss indicators in emission, the error is somewhat lower. Errors on v_∞ are on the order of ± 100 km s^{-1}, taken from Massey et al., and we estimate the errors on $v \sin i$ and v_{mac} as ± 10 to 20 km s^{-1}. A rough estimate on the error of Y_{He} is ± 0.01 to 0.02. Regarding [N], we adopt a conservative value of ± 0.15 to 0.20 dex to account for the dependence on stellar and wind parameters.

6.4. Comparison with results from Massey et al.

In the following, we briefly discuss overall differences between the stellar/wind parameters derived within this work and by Massey et al. for overlapping objects, also regarding BI237 and BI253 which were already analyzed in Paper II. For details, see Appendix B.

For the majority of objects, where we still could use the He I/He II balance as a primary temperature indicator (but also accounting for nitrogen, see Sect. 6.3), we derived slightly cooler T_{eff}, on the order of 0.5 to 1 kK. This is not too disturbing, however, as one often finds systematic differences of this order when different elements are used to derive T_{eff} for hot stars, as, e.g., in the case of using Si vs. He for early B-/late O-type stars (e.g., Hunter et al. 2007). The maximum difference amounts to $\Delta T_{\mathrm{eff}} = -2$ kK for LH 81:W28-23, on the margin of the adopted errors.

For a few objects (BI237, BI253, NGC 346-355, R136-018, and Sk–67° 22) where we needed to exploit the nitrogen ionization balance to break the helium degeneracy, we inferred considerably hotter temperatures ($\Delta T_{\mathrm{eff}} \sim$ 2-7 kK). Admittedly, and owing to the restricted quality of the data for some of the earliest objects with weak N III triplet emission and very weak He Iλ4471, the effective temperatures derived might by affected by uncertainties due to noise and continuum placement. Nevertheless, the fact that also here the differences are systematic suggests that the solution to this problem may not be purely observational.

We also derived quite similar values for log g, except for the five objects explicitly mentioned above, which indicated higher gravities (mostly because of the higher T_{eff}), with a maximum difference of roughly 0.25 dex for BI253. Our $\dot{M}$ values are systematically lower, mostly because of the lower T_{eff}. For those stars with increased T_{eff}, the reduction is caused by lower R_* and/or higher β, where the latter effect is particularly strong for BI253 which displays the largest difference, $\Delta \log \dot{M} = -0.51$ dex. Helium abundances agree quite well except for those

---

[14] Regarding the impact of clumping on the synthetic nitrogen spectra, see Paper II.

[15] As implemented and tested in the OB-star range by Simón-Díaz et al. (2006) and Simón-Díaz & Herrero (2007).

[16] In this case, one is unable to derive β from line-fitting, and the uncertainty in β reflects in quite a large error for $\dot{M}$ (Markova et al. 2004).

Table 5. Fundamental parameters for the early O-star sample, assuming unclumped mass-loss.

Star	Spectral type	Nitrogen $T_{\rm eff}$ diag.	$T_{\rm eff}$ (kK)	$\log g$ (cgs)	$\log g_{\rm true}$ (cgs)	R_* ($R_\odot$)	$\log L_*$ ($L_\odot$)	$\dot{M}^c$	$\log Q$	β	v_∞ (km s^{-1})	$v \sin i$ (km s^{-1})	$v_{\rm mac}$ (km s^{-1})	$Y_{\rm He}$	[N]
							Dwarfs								
BI253[a]	O2 V((f*))	N IV/N V	54.8	4.18	4.20	10.7	5.97	1.53	-12.61	1.21	3180	230	-	0.08	7.90
BI237[a]	O2 V((f*))	N IV/N V	53.2	4.11	4.12	9.7	5.83	0.62	-12.98	1.26	3400	140	-	0.09	7.38
R136-040	O2-3.5 V	-	>51.0	4.01	4.02	10.3	5.81	1.93	-12.53	0.80	3400	120	-	0.08	6.90
N11-060[a]	O3 V((f*))	N III/N IV/N V	48.0	3.97	3.97	9.5	5.63	0.51	-12.92	1.26	2740	68	40	0.12	8.20
		N IV/N V	51.0	4.10	4.10	9.2	5.71	0.48	-12.92						8.15
AV 435[b]	O3 V((f*))	N III/N IV	46.0	3.90	3.91	13.8	5.88	0.21	-13.15	0.80	1500	110	-	0.10	7.58
LH 81:W28-23	O3.5 V((f+))	N III/N IV/N V	47.0	3.80	3.82	10.0	5.65	1.57	-12.53	1.00	3050	146	-	0.25	8.40
LH 101:W3-24	O3.5 V((f+))	-	47.0	4.00	4.01	8.1	5.46	0.27	-13.00	0.80	2400	120	-	0.10	7.78
LH 81:W28-5	O4 V((f+))	N III/N IV/N V	44.0	3.80	3.81	9.8	5.51	1.08	-12.60	0.80	2700	120	80	0.15	8.38
AV 177[b]	O4 V((f))	-	44.0	3.80	3.85	8.8	5.42	0.23	-13.19	0.80	2650	220	-	0.15	7.78
							Giants								
N11-031[a]	ON2 III(f*)	N III/N IV	47.8	3.95	3.95	13.4	5.92	2.02	-12.64	1.08	3200	71	60	0.11	7.83
		N IV/N V	56.0	4.00	4.00	12.2	6.12	2.20	-12.54						8.30
NGC 346-355[b]	ON2 III(f*)	N IV/N V	55.0	4.00	4.01	12.0	6.08	2.50	-12.39	0.80	2800	140	-	0.10	8.10
		N III/N IV	51.0	4.00		12.5	5.98	2.00	-12.51				-		7.98
N11-026[a]	O2 III(f*)	N III/N IV/N V	49.0	4.00	4.00	11.3	5.82	1.56	-12.63	1.08	3120	72	60	0.10	7.80
		N IV/N V	52.0	4.10	4.10	11.0	5.89	1.49	-12.63						7.75
R136-018	O3 III(f*)	N III/N IV/N V	47.0	3.90	3.92	14.2	5.95	1.68	-12.76	0.80	3200	180	-	0.10	8.18
LH 90:ST 2-22	O3.5 III(f+)	N III/N IV/N V	44.0	3.70	3.71	18.8	6.08	4.56	-12.36	0.80	2560	120	80	0.15	8.58
							Supergiants								
Sk–67° 22	O2 If*/WN5	N III/N IV/N V	46.0	3.70	3.74	12.4	5.80	15.00	-11.60	0.80	2650	200	-	0.30	8.78
LH 101:W3-19	O2 If*	N III/N IV/N V	44.0	3.90	3.91	25.3	6.34	20.86	-11.97	0.80	2850	180	-	0.10	8.18
Sk–65° 47	O4 If	N III/N IV	40.5	3.60	3.62	19.8	5.98	11.00	-11.89	0.80	2100	160	-	0.12	7.78

[a] Stellar/wind parameters derived in Paper II; [b] SMC star; [c] in units of $10^{-6}\,M_\odot{\rm yr}^{-1}$

Notes. $\log g_{\rm true}$ is the surface gravity corrected for centrifugal effects. For each star, the additional (or even primary) $T_{\rm eff}$ diagnostics used in parallel with the He I/He II ionization equilibrium is indicated. For four stars, two parameter sets are provided, because we had problems to reach a simultaneous fit for all considered lines from three nitrogen ionization stages. For N11-026 and N11-060 the first entry is our preferred one, and the second entry is a (disfavored) alternative, whereas for N11-031 (see Paper II) and NGC 346-355 we consider both solutions as possible. For errors, see text.

few stars with a larger change in $T_{\rm eff}$, where we had to adapt $Y_{\rm He}$ to preserve the fit quality of the helium lines. The largest difference found amounts to about 0.05 in $Y_{\rm He}$ for LH 90:ST 2-22. Finally, most of our $v \sin i$ are in good agreement with the Massey et al. values, and only three objects displayed substantial differences, with the largest one of about 30 km s^{-1} for BI253.

One of the major implications of our re-analysis of the earliest O-stars as considered by Massey et al. can be stated already now: We do not find the pronounced degeneracy of the N IV/N III emission line ratio as claimed by Mas05 (for details, see Sect. 7.3). For instance, these authors questioned the monotonicity of the classification scheme with respect to $T_{\rm eff}$, because, among other problems, they inferred similar $T_{\rm eff}$ for two dwarfs, LH 101:W3-24 (O3.5) and BI237 (O2), which on the other hand displayed considerable differences in their N IV/N III emission line ratios. These $T_{\rm eff}$ were derived by a pure H/He analysis. By exploiting the nitrogen ionization balance, we are now able to break this degeneracy, since, e.g., we find a considerably hotter temperature for BI237 (see table 5), similar to the temperature derived for BI253, the other O2 dwarf from the sample.

## 7. Discussion

7.1. Nitrogen abundances

Though not the major topic of our present work, let us briefly comment on the nitrogen abundances derived within this analysis. Globally, these are consistent with our results from Paper II.

The bulk of the LMC stars displays a considerable enrichment, stronger than expected from tailored evolutionary calculations (Brott et al. 2011b), and supporting the idea of an efficient mixing during very early phases of O-star evolution. We confirm the tight correlation between the derived helium and nitrogen content.

Only three dwarfs (note that only one prototypical case of nitrogen-weak objects, R136-040, has been analyzed) seem to be unenriched, visible already in the absence of nitrogen lines in their spectra. The star with the highest enrichment within the sample is Sk–67° 22 (O2 If*/WN5), and the derived [N] lies roughly 1.9 dex above the LMC baseline abundance, larger than any of the values found in Paper II. In analogy, also its helium content is extreme, and both findings support the evolved nature indicated by its 'slash' designation.

Although the nitrogen content (in absolute numbers) of the few SMC sample members lies below that of most of our LMC stars, all of them are strongly enriched, by more than one dex above the SMC nitrogen baseline abundance[17]. The largest enrichment (by ~1.6 dex, [N] = 7.98. . . 8.10) was found for NGC 346-355, in agreement with its 'ON' designation. A very similar abundance, [N] = 7.92, together with similar stellar parameters, has been previously derived by both Bouret et al. (2003) and Heap et al. (2006) for this star, see Appendix B.

---

[17] According to Hunter et al. (2007), [N]$_{\rm baseline}$ = 6.5
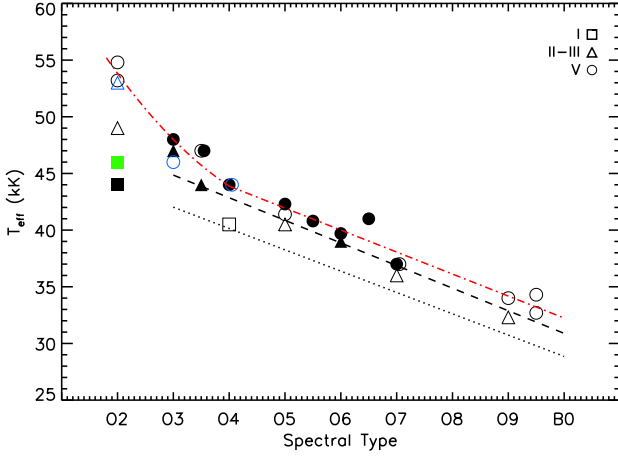
Fig. 12. Effective temperatures as a function of spectral type, for LMC and SMC O-stars analyzed within this work and Paper II (N11-031 and R136-040 discarded, see text). For NGC 346-355 (ON2 III(f*), SMC), T_{eff} according to our 'average' solution, see text. Black symbols: LMC objects; blue symbols: SMC objects; green symbol: Sk–67° 22 (O2 If*/WN5, LMC). Squares refer to supergiants, triangles to (bright) giants, and circles to dwarfs. Filled symbols correspond to objects with [N] ≥ 8.0, and open ones with [N] < 8.0. The dashed-dotted (red) line displays a least square linear and quadratic fit to all dwarfs, according to Eq. 1. The T_{eff} calibration from Martins et al. (2005) for Galactic O-dwarfs (dashed) and supergiants (dotted) is displayed for comparison. For clarity, some objects have been slightly shifted horizontally.

7.2. Effective temperatures vs. spectral types

In Fig. 12, we display the derived effective temperatures as a function of spectral type for our present stellar sample (Table 4), augmented by all (LMC-) stars later than O4 from Paper II to extend the sampling toward cooler types analyzed in a uniform way.

Because it was not possible to assign a specific spectral type to R136-040 (see above), this star is not contained in Fig. 12. We also discarded N11-031 (ON2 III(f*)) from this diagram, owing to severe problems in the determination of its T_{eff}. In Paper II we were not able to derive a unique effective temperature from He I and all three nitrogen ionization stages in parallel, whilst using either He I/N III/N IV or N IV/N V resulted in a difference of $\Delta T_{\mathrm{eff}} = 8$ kK, which is too large to allow for further conclusions. Nevertheless, our sample contains another ON2 giant, NGC 346-355 from the SMC. Also for this object, we were only able to obtain a hotter (based on N IV/N V) and a cooler (based on N III/N IV) solution, but the difference is much smaller, $\Delta T_{\mathrm{eff}} = 4$ kK. In Fig. 12 we assigned a mean value, $T_{\mathrm{eff}} = 53$ kK (accounting for larger errors than typical, on the order of 3 kK), to remain unbiased from a somewhat subjective view, but note that both the hot and the mean temperature are considerably higher than what we would have derived using just the He II/He I lines alone. Further comments on the ON2 stars are given at the end of this section.

To check the impact of [N] on the T_{eff} estimates for a given spectral type, in Fig. 12 we denote objects with nitrogen abundances above and below [N] = 8.0 by filled and open symbols, respectively. This threshold has been chosen according to our findings from Paper II, roughly separating LMC objects with

mild or typical enrichment from those with unexpectedly strong enrichment. We note that this value would be too high for SMC objects if one would be interested in displaying the actual enrichment,[18] but for our purpose of testing and comparing the impact of [N], only the absolute value and not the enrichment is decisive (see Sect. 4.2.3).

The complete LMC sample considered in Fig. 12 covers 26 stars spread over (almost) the full range of spectral subtypes, comprising 16 dwarfs, 7 (bright) giants, and 3 supergiants. On the other hand, only three early SMC objects (two dwarfs and one giant) have been analyzed, preventing firm conclusions.

Before we concentrate on the earliest types, we highlight some general trends. From a first glance, and even though the number of supergiants and (bright) giants within our sample is lower than the number of dwarfs, it is obvious that T_{eff} increases from supergiants to dwarfs for all spectral types, similar to Galactic conditions (e.g., Repolust et al. 2004, Martins et al. 2005). At least for types later than O3.5, giants and supergiants are about 1 kK and 4 kK cooler than dwarfs, respectively. The latter difference is similar to what has been found in previous studies, e.g., by Mas05, Mokiem et al. (2007a), and Mas09. For the earliest types, on the other hand, this difference becomes much larger, about 10 kK at O2.

We can also clearly distinguish different behaviors of the spectral-type-T_{eff} relation. For luminosity classes V and II-III, later types follow a linear trend, whilst the increase in T_{eff} is much steeper for the earliest ones. On the other hand, the few early supergiants of our sample seem to follow a linear trend with a slope similar to cooler objects.

At least for the dwarfs, we are able to provide a *typical* relation, when ignoring any differences in Z and [N]. Using a linear and a quadratic least-square fit for the objects later/including and earlier than O4, respectively, we find

$$T_{\mathrm{eff}} = \begin{cases} 51.64 - 1.94 \times ST & \text{if } ST \geq 4 \\ 70.87 - 10.29 \times ST + 0.88 \times ST^2 & \text{if } 2 \leq ST < 4, \end{cases} \quad (1)$$

where ST is the spectral type for O-dwarfs, and T_{eff} is expressed in kK. At the present state of knowledge, this relation might be applied to LMC stars only, since the low number of analyzed SMC-dwarfs as well as other arguments (see Sect. 7.5) prohibit an application for stars from the SMC.

For comparison, we show in Fig.12 the observed spectral-type-T_{eff} relation for Galactic dwarfs (dashed) and supergiants (dotted) from Martins et al. (2005). For the dwarfs, there is a typical offset of roughly 1 kK, whereas the (cooler) O2 and O4-supergiant seem to follow the Galactic calibration.

A similar comparison between their LMC sample and Galactic dwarfs was provided by Mokiem et al. (2007a), who found a somewhat larger offset by ∼ 2 kK. This difference is caused by lower T_{eff} as resulting from the updated version of FASTWIND for later spectral types (see Paper II).

Reassuringly, the scatter in the spectral-type-T_{eff} relation for objects later than O4 is small (∼1 kK), since the spectral types (as well as our primary T_{eff} indicator) rely on the He I/He II line strength (or E.W.) ratio, which is a rather monotonic function of T_{eff} for a given luminosity class (controlling gravity and wind-strength) and background abundance.[19] The only outlier is N11-

---

[18] Indeed, all SMC objects in Fig. 12 appear with open symbols, despite their strong enrichment. Because of the lower baseline abundance, a threshold of [N] = 8.0 corresponds to an enrichment of 1.5 dex, which is very unlikely to occur except for extreme objects such as NGC 346-355 located close to this value.

[19] All our cool objects are LMC stars.

065, an O6.5 dwarf. The analysis of this star was quite difficult, and for the determination of T_{eff} (and other parameters) we used also the N III/N IV ionization balance, in parallel with He I/He II. Nevertheless, we found considerable problems in fitting the emission at N III$\lambda\lambda 4634 - 4640 - 4642$ together with the pronounced absorption at N IV$\lambda 4058$ and remaining nitrogen lines. Even though this problem became somewhat relaxed by allowing for wind-clumping, it seems that there was indeed a problem in the analysis of this star, and that it might be cooler.

Our sample includes two O4 dwarfs, one from the LMC (LH 81:W28-5) and the other from the SMC (AV 177). For these stars we derive similar T_{eff} and $\log g$, see Table 5, though the SMC star (because of lower Z and weaker winds) should be hotter (e.g., Bouret et al. 2003, Heap et al. 2006, Mokiem et al. 2006). Mas04/05, who came to the same general conclusion, found from a pure H/He analysis the same T_{eff} for AV177 (SMC), whilst they derived an even higher T_{eff} for LH 81:W28-5 (LMC). We note that the present spectrum of the latter shows weak emission in N IV$\lambda 4058$ (Fig. B.4), so that the star might be alternatively classified as O3.5. Since also the gravities are quite low for lc V stars, the situation for both objects remains somewhat unclear, even though the derived parameters are fully consistent with the observed N IV and N III lines.

We concentrate now on the impact of different parameters such as [N], Z, and $\dot{M}$, on the spectral-type-T_{eff} relation for the earliest O-types (O2-O3.5), for which the spectral classification depends crucially on the N IV/N III emission lines, whilst our T_{eff} diagnostics includes additional lines from those ions as well as from N V when visible. To allow for an easy understanding of the following, we summarize the results from our parameter study in Sect. 4: For a given emission line ratio (i.e., spectral type), the derived T_{eff} should increase with [N] and $\log g$, and decrease with Z (at least for higher T_{eff}, see Fig. 6) and $\dot{M}$ (more precisely, $\log Q$).

Thus, the general T_{eff}-difference between dwarfs, (bright) giants, and supergiants can be easily attributed to differences in $\log g$ and $\log Q$, which increase and decrease for increasing luminosity class, respectively. In this way, both effects add up, leading to $T_{eff}(lc V) > T_{eff}(lc III) > T_{eff}(lc I)$, at least for comparable [N] and Z. Regarding this general trend, a classification in terms of nitrogen (early O-types) and helium (late O-types) provides similar effects.

- For the two LMC O3.5 dwarfs (LH 81:W28-23 and LH 101:W3-24), we find the same T_{eff}, though $\log g$ differs by 0.2 dex. The effect produced by the larger [N] of LH 81:W28-23 (Δ[N] $\approx$ 0.6 dex compared to LH 101:W3-24, implying a shift towards higher T_{eff}) is counteracted by both its denser wind and a lower $\log g$. Anyway, it is not clear whether LH 81:W28-23 is correctly designated as a dwarf. Indications of a giant nature are its low surface gravity ($\log g = 3.8$), the wind-strength, and the trace of a P-Cygni profile at He II$\lambda 4686$ (Fig B.2). If this would be the case, the inferred T_{eff} might be too high for this luminosity class when compared to the 'other' O3.5 giant, LH 90:ST 2-22.

- The two O3 dwarfs, N11-060 from the LMC and AV 435 from the SMC, show different T_{eff}. Astonishingly, the LMC star is hotter than the SMC one, by 3 kK, contrary to what might be expected. Here, the [N] effect outweighs the corresponding one associated to Z[20], whilst differences in $\log g$

and wind-strength compensate each other. We will come back to this finding and probable consequences in Sect. 7.5.

- The largest T_{eff} spread seen in our analysis occurs for the O2 stars, with T_{eff} ranging from 44 to 55 kK when accounting for all luminosity classes. Again, the more enriched of the two dwarfs (BI253 vs. BI237) is the hotter one, since the [N] effect dominates over the larger wind-strength. For the two supergiants (Sk–67° 22 and LH 101:W3-19), we find a similar T_{eff} difference, consistent with our predictions for a combination of [N] and $\log Q$. Interestingly, the effect from a lower $\log g$ (3.70 vs. 3.90), as seen for the O3 dwarfs, becomes inhibited by the extreme mass-loss. In Fig. 7, we noted that the N IV/N III emission line ratio begins to loose its sensitivity on $\log g$ at the 'F'-series of our model-grid. The wind-densities of the two supergiants are even higher (roughly corresponding to 'G'), and in this situation the surface gravity does not play any role for determining the line ratio. Finally, the difference between two O2 giants (N11-026 from the LMC and NGC 346-355 from the SMC), $\Delta T_{eff} = 3$ kK with respect to the 'average' solution for NGC 346-355, is larger than expected, since all other parameters except for Z are quite similar, and the Z effect alone should amount to 1 kK (see Fig. 6). Note, however, that the errors in T_{eff} for both objects are larger than typical (≥ 3 kK), related to the problems we encountered for ON2 (III) stars.

The ON2 (III) stars. Let us point out already here that there seems to be a general, severe problem with the ON2 III class, as indicated from our results for N11-031 and NGC 346-355, and the inspection of LH 64-16 (see Sect. 6.1). This problem must relate to some unknown physical process allowing for the presence of strong N III, N IV and N V lines in combination with weak, but still visible He I. Having explored hundreds of models (both from our grid and additional, fine-tuned ones), varying the N abundances as well as other parameters, it turned out that these lines could not be synthesized in parallel. Moreover, we explored a variety of potential sources also from the CMFGEN side, manipulating the photosphere-wind transition zone, including wind-clumping with a variety of clumping laws, and near-photospheric X-rays,[21] etc., and found that none of these would solve the problem. Thus, we can be also sure that the problem is neither related to FASTWIND nor to our present nitrogen model atom.

Also the mass-discrepancy found for these objects underpins their problematic nature. Using the hotter solutions for N11-031 and NGC 346-355, we derived spectroscopic masses of 60 and 53 $M_\odot$, respectively. Evolutionary masses from non-rotating tracks by Charbonnel et al. (1993) and Schaerer et al. (1993)[22] yield 90-95 $M_\odot$ for both stars. Note however that also for a cooler solution for NGC 346-355, at $T_{eff} = 49.5$ kK, already Mas05 stated quite a mass discrepancy, in this case 50 (spectroscopic) vs. 75 $M_\odot$ (evolutionary). For another LMC ON2 III star, LH 64-16, not analyzed during the present work, Mas05 found an even larger discrepancy, 26 vs. 76 $M_\odot$. The authors suggested that the latter star might be the result of binary evolution, since it shows highly processed material at the surface, and since this star appeared to be located to the left of the ZAMS. This seems also to be the case for N11-031 (at least for the hot solution), but not

---

[20] In cooler stars, the He I/He II ionization balance used for classification is almost only affected by background abundance (less Z, less EUV line-blocking), see Repolust et al. (2004).

[21] which do not help because of the destruction of N III and He I, see Paper II.

[22] For the hottest stars, the inclusion of rotation has only a modest effect, resulting in ~10 % lower masses, e.g., Mas05, as long as the initial rotation is not high enough to induce quasi-homogeneous evolution.

for NGC 346-355. A similar problem was also found for some of the close binaries in the R136 cluster (Massey et al. 2002), supporting the idea that these stars suffered from binary interactions. An alternative to binarity might be quasi-homogeneous evolution, but the low $v \sin i$ values measured for our objects (on the order of 100 km s^{-1}) render this possibility as unlikely.

7.3. N IV/N III emission line ratio

To further test the significance of the Walborn et al. (2002) classification scheme, we investigated the relation between the N IV/N III emission line ratio and T_{eff} for our O2-O4 sample stars in a quantitative way, similar to previous work by Mas05, but using our updated parameters (see Sect. 6.4). Unlike Mas05 who used EW ratios, we employed the line-strength ratios to be consistent with the classification scheme. Later on, we also consider an alternative line ratio, N vλ4603/N IVλ6380 (hereafter N v/N IV), to check its potential for classification purposes, and to test whether this ratio might break potential degeneracies inherent to N IV/N III.

Table 6 lists the line ratios for our targets, as derived both from the observations and from the synthetic models associated to our best-fitting solutions. Again, we discarded N11-031 and R136-040 (see Sect. 7.2). Note that at the lower and upper end of the scheme the errors on the observed line ratios can become significant, due to noise and/or absence of N IVλ4058 or N IIIλ4640. In those cases, we provide corresponding lower or upper limits and their uncertainties. Typical errors are on the order of 0.1 to 0.2 dex.

Figure 13 displays the derived effective temperatures as a function of the observed (upper panel) and 'model' (lower panel) N IV/N III line ratios, expressed logarithmically. Number designations for each object refer to Table 6. Different colors are used for each spectral type: O2 (black), O3 (red), O3.5 (blue), and O4 (purple). Symbols referring to luminosity classes and filling referring to [N] are as in Fig. 12.

If we examine the *observed* emission line ratio, we find quite a monotonic behavior, confirming its T_{eff} sensitivity, and similar trends as in the previous section. On the one hand, dwarfs and giants behave rather similar (though the giants seem to be a little cooler), except for the O2 types where the spread is larger. On the other, the observed relation for supergiants lies in parallel to the relation for dwarfs, but at considerably lower T_{eff}. As already pointed out, this is caused by the different gravities and wind-strengths. E.g., from Table 5 we find $\log Q$ values in the ranges $[-13.00, -12.53]$ for the LMC dwarfs, around -13.2 for the SMC dwarfs, $[-12.76, -12.36]$ for the giants, partly overlapping with the dwarfs, and $[-11.97, -11.60]$ for the supergiants.

The various spectral subtypes are located in quite different ranges (by definition, consistent with the Walborn et al. 2002 scheme): All O2 stars are located at $\log$ N IV/N III ≥ 0.4, and O3 dwarfs and O3.5 giants around $\log$ N IV/N III ~ 0 (N IV $\sim$ N III). Finally, one of the O4 dwarfs is located at $\log$ N IV/N III ≈ -0.7, for the other one (#8) we are only able to provide an upper limit, $\log$ N IV/N III $\lesssim -0.3$, whilst the O4 supergiant (#15) lies close to the O3.5 border.

We see small [N] effects[23] on the line ratio, where a larger abundance tends (but not necessarily) to increase the emission line ratio within a given spectral subtype, in particular for the following pairs of stars: O3.5 dwarfs – LH 101:W3-24 (#6, upper limit) and LH 81:W28-23 (#5); O3 dwarfs – AV435 (#4, SMC) and N11-060 (#3); O2 dwarfs – BI237 (#2) and BI253 (#1); O2
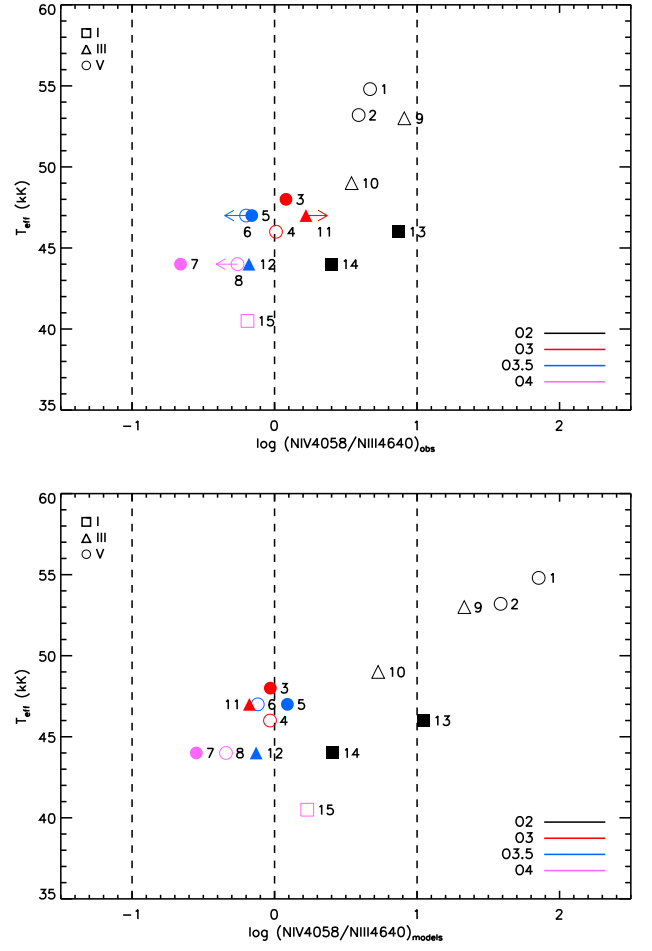
Fig. 13. Effective temperatures as a function of $\log$ N IV/N III, for O2-O4 sample stars. Spectral types distinguished according to legend. Upper panel: observed emission line ratios, limits indicated by arrows; lower panel: emission line ratios predicted from the (globally) best-fitting models. Objects numbered according to Table 6. Filling and symbols as in Fig. 12. Dashed vertical lines (at $\log$ N IV/N III = -1, 0, 1) correspond to the limits used in Fig. 6. For object #9 (NGC 346-355), T_{eff} and theoretical line ratio according to our 'average' solution. Stars #4, #8, and #9 are SMC stars.

supergiants – LH 101:W3-19 (#14) and Sk–67° 22 (#13). Since, on the other hand, the emission line ratio should decrease for enhanced [N] when keeping all other parameters fixed, a consistent solution requires these objects to have a *higher* T_{eff}. For the pair of O4 dwarfs – AV177 (#8, SMC) and LH 81:W28-5 (#7), we note that the star with the higher abundance (#7) seems to have a lower emission line ratio,[24] but this is consistent with the *similar* T_{eff} of these stars.

Indeed, there are not only [N] effects, but also mass-loss effects on the emission line ratio. For all pairs considered above, the object with higher [N] has also a higher wind strength, $\log Q$ (cf. Table 5), which potentially counteracts the [N] effect. Comparing the differences in [N] with the differences in $\log Q$, it turns out that the [N] effect should dominate in all cases though.

Taken together, our findings explain the almost monotonic increase of T_{eff} with N IV/N III also within the individual spectral subtypes, consistent with the derived scatter of T_{eff} per subtype.

---

[23] slightly contaminated by mass-loss effects, see below.

[24] but note also the quite large uncertainty for object #8.

Table 6. Observed and predicted line-strength ratios for N IV/N III and N V/N IV, for the O2-O4 stars analyzed within this work. Observed ratios (or limits) inclusive errors. Numbers refer to Figs. 13 and 14.

Star	#	SpT	$T_{\rm eff}$ (kK)	$\log(\frac{NIV}{NIII})$ obs		$\log(\frac{NIV}{NIII})$ model	$\log(\frac{NV}{NIV})$ obs		$\log(\frac{NV}{NIV})$ model	Comments
BI253	1	O2 V((f*))	54.8	0.67	±0.15	1.85	0.53	±0.23	0.43	N IIIλ4640 and N IVλ4058 underpredicted[a]
BI237	2	O2 V((f*))	53.2	0.59	±0.14	1.58	0.36	±0.14	0.21	N IIIλ4640 underpredicted[a]
N11-060	3	O3 V((f*))	48.0	0.08	±0.02	−0.03	−0.07	±0.03	−0.30	N IVλ4058 and N Vλ4603 underpredicted[a,b]
AV 435	4	O3 V((f*))	46.0	0.01	±0.18	−0.03	< −0.30	(+0.10)	−0.46	N Vλ4603 diluted in noise
LH 81:W28-23	5	O3.5 V((f+))	47.0	−0.16	±0.04	0.09	−0.01	±0.05	−0.18	N IIIλ4640 underpredicted
LH 101:W3-24	6	O3.5 V((f+))	47.0	< −0.20	(+0.12)	−0.12	< −0.28	(+0.14)	−0.38	N IIIλ4640 underpredicted
LH 81:W28-5	7	O4 V((f+))	44.0	−0.66	±0.10	−0.55	−0.53	±0.13	−0.60	Satisfactory fits
AV 177	8	O4 V((f))	44.0	< −0.26	(+0.13)	−0.34	< −0.36	(+0.09)	−0.57	Only N IIIλ4640 and N IVλ6380 visible
NGC 346-355	9	ON2 III(f*)	53.0	0.91	±0.09	1.33	0.19	±0.04	0.21	N IIIλ4640, N IVλ4058, N Vλ4603 underpred.[c]
N11-026	10	O2 III(f*)	49.0	0.54	±0.06	0.73	0.14	±0.02	−0.08	N IIIλ4640, N IVλ4058, N Vλ4603 underpred.[a,b]
R136-018	11	O3 III(f*)	47.0	> +0.22	(−0.21)	−0.18	> −0.20	(−0.13)	−0.32	N IIIλ4640 and N IVλ4058 underpredicted
LH 90:ST 2-22	12	O3.5 III(f+)	44.0	−0.18	±0.06	−0.13	−0.20	±0.04	−0.39	Satisfactory fits
Sk−67° 22	13	O2 If*/WN5	46.0	0.87	±0.14	1.04	0.35	±0.03	0.31	N Vλ4603 under, N IVλ4058 overpredicted
LH 101:W3-19	14	O2 If*	44.0	0.40	±0.07	0.41	0.05	±0.14	0.00	N Vλ4603 overpredicted
Sk−65° 47	15	O4 If	40.5	−0.19	±0.12	0.23	< −0.38	(+0.08)	−0.52	N IVλ4058 overpredicted

[a] For fits, see Paper II, Appendix C; [b] Compromise solution, see Paper II; [c] 'Average' solution.

Notes. Errors in brackets provide uncertainties of lower or upper limits. Predicted line ratios ('model') drawn from best-fitting synthetic spectra. N11-031 and R136-040 discarded, see text.

Differences in background metallicity and wind-strength seem to play a secondary role, compared with the larger impact of [N].

If we now inspect the line ratios *predicted* by our best-fitting models (lower panel), we mostly find quite similar values and trends. For the bulk of the stars there are only small shifts due to minor problems in properly fitting the lines (see Table 6 for particular comments on each star). However, more severe differences are present for BI237 (#1), BI253 (#2), and NGC 346-355 (#9, SMC). For the former O2 dwarfs, we predict too weak N III emission, thus overestimating the line ratio, but note that the *observed* emission is also rather weak for these stars. For NGC 346-355, the problem is different since we are not able to reproduce both lines using the 'average' solution (see Fig.B.12) displayed here.

We conclude that, for a given luminosity class, the effective temperatures are a rather monotonic function of log N IV/N III, that the scatter within a spectral subtype is mostly due to abundance effects, and that our models are in fair agreement with the observed line-ratios, except for the hottest objects where we underestimate the observed (low) N III emission strength.

7.4. N V/N IV line ratio

Since both N IVλ6380 and N Vλ4603 are absorption lines (i.e, less affected by complex formation processes), since they turned out to be quite reliable during our analyses, and since N Vλ4603 is very $T_{\rm eff}$ sensitive (Sect. 5), we checked the corresponding line ratio as a potential diagnostic tool, which might be even used for future classification purposes.

From Fig. 14, we see that the relation $T_{\rm eff}$ vs. log N V/N IV is remarkably monotonic. By inspection of the *observed* line ratios (upper panel), we find again two different trends, one for dwarfs and (bright) giants and another one for supergiants. The objects are basically grouped together within three regions: O2 stars with log (N V/N IV)$_{\rm obs}$ > 0, O3/O3.5 dwarfs and giants around log (N V/N IV)$_{\rm obs}$ ≈ −0.3...0, and the O4 stars with log (N V/N IV)$_{\rm obs}$ ≲ −0.4. The only discrepant object seems to be the SMC O3-dwarf AV 435 (#4), which appears at the edge

of the O4-region. However, this 'erroneous' position could be
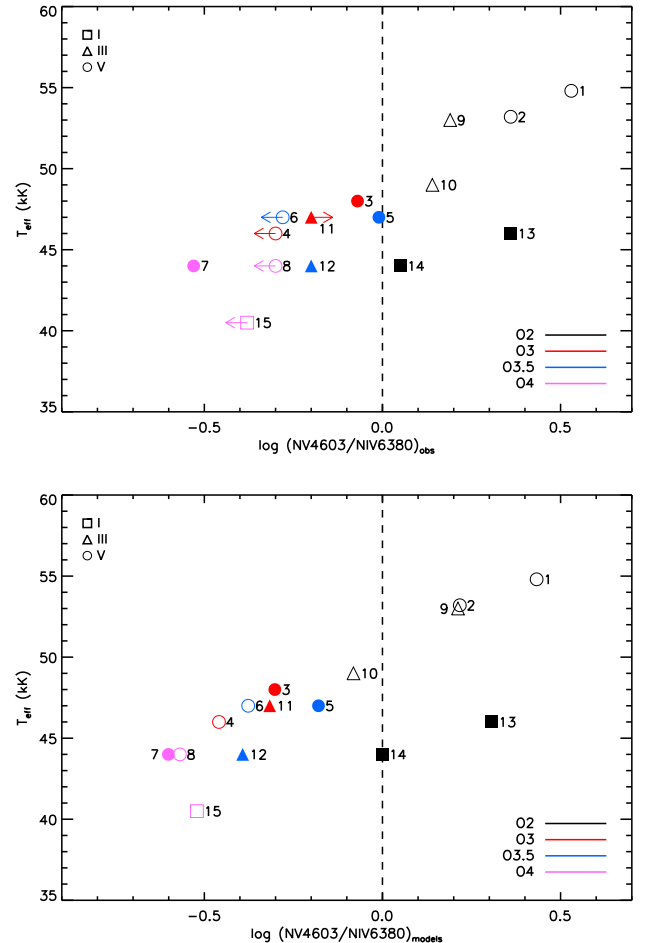
Fig. 14. As Fig. 13, but for the N vλ4603/N ivλ6380 line ratio.

tracked down to a considerable error in the measured line ratio, because of very weak N v lines diluted in the continuum (Fig. B.10).

Compared to the N IV/N III emission line ratio, there seems to be a clearer separation between the different subtypes, e.g., Sk–65° 47 (#15) is located closer to the remaining O4 objects, whilst regarding N IV/N III it is closer to the O3 V/O3.5 III group. Moreover, there is a clear separation between the two O2 dwarfs (#1,2) and the ON2 giant (#9, SMC) because of weaker N IVλ6380.

Comparing now with the *predicted* line ratios (lower panel), we see that predicted and observed ones agree quite well *over the complete range*. Still, there are certain shifts because of a non-perfect representation by our synthetic lines (Table 6), but interestingly we do no longer find the extreme differences for BI237, BI253, and NGC 346-355 as present in the N IV/N III diagram, which indicates that we are able to obtain a satisfactory representation of the N IV/N V ionization balance. So far, we cannot comment on any [N] related bias, since we did not perform corresponding theoretical studies. In case the N V/N IV line ratio might be used in future classification schemes, this will become certainly necessary.

The monotonic behavior of the N V/N IV line ratio illuminates its promising potential, particularly for the hottest objects (O2), simply because there is more N V than N III present at these temperatures. We suggest to investigate this possibility when larger samples become available.

7.5. Caveats for low-metallicity stars

Summarizing our findings, we conclude that already the present Walborn et al. (2002) classification scheme allows for a reasonable relation between spectral type and effective temperature, *as long as it possible to discriminate the luminosity class*. The only significant bias in the scheme might be produced by nitrogen abundance effects (or *extreme* variations in wind strength). E.g., if the nitrogen abundance is not the same in an O3 III and an O3.5 III star, then the O3 III star is not necessarily hotter than the O3.5 III.

However, there are also important caveats regarding low-metallicity (e.g., SMC) stars. As it is well-known, effective temperatures increase with decreasing Z for a given spectral type if the classification is based on the helium ionization balance, i.e., the He I/He II line-strength ratio (O4-O9.7 stars, e.g., Bouret et al. 2003, Mas04/05, Heap et al. 2006, Mokiem et al. 2006, 2007b). According to our predictions, this no longer needs to be true for the earliest O-stars classified by means of nitrogen.

(i) *O2/O3 stars.* Though for similar [N] a lower metallicity implies a higher $T_{\rm eff}$ (at least for spectral types O3(dwarfs)/O3.5(giants and supergiants) and earlier, see Fig. 6), this effect might be counteracted by a different nitrogen content if we assume typical (maximum) enrichments, of roughly +0.6, +0.9, and +1.0 dex above the corresponding MW, LMC, and SMC baseline abundance, as predicted by Brott et al. (2011a) for a 40 $M_\odot$ star at an initial rotation of 270 km s^{-1}. As visible from Fig. 8, for an O3 dwarf with log g = 4.0 dex, our predictions indicate $T_{\rm eff} \approx$ 47-48 kK for the Galaxy and $T_{\rm eff} \approx$ 46 kK for the LMC/SMC.[25] Such cooler or at least similar $T_{\rm eff}$ for stars in a lower Z environment should be present only for typical nitrogen abundances;

objects with a considerably different enrichment will contribute to enlarging the spread.

(ii) *O3.5/O4 stars.* In view of the results from Sect. 4.2.1, there might be an additional problem around O3.5/O4. From Fig. 6, SMC stars should be *cooler* than corresponding LMC ones, even at a similar [N], for a line ratio around N IV/N III = 0.1 (which represents a lower limit for O3.5 V and O4 I/III). Since the SpT-$T_{\rm eff}$ relation is rather monotonic for LMC stars at *all* spectral types, derived either by helium or nitrogen (see Fig. 12), the corresponding relation for SMC stars might be not monotonically connected between these two regime: Even though there seems to be a monotonic relation between N IV/N III and $T_{\rm eff}$ on the hot side, the potential 'jump' would be caused by the fact that the SMC SpT-$T_{\rm eff}$ relation on the cooler side (based on He I/He II) lies above the LMC relation.

To confirm or disprove these predictions and caveats, a thorough analysis of a large sample of SMC stars is certainly required, given the few SMC objects investigated so far.

7.6. SMC Of-stars

The luminosity criteria for O-type stars are based primarily on their "Of" characteristics; i.e., the strength of the N III triplet and the He IIλ4686 emission.[26] As already emphasized by Mas04/05/09, this can lead to significant problems with luminosity classification of O-stars found in low metallicity environments, such as the SMC.

The problem is that the emission strengths of the Of features are tied to mass-loss rates (both for He II and N III), which in turn scale with metallicity, and to (average) nitrogen abundances (for N III).[27] One thus expects a star in the SMC to show weaker Of-characteristics for the same physical properties than would a similar star in the Milky Way. As demonstrated in Sect. 3.1, in particular the N III emission strength of the SMC star should be lower, unless the nitrogen abundances of the two objects were similar, which would mean the rare case of an *extreme* enrichment of the SMC star.

Throughout their studies of Magellanic Cloud O-type stars, and particularly those in the SMC, Mas04/05/09 found numerous examples where the Of-type properties indeed were weaker than would be expected given the absolute magnitude of those stars[28]. We can demonstrate the weakness of Of-features statistically as follows. If we restrict ourselves to the SMC O-type stars with spectral subtypes determined from slit spectroscopy (Table 6 of Massey 2002) we find 74 stars, only 5 (7%) have "f" type designations. Similarly, of the 83 O-type stars listed by Evans & Howarth (2008), only 7 (8%) have any "f" designation, and all of these are either "(f)" or "((f))" indicating that He IIλ4686 is weakly in emission or in absorption. In contrast, Of-characteristics abound among O-type stars in the Milky Way. Of the 378 Galactic O-type stars catalogued by Maíz-Apellániz et al. (2004), 160 (42%) display Of-characteristics. Since Of-type stars are brighter than non-Of stars (at least in the Milky Way), this may overestimate the true per-

---

[25] See also Fig. 12, where the SMC O3 dwarf AV 435 indeed is cooler than the corresponding LMC objects.

[26] These emission features were linked with luminosity for Galactic stars (see, for example, Walborn 1972), a refinement over previous luminosity criteria based primarily on the Si IVλ4089 to He Iλ4143 ratio.

[27] Counteracting the increase of N III emission because of less blocking in a low Z environment.

[28] The alternative explanation that all such discrepant stars were too bright owing to their being binaries was contradicted by the excellent fits obtained to the spectral features; this would require both components of a binary to be of identical spectral subtype and brightness.

centage. If we instead restrict ourselves just to the sample of 24 O-type stars with well-established distances by HIPPARCOS (Maíz-Apellániz et al. 2004 Table 7) we find that 7 (29%) have Of-characteristics.

Thus we conclude that there are strong indications for a significantly lower percentage of SMC Of-stars, compared to Galactic ones, which we attribute to the effects outlined in Sect. 3.1. Remember, however, that a lower wind-strength alone is not sufficient to explain this finding (Fig. 2, upper panel), but that a lower average nitrogen content needs to be present as well.

8. Summary and conclusions

We investigated open questions raised by our previous studies on the formation of N $_{\rm III}\lambda4640$ and N $_{\rm IV}\lambda4058$. We provided first theoretical predictions for the N $_{\rm IV}$/N $_{\rm III}$ emission line ratio, and confronted these predictions with observational findings, concentrating on a sample of early-type O-stars. The results of this work can be summarized as follows.

1. The emission strength of the N $_{\rm III}$ triplet from objects with similar $T_{\rm eff}$ and $\log g$ depends on their metallicity, associated mass-loss, and nitrogen content. Whilst even under SMC conditions lower mass-loss rates alone are not able to compensate the increase in emission for decreasing Z, a lower [N], coupled to a significantly lower base-line abundance, can easily outweigh the Z effect and lead to overall lower emission strengths. This might explain the relatively low number of SMC 'Of' stars.

2. Our models predict an only weak Z-dependence of N $_{\rm IV}\lambda4058$ (contrasted to the N $_{\rm III}$ triplet). SMC-abundance models with $T_{\rm eff} \leq 45$ kK display slightly more emission than their Galactic counterparts, and vice versa for hotter temperatures. Much stronger is the impact of wind-strength though.

3. It turned out that N $_{\rm IV}\lambda4058$ behaves quite unexpectedly when [N] is increased in low-$\dot{M}$ models. For almost the whole temperature range, we either obtain more absorption or less emission, compared to models with a lower nitrogen content. For a specific temperature range, N $_{\rm IV}\lambda4058$ can even switch from emission to absorption when increasing [N]. For Galactic stars at 44 kK $\leq T_{\rm eff} \leq 50$ kK and comparatively low $\dot{M}$, our models imply that if N $_{\rm IV}\lambda4058$ is observed in absorption, this would indicate a strong nitrogen enrichment.

4. We provided first theoretical predictions on the N $_{\rm IV}$/N $_{\rm III}$ emission line ratio, as a function of Z, $\log Q$, and [N], by studying line-ratio iso-contours in the $T_{\rm eff}$-$\log g$ plane. For an emission line ratio of unity (i.e., a spectral type of O3.5 I/III or O3 V), the corresponding $T_{\rm eff}$ increases with [N] ($\sim$1 kK per increment of 0.2 dex in [N]) and $\log g$ ($\sim$1 kK per increment of 0.1 dex in $\log g$). In addition, it should decrease with Z, at least for higher $T_{\rm eff}$ ($\sim$2-3 kK difference between SMC and MW objects), and $\log Q$ ($\sim$2-4.5 kK between low- and high-$\dot{M}$ models).

5. We performed a comparison with results from the alternative model atmosphere code CMFGEN, for a small grid of early O-type dwarfs and supergiants. Our basic predictions regarding the impact of [N] on (i) N $_{\rm IV}\lambda4058$ for low-$\dot{M}$ models (see item 3), and (ii) on the N $_{\rm IV}$/N $_{\rm III}$ emission line ratio (see item 4) were confirmed by corresponding CMFGEN results. Regarding specific line predictions, we found a mostly satisfactory agreement, except for some systematic deviations: For early O-stars, FASTWIND produces more emission at the N $_{\rm III}$ triplet, less emission at N $_{\rm IV}\lambda4058$, and mostly much

more absorption at N $_{\rm IV}\lambda6380$. This would lead to lower $T_{\rm eff}$ and quite different [N] in analyses performed by means of CMFGEN, if concentrating on the N $_{\rm III}$ triplet and N $_{\rm IV}\lambda4058$ alone. Fortunately, the remarkably good agreement of the H/He lines in both codes enables an identification of potential problems regarding the nitrogen lines, as long as the helium ionization balance is used to constrain $T_{\rm eff}$. In the hot O-star domain, the latter approach is no longer feasible because of vanishing He $_{\rm I}$. Nevertheless, potential problems should become obvious also here when relying on the N $_{\rm V}\lambda\lambda4603$-4619 doublet, which turned out to be very sensitive on $T_{\rm eff}$ as well as code-independent.

6. We confronted our theoretical predictions with results from an analysis of a medium-size sample of LMC/SMC O-stars, drawn from studies by Massey et al. (early types), and from Paper II. The basic difference to the Massey et al. analyses is found in the procedure for deriving $T_{\rm eff}$, where we used the nitrogen ionization balance in the hotter $T_{\rm eff}$ regime instead of the helium one, to avoid any degeneracy. For the cooler objects of our sample ($T_{\rm eff} \leq 44$ kK) we mainly relied, when possible, on helium, using nitrogen as a consistency check. For these stars we found similar or slightly cooler $T_{\rm eff}$ compared to Massey et al.. Considerably hotter $T_{\rm eff}$, on the other hand, were inferred for the earliest O-stars, by means of the nitrogen diagnostics. Nevertheless, in most cases the corresponding synthetic He $_{\rm II}$/He $_{\rm I}$ lines were still consistent with the observations, or indicated only slightly lower temperatures. Notable exceptions are the ON2 III stars (see below). The nitrogen abundances derived within our analysis are consistent with our results from Paper II: again, the bulk of the stars displays a considerable enrichment.

7. By inspecting the inferred effective temperatures, we saw that $T_{\rm eff}$ increases from supergiants to dwarfs for all spectral types, consistent with earlier results. For spectral types later than O3.5 (down to O9.5), LMC giants are cooler by $\sim$1 kK, and supergiants are cooler by $\sim$4 kK, compared to dwarfs. For types earlier than O3.5, this difference (and also the scatter) becomes larger, amounting to $\sim$10 kK at O2 when comparing supergiants and dwarfs. For LMC dwarfs and giants later than O3.5, and for all LMC supergiants, we found linear relations between $T_{\rm eff}$ and spectral type, again consistent with previous work. The earliest dwarfs and giants, on the other hand, display a much steeper increase in $T_{\rm eff}$. The dominating effect responsible for the scatter in the SpT-$T_{\rm eff}$ relation at earliest types was attributed to difference in [N], where for a given spectral type more enriched objects are typically hotter.

8. The relation between the observed N $_{\rm IV}$/N $_{\rm III}$ emission line ratio and $T_{\rm eff}$ turned out to be quite monotonic, if discriminating for luminosity class. Because of the high $T_{\rm eff}$ derived for the earliest stars by means of the nitrogen ionization balance, we did not find the pronounced degeneracy of the N $_{\rm IV}$/N $_{\rm III}$ emission line ratio as claimed by Mas05. The scatter found within a spectral subtype is, again, primarily produced by abundance effects. Our model predictions are in fair agreement with the observed line-ratios, except for the hottest objects where we underestimate the observed (low) N $_{\rm III}$ emission-strength.

9. We provided first insights into the relation between $T_{\rm eff}$ and the N $_{\rm V}\lambda\lambda4603$-4619/N $_{\rm IV}\lambda6380$ absorption line ratio, which is remarkably monotonic, particularly for the hottest objects in our sample, and we highlighted the promising potential of this line ratio for future classification schemes.

Both our theoretical predictions and our observational analysis suggest that the Walborn et al. (2002) classification scheme is able to provide a meaningful relation between spectral type and effective temperature. In particular, and as one might have expected, the N IV/N III emission line ratio changes with effective temperature, all other factors being equal. However, this ratio is also sensitive to surface gravity, mass-loss rate, and to nitrogen abundance, which are expected to vary among a sample of stars. Thus, the significance of the classification scheme (within the uncertainties caused by nitrogen abundance) might be only warranted as long as it is possible to fairly discriminate the luminosity class (as a proxy to gravity), and as long as there is a strong correlation between spectral type/luminosity class and wind-strength. If, e.g., there would be weak-winded stars (Marcolino et al. 2009, Najarro et al. 2011 and references therein) also in the early O-type regime and not only at later spectral types, the monotonicity with respect to $T_{\rm eff}$ might become severely disturbed.

A clear identification of early O-type luminosity classes from spectral morphology alone becomes difficult in low-Z environments such as the SMC. We emphasize the same point as made by Mas04/05/09, that the standard luminosity classification criterion, primarily based on the morphology of He IIλ4686, is significantly biased on mass-loss rates. Owing to lower wind-strengths for SMC conditions, He IIλ4686 is typically in absorption not only for lc V, but also for lower gravity objects which under Galactic conditions would correspond to lc I/III. Thus, there are O-type stars in the SMC whose physical properties (visual luminosities and surface gravities) might be in accord with them being giants or supergiants whereas their spectroscopically determined luminosity classes may be dwarfs or giants, respectively. To circumvent this caveat, other information, such as the absolute visual magnitude of the system, may have to be appealed to. Without such additional information, an appropriate classification may rest on a more precise determination of the surface gravity, e.g., using a visual inspection of the wings of H_γ. Another possibility is to extend the classification scheme by including the strength of H_α (which needs to be carefully calibrated, since also this wind-line remains in absorption).

Our study also implies important consequences which need to be validated or investigated in future work:

(i) The SpT-$T_{\rm eff}$ scale constrained from our LMC sample turned out to be, for a given luminosity class, more or less monotonic. However, the majority of the analyzed objects displayed a considerable nitrogen enrichment. To quantify the actual impact of nitrogen abundance would require the analysis of a significant number of un- or mildly enriched earliest MW/LMC objects[29] that according to our predictions should be cooler than the enriched ones.

(ii) Typical SMC stars of earliest spectral types might have effective temperatures below corresponding LMC objects, and the overall SpT-$T_{\rm eff}$ relation for SMC stars might be non-monotonic around O3.5/O4.

(iii) Our predictions suggest that there should be (enriched) Galactic O4 dwarfs with emission at N IIIλ4640 and absorption at N IVλ4058 (item 3 from above). So far, the Walborn et al. (2002) classification scheme only states that N IVλ4058 should be absent for such objects. A quick

inspection of the IACOB database of Galactic OB stars (Simón-Díaz et al. 2011) allowed us to find a first indication of this effect, for HD 46223 (O4 V((f))), and we were able to reproduce its strong emission at N IIIλ4640 together with a pronounced absorption at N IVλ4058, for a considerable nitrogen enrichment.

(iv) As became apparent throughout this work (first indications were already found in Paper II), we encountered severe problems for ON2 III stars. For these objects, we were not able to find a simultaneous fit of the pronounced N III/N IV/N V lines and the weak, but still clearly present He Iλ 4471, independent whether we used FASTWIND or CMFGEN. Though we were able to derive a cooler (fitting N III/N IV and He I) and a hotter solution (fitting N IV/N V), we were not able to favor one of those. In some cases, the $T_{\rm eff}$ difference between the hotter and the cooler solution is extreme, e.g., for N11-031 analyzed in Paper II. Because of the restricted quality of our present dataset, new observations with higher S/N and higher resolution would be extremely valuable to verify our results using the nitrogen ionization balance and/or the pure He II/He I results from Massey et al. when He I (and N III) become extremely weak.

Future work is certainly needed to address the aforementioned issues. Upcoming analyses of extensive O-star samples, e.g., from the VLT-FLAMES Tarantula survey and the IACOB data base, will be fundamental for trying to explain these open questions.

References

Asplund, M., Grevesse, N., & Sauval, A. J. 2005, in Cosmic Abundances as Records of Stellar Evolution and Nucleosynthesis, ed. T. G. Barnes III & F. N. Bash, Vol. 336 (San Francisco, ASP), 25
Asplund, M., Grevesse, N., Sauval, A. J., & Scott, P. 2009, ARA&A, 47, 481
Azzopardi, M. & Vigneau, J. 1982, A&AS, 50, 291
Bouret, J.-C., Lanz, T., Hillier, D. J., et al. 2003, ApJ, 595, 1182
Breysacher, J., Azzopardi, M., & Testor, G. 1999, A&AS, 137, 117
Brott, I., de Mink, S. E., Cantiello, M., et al. 2011a, A&A, 530, A115
Brott, I., Evans, C. J., Hunter, I., et al. 2011b, A&A, 530, A116
Brunet, J. P., Imbert, M., Martin, N., et al. 1975, A&AS, 21, 109
Charbonnel, C., Meynet, G., Maeder, A., Schaller, G., & Schaerer, D. 1993, A&AS, 101, 415
Crowther, P. A. 2000, A&A, 356, 191
Crowther, P. A. & Walborn, N. R. 2011, MNRAS, 416, 1311
Doran, E. I. & Crowther, P. A. 2011, Bulletin de la Societe Royale des Sciences de Liege, 80, 129
Evans, C. J. & Howarth, I. D. 2008, MNRAS, 386, 826
Evans, C. J., Lennon, D. J., Smartt, S. J., & Trundle, C. 2006, A&A, 456, 623
Evans, C. J., Taylor, W. D., Hénault-Brunet, V., et al. 2011, A&A, 530, A108
Gray, D. F. 1976, The observation and analysis of stellar photospheres, Vol. 484 (Research supported by the National Research Council of Canada. New York, Wiley-Interscience)
Grevesse, N. & Sauval, A. J. 1998, Space Science Reviews, 85, 161
Heap, S. R., Lanz, T., & Hubeny, I. 2006, ApJ, 638, 409
Herrero, A. 2003, in Astronomical Society of the Pacific Conference Series, ed. C. Charbonnel, D. Schaerer, & G. Meynet, Vol. 304 (San Francisco, ASP)
Herrero, A. & Lennon, D. J. 2004, in IAU Symposium, Vol. 215, Stellar Rotation, ed. A. Maeder & P. Eenens (San Francisco, ASP), 209

---

[29] For SMC objects, the nitrogen baseline abundance is too low to allow for a clear-cut classification and spectroscopic analysis by nitrogen lines, at least in the optical. This was already a problem for unenriched LMC stars, e.g., R136-040, and the similar objects R136-033 and R136-055.

Hillier, D. J. & Miller, D. L. 1998, ApJ, 496, 407
Hubeny, I. & Lanz, T. 1995, ApJ, 439, 875
Hunter, I., Dufton, P. L., Smartt, S. J., et al. 2007, A&A, 466, 277
Kudritzki, R.-P. 1980, A&A, 85, 174
Kudritzki, R.-P. & Puls, J. 2000, ARA&A, 38, 613
Leitherer, C., Robert, C., & Drissen, L. 1992, ApJ, 401, 596
Lenorzer, A., Mokiem, M. R., de Koter, A., & Puls, J. 2004, A&A, 422, 275
Lucke, P. B. 1972, PhD thesis, University of Washington
Maíz-Apellániz, J., Walborn, N. R., Galué, H. Á., & Wei, L. H. 2004, ApJS, 151, 103
Malumuth, E. M. & Heap, S. R. 1994, AJ, 107, 1054
Marcolino, W. L. F., Bouret, J., Martins, F., et al. 2009, A&A, 498, 837
Markova, N., Puls, J., Repolust, T., & Markov, H. 2004, A&A, 413, 693
Markova, N., Puls, J., Scuderi, S., Simón-Díaz, S., & Herrero, A. 2011, A&A, 530, A11
Martins, F., Escolano, C., Wade, G. A., et al. 2012a, A&A, 538, A29
Martins, F., Mahy, L., Hillier, D. J., & Rauw, G. 2012b, A&A, 538, A39
Martins, F., Schaerer, D., & Hillier, D. J. 2005, A&A, 436, 1049
Massey, P. 2002, ApJS, 141, 81
Massey, P., Bresolin, F., Kudritzki, R. P., Puls, J., & Pauldrach, A. W. A. 2004, ApJ, 608, 1001
Massey, P. & Hunter, D. A. 1998, ApJ, 493, 180
Massey, P., Parker, J. W., & Garmany, C. D. 1989, AJ, 98, 1305
Massey, P., Penny, L. R., & Vukovich, J. 2002, ApJ, 565, 982
Massey, P., Puls, J., Pauldrach, A. W. A., et al. 2005, ApJ, 627, 477
Massey, P., Zangari, A. M., Morrell, N. I., et al. 2009, ApJ, 692, 618
Mihalas, D. & Hummer, D. G. 1973, ApJ, 179, 827
Mokiem, M. R., de Koter, A., Evans, C. J., et al. 2007a, A&A, 465, 1003
Mokiem, M. R., de Koter, A., Evans, C. J., et al. 2006, A&A, 456, 1131
Mokiem, M. R., de Koter, A., Vink, J. S., et al. 2007b, A&A, 473, 603
Morel, T. 2009, Communications in Asteroseismology, 158, 122
Najarro, F., Hanson, M. M., & Puls, J. 2011, A&A, 535, A32
Najarro, F., Hillier, D. J., Puls, J., Lanz, T., & Martins, F. 2006, A&A, 456, 659
Oey, M. S. 2006, in The Local Group as an Astrophysical Laboratory, ed. M. Livio & T. M. Brown (Cambridge: Cambridge Univ. Press), 72
Oey, M. S. & Kennicutt, Jr., R. C. 1997, MNRAS, 291, 827
Parker, J. W., Garmany, C. D., Massey, P., & Walborn, N. R. 1992, AJ, 103, 1205
Puls, J., Urbaneja, M. A., Venero, R., et al. 2005, A&A, 435, 669
Repolust, T., Puls, J., & Herrero, A. 2004, A&A, 415, 349
Rivero González, J. G., Puls, J., & Najarro, F. 2011, A&A, 536, A58
Rivero González, J. G., Puls, J., Najarro, F., & Brott, I. 2012, A&A, 537, A79
Sanduleak, N. 1970, Contributions from the Cerro Tololo Inter-American Observatory, 89
Santolaya-Rey, A. E., Puls, J., & Herrero, A. 1997, A&A, 323, 488
Schaerer, D., Meynet, G., Maeder, A., & Schaller, G. 1993, A&AS, 98, 523
Simon, K. P., Kudritzki, R. P., Jonas, G., & Rahe, J. 1983, A&A, 125, 34
Simón-Díaz, S., Castro, N., Garcia, M., Herrero, A., & Markova, N. 2011, Bulletin de la Societe Royale des Sciences de Liege, 80, 514
Simón-Díaz, S. & Herrero, A. 2007, A&A, 468, 1063
Simón-Díaz, S., Herrero, A., Esteban, C., & Najarro, F. 2006, A&A, 448, 351
Smith, L. F., Shara, M. M., & Moffat, A. F. J. 1996, MNRAS, 281, 163
Sota, A., Maíz Apellániz, J., Walborn, N. R., et al. 2011, ApJS, 193, 24
Walborn, N. R. 1971, ApJ, 167, L31
Walborn, N. R. 1972, AJ, 77, 312
Walborn, N. R., Howarth, I. D., Lennon, D. J., et al. 2002, AJ, 123, 2754
Walborn, N. R., Morrell, N. I., Howarth, I. D., et al. 2004, ApJ, 608, 1028

Appendix A: Comparison with CMFGEN

Figures A.1 to A.8 provide a detailed comparison between H/He and N III/N IV/N V CMFGEN spectra for models d2v, d4v, s2a, and s4a (see Table 3), and corresponding FASTWIND profiles from closest or almost closest grid models, for a nitrogen abundance of [N] = 8.78 and [N] = 7.78. If not explicitly stated else, no convolution has been applied to the spectra. For details, see Sect. 5.
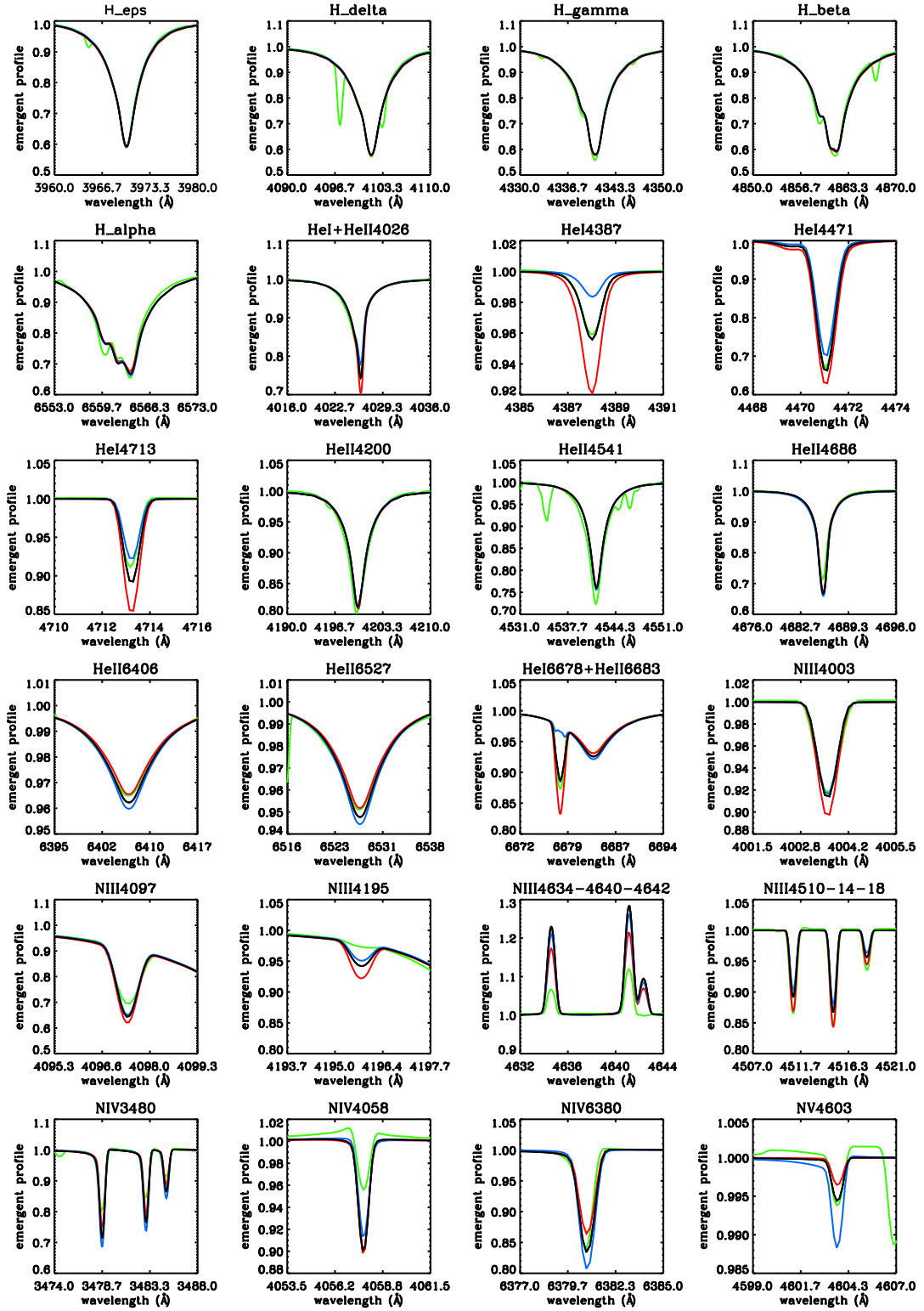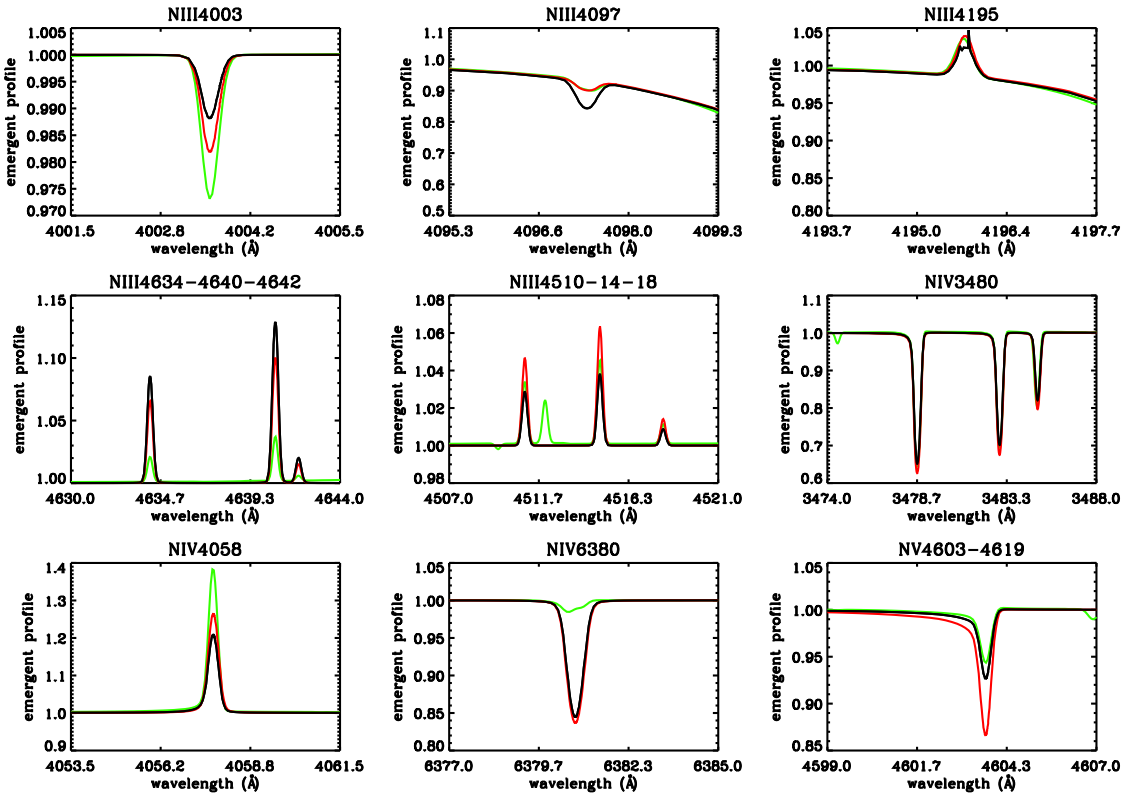

Fig. A.1. Model d4v at [N] =8.78. Comparison of H/He/N spectra from CMFGEN (green) and FASTWIND, at the closest grid-model (black: T_{eff} = 41 kK, log g = 4.0, log Q = −12.8, [N] = 8.78) and at neighboring grid models with T_{eff} = 40 kK (red) and T_{eff} = 42 kK (blue). To allow for an easier comparison, all profiles have been convolved with $v \sin i$ = 30 km s^{-1}.
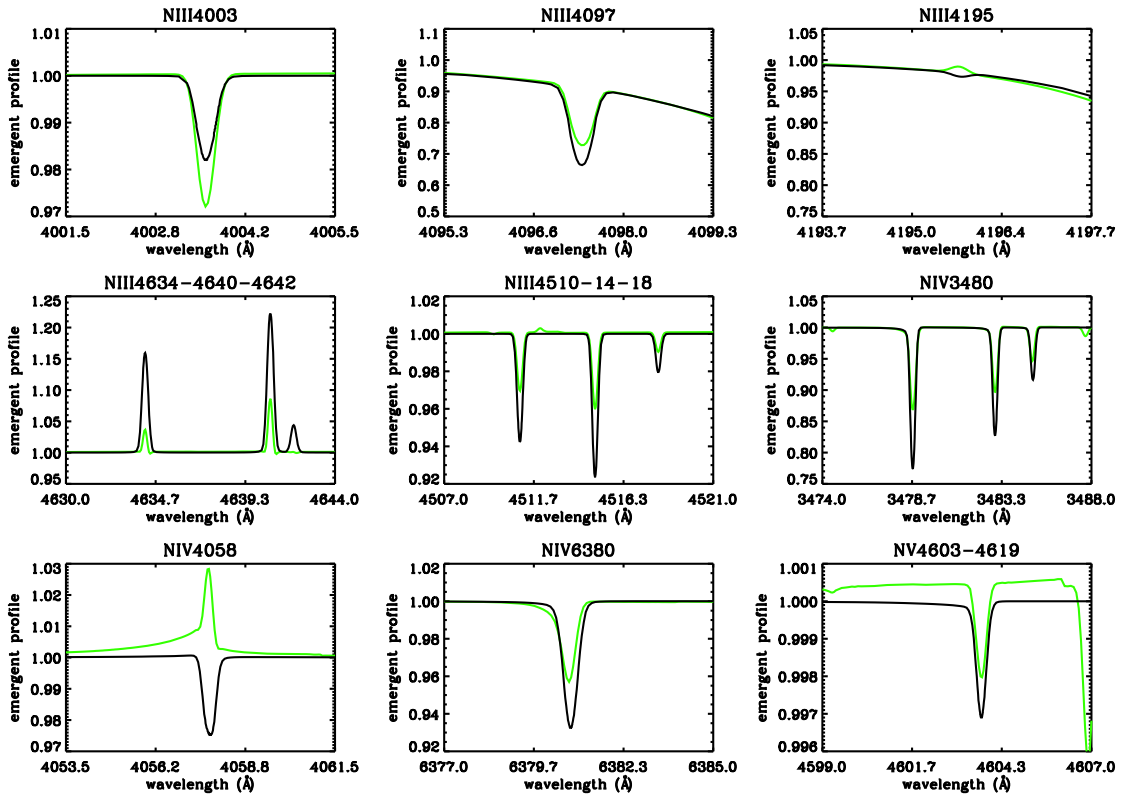
Fig. A.2. Model d4v at [N] =7.78 (solar). Comparison of N spectra from CMFGEN (green) and FASTWIND, at the closest grid-model. (black: T_{eff} = 41 kK, log g = 4.0, log Q = −12.8, [N] = 7.78). The H/He spectra remain as in Fig. A.1. No convolution applied.

Fig. A.3. Model d2v at [N] =7.78 (solar). Comparison of N spectra from CMFGEN (green) and FASTWIND, at the closest grid-model (black: T_{eff} = 46 kK, log g = 4.0, log Q = −12.45, [N] = 7.78), and at the neighboring grid model with T_{eff} = 47 kK (red). The H/He spectra remain as in Fig. A.4.
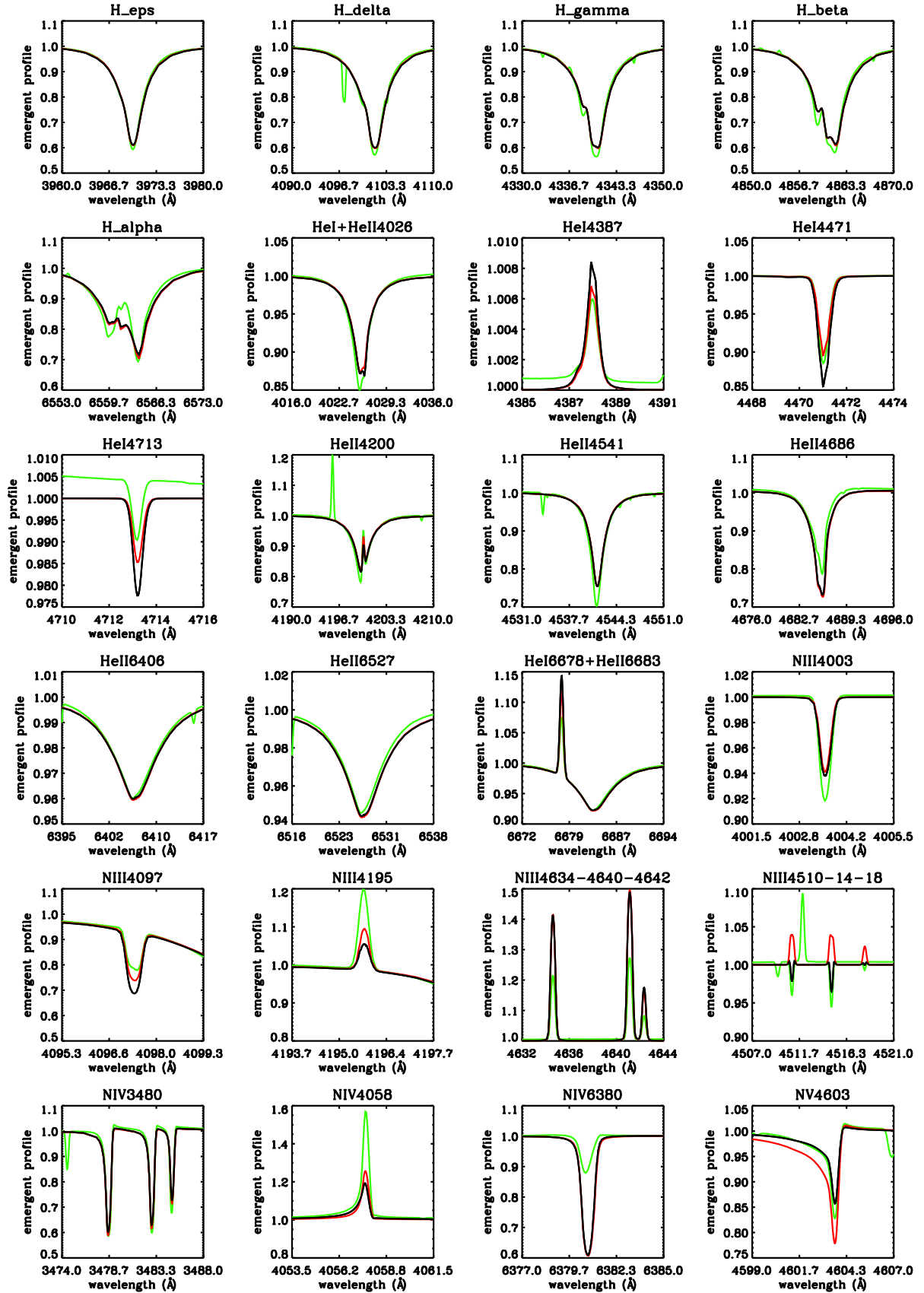
Fig. A.4. Model d2v at [N] =8.78. Comparison of H/He/N spectra from CMFGEN (green) and FASTWIND, at the closest grid-model (black: $T_{\rm eff}$ = 46 kK, log g = 4.0, log Q = −12.45, [N] = 8.78) and at neighboring grid model with $T_{\rm eff}$ = 47 kK (red). No convolution has been applied.
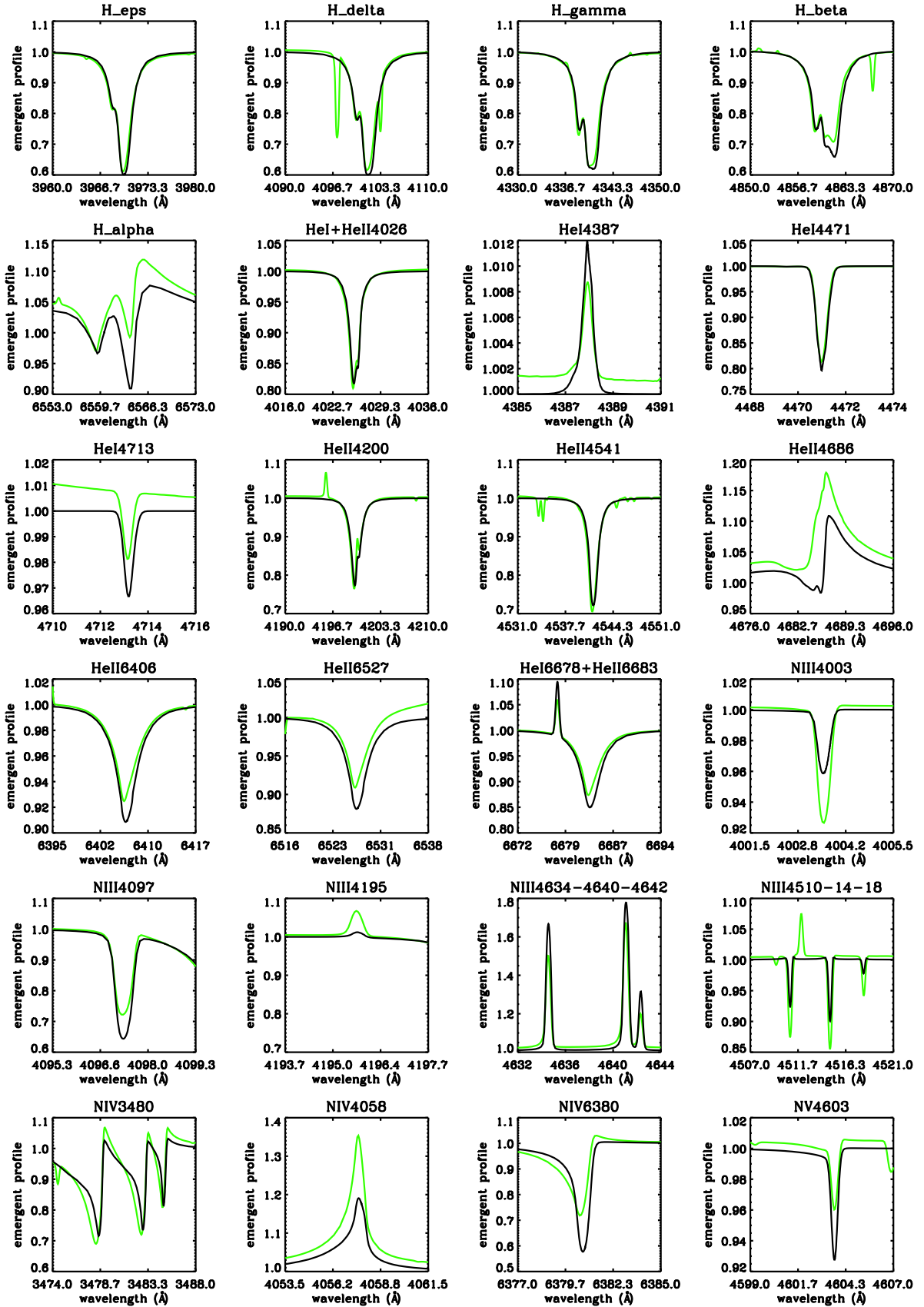
Fig. A.5. Model s4a at [N] =8.78. Comparison of H/He/N spectra from CMFGEN (green) and FASTWIND, at the closest grid-model (black: T_{eff} = 39 kK, log g = 3.5, log Q = −12.10, [N] = 8.78).
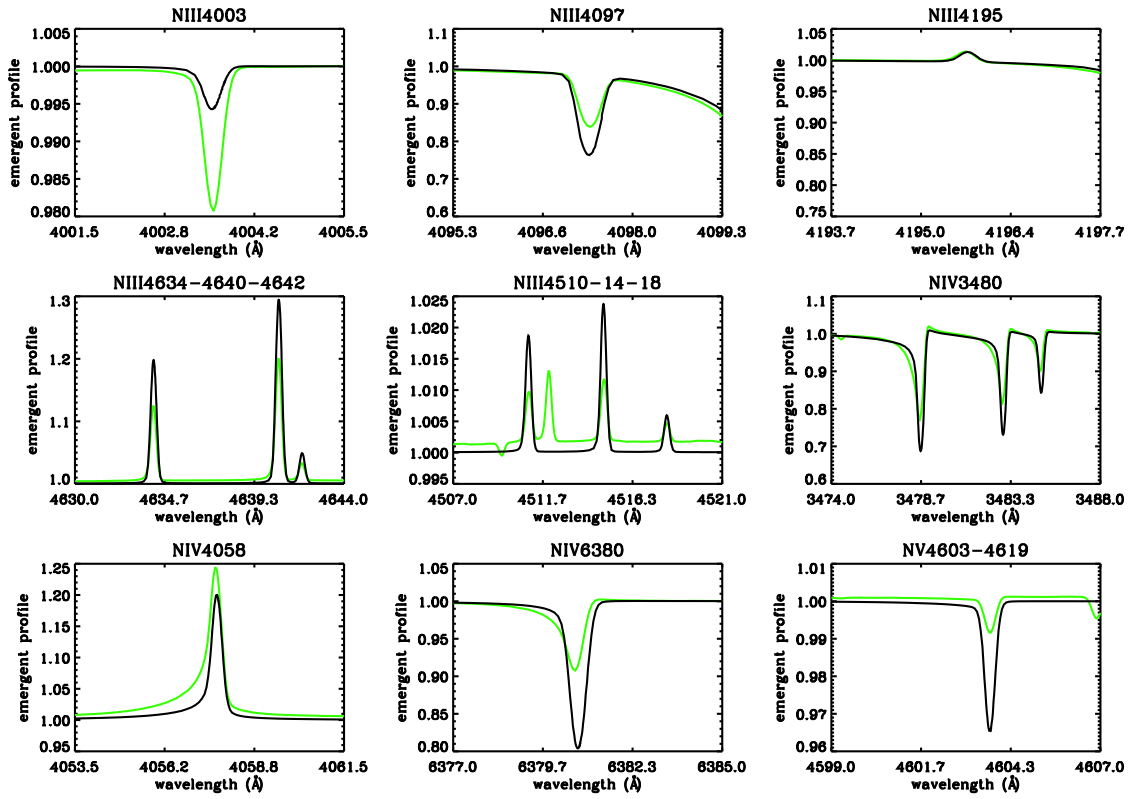
Fig. A.6. Model s4a at [N] =7.78 (solar). Comparison of N spectra from CMFGEN (green) and FASTWIND, at the closest grid-model (black: $T_{\rm eff}$ = 39 kK, log g = 3.5, log Q = −12.10, [N] = 7.78). The H/He spectra remain as in Fig. A.5.
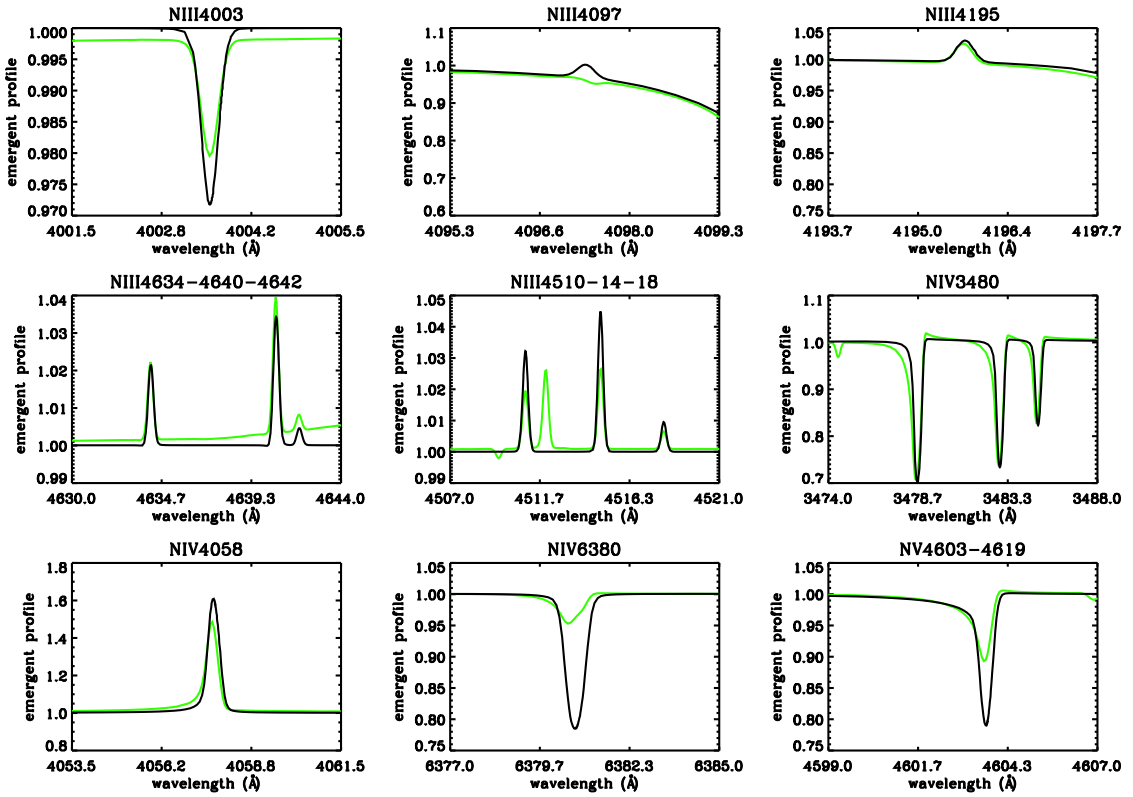
Fig. A.7. Model s2a at [N] =7.78 (solar). Comparison of N spectra from CMFGEN (green) and FASTWIND, at the (almost) closest grid-model (black: $T_{\rm eff}$ = 46 kK, log g = 3.8, log Q = −12.10, [N] = 7.78). The H/He spectra remain as in Fig. A.8.
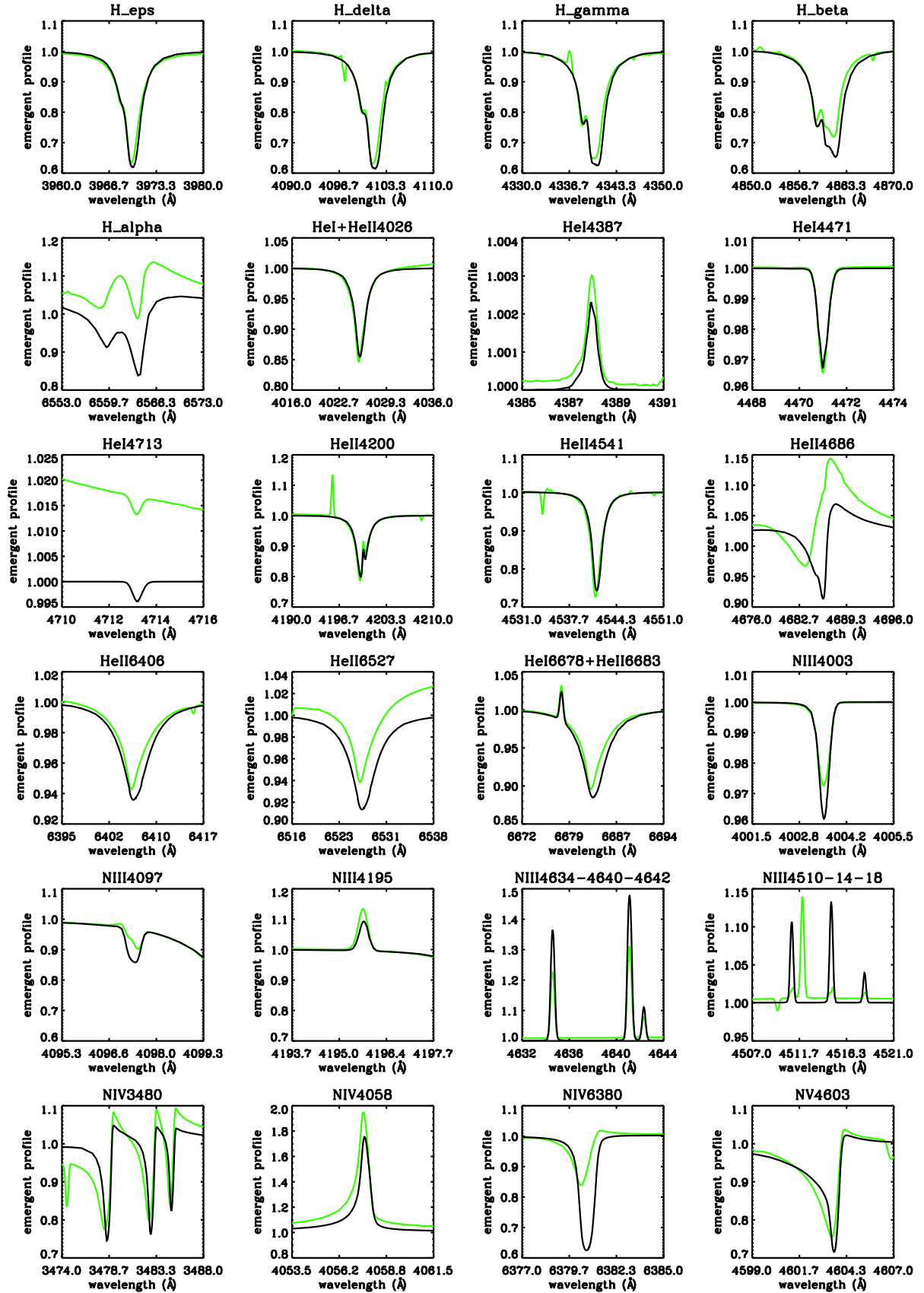
Fig. A.8. Model s2a at [N] =8.78. Comparison of H/He/N spectra from CMFGEN (green) and FASTWIND, at the (almost) closest grid-model (black: T_{eff} = 46 kK, $\log g$ = 3.8, $\log Q$ = −12.10, [N] = 8.78).

Appendix B: Comments on the individual objects

In the following, we give specific comments on the individual objects, regarding peculiarities and problems found during our analysis. We separate between galaxy membership, and sort by luminosity class and spectral type. Line fits are displayed in Figs. B.1 to B.12, for important H/He/N lines: H_α, H_β, H_γ, H_δ, H_ϵ, He I$\lambda\lambda$ 4387, 4471, 4713, He II(+He I)λ4026, He II$\lambda\lambda$4200, 4541, 4686, 6406, 6527, 6683, N III$\lambda\lambda$ 4003, 4097, 4195, 4379, $\lambda\lambda$4634 − 4640 − 4642, and $\lambda\lambda$4510 − 4514 − 4518, N IV$\lambda\lambda$ 4058, 6380, and N V$\lambda\lambda$4603/4619. All spectra were corrected for radial velocity shifts.

If not explicitly stated, any comparison made in the following text refers to the results from Mas05.

B.1. LMC stars

R136-040 – O2-3.5 V (Fig. B.1). This star could not been classified by Mas05 using the scheme by Walborn et al. (2002), because neither N III$\lambda\lambda$4634 − 4640 − 4642 nor N IVλ4058 were visible in the spectra. As outlined in Sect. 6.2, for the R136 stars we have spectra from both STIS and FOS available. Taking advantage of the better quality of the STIS data and using H_α, H_γ, and He IIλ4541, we derived a similar lower limit (no He I and no nitrogen lines)! on T_{eff} as Mas04, but a substantially larger (by 0.2 dex) gravity, which agrees better with its dwarf designation. Our analysis also resulted in a low helium content, $Y_{\text{He}} = 0.08$ (Mas04: $Y_{\text{He}} = 0.1$). Note the discrepancy in the cores of H_δ, H_ϵ, and He II$\lambda\lambda$4026, 4200 when comparing with the FOS data. Such a discrepancy was also found for the remaining H/He II lines in the FOS data, when used instead of the STIS spectra.

The missing nitrogen lines imply an upper limit for the nitrogen content corresponding to the LMC baseline abundance [N] = 6.90, which also agrees quite well with the low He content.

LH 81:W28-23 – O3.5 V((f+)) (Fig. B.2). The modeling of this star was straightforward, and we obtained similar results as Mas05. However, we considered a larger $\beta = 1.0$ to better reproduce the marginal P-Cygni profile at He IIλ4686, which might indicate a luminosity class III object (see Walborn et al. 2002). To preserve the fit of H_α, we needed to reduce $\dot{M}$. All nitrogen lines are consistent with the temperature derived from the helium ionization equilibrium. The quite large nitrogen abundance ([N] = 8.40) agrees well with the helium abundance $Y_{\text{He}} = 0.25$, indicating an evolved nature of this object.

LH 101:W3-24 – O3.5 V((f+)) (Fig. B.3). We derived a somewhat cooler T_{eff} (by 1 kK) together with a lower helium content, $Y_{\text{He}} = 0.10$, which was consistent for all helium lines. Nitrogen lines are barely visible, because the spectrum of this star displays more noise than the bulk of our sample stars, caused by the use of a narrow extraction aperture to reduce effects from nebular emission for the ground-based observations (cf. Sect 6.2). Due to the noisy spectrum, we were only able to infer an upper limit for the nitrogen abundance, [N] ≤ 7.78.

LH 81:W28-5 – O4 V((f+)) (Fig. B.4). This is one of the standards used by Walborn et al. (2002) for defining the O4 V((f+)) class. A consistent analysis of the helium and nitrogen ionization equilibrium yielded a cooler temperature, $T_{\text{eff}} = 44$ kK,

which required a helium abundance of $Y_{\text{He}} = 0.15$ to reproduce He Iλ4471. An excellent fit to most nitrogen lines from all three ionization stages was achieved for this star, indicating a significant enrichment, [N] = 8.38.

R136-018 – O3 III(f*) (Fig. B.5). Also for this O3 giant we have used data from both STIS and FOS. A consistent analysis of the H/He lines from STIS and nitrogen lines (mostly from FOS) suggested a hotter T_{eff}, by 2 kK, as well as a higher surface gravity, by ~0.1 dex. Again, we found discrepancies in the cores of the H/He II lines from the FOS spectra, except for He IIλ4686. An acceptable fit for N III/N IV/N V using [N] = 8.18 was possible, where only N IVλ4058 was slightly underpredicted. Even though the nitrogen lines contained in the STIS dataset, N III$\lambda\lambda$4510 − 4514 − 4518 and N IVλ6380, are diluted in the continuum, they support our analysis.

LH 90:ST 2-22 – O3.5 III(f+) (Fig. B.6). An unproblematic analysis provided the same results as obtained by Mas05, except that we opted for a lower helium abundance, $Y_{\text{He}} = 0.15$. Again, a remarkable fit to the nitrogen lines was possible, at [N] = 8.58, indicating an extreme enrichment.

Sk–67° 22 – O2 If*/WN5 (Fig. B.7). This star was re-classified[30] as O2 If*/WN 5 by Crowther & Walborn (2011) using their updated classification scheme, because of the H_β P-Cygni profile. Using lines from N III/N IV/N V, we inferred $T_{\text{eff}} = 46$ kK which is hotter than the lower limit (from very weak He Iλ4471) quoted by Mas05. Our fit seems to slightly overpredict the emission in N IVλ4058 and to underpredict the N V doublet. An extreme nitrogen abundance, [N] = 8.78, was required, the largest one found in our sample. Such an abundance would be certainly too large when comparing even with strongly nitrogen-enhanced O-stars, and also with predictions from evolutionary calculations tailored for the LMC (Brott et al. 2011b and paper II), thus supporting a rather evolved nature of this object and its 'slash-star' designation. This star was also analyzed by Doran & Crowther (2011) using N IV/N V lines (without discussion of He I and N III), only providing a $T_{\text{eff}} = 49.3$ kK for this object. Such hotter temperature would improve our fits for N IVλ4058 and the N V doublet, but is inconsistent with the observed strength of N III.

LH 101:W3-19 – O2 If* (Fig. B.8). For this supergiant, a consistent He/N analysis allowed us to derive $T_{\text{eff}} = 44$ kK, hotter than the lower limit (marginal He Iλ4471) assigned by Mas05. Using N III/N IV/N V in parallel, we achieved an almost excellent fit for the nitrogen lines at [N] = 8.18.

Sk–65° 47 – O4 If (Fig. B.9). The parameter set derived for this star using H/He/N lines is quite similar to the results from Mas05, with somewhat larger $Y_{\text{He}} = 0.12$, A potential discrepancy provides N IVλ4058, where we might slightly overpredict the observed emission.

B.2. SMC stars

AV 435 – O3 V((f*)) (Fig. B.10). The only discrepancies found during our analysis correspond to an overprediction of He II$\lambda\lambda$6406, 6527, 6683. Both the He I/He II and the N III/N IV

---

[30] Mas05: O2 If*

ionization equilibrium suggest a hotter temperature than quoted by Mas05, $T_{\rm eff}$ = 46 kK. This temperature seems to be somewhat cool for its spectral type O3 V assigned by Mas05 because of N ɪᴠλ4058 ≳ N ɪɪɪλ4640, but quite consistent with our predictions for the derived wind-strength and nitrogen content, [N] = 7.58 (cf. Figs. 7 and 8).

AV 177 – O4 V((f)) (Fig. B.11). The H/He analysis of this star produced similar parameters as found by Mas05. Owing to a high rotation, $v \sin i$ = 220 km s^{-1}, nitrogen lines are barely visible in the spectrum. Weak traces of emission at N ɪɪɪ$\lambda\lambda$4634 − 4640 − 4642 and N ɪɪɪ$\lambda\lambda$4510 − 4514 − 4518 together with weak absorption at N ɪᴠλ6380 are fitted consistently at [N] = 7.78.

NGC 346-355 – ON2 III(f*) (Fig. B.12). This star was considered as a standard for the O2 III(f*) category by Walborn et al. (2002), and later on updated to ON2 III(f*) by Walborn et al. (2004). As for N11-031 (same type!) analyzed in paper II, we found problems to fit all N ɪɪɪ/N ɪᴠ/N ᴠ lines in parallel, but to a lesser extent. The basic difference is related to He ɪλ4471, which is not as clearly visible as for N11-031. During our analysis, we considered two possible parameter sets: a cooler solution with $T_{\rm eff}$ = 51 kK (red) and a hotter one with $T_{\rm eff}$ = 55 kK (black), using either the N ɪɪɪ/N ɪᴠ or the N ɪᴠ/N ᴠ ionization equilibrium. By inspection of He ɪλ4471, we note that both temperatures might be consistent with the very weak observed feature. For a similar nitrogen abundance, [N] = 7.98, we were able to fit either N ɪɪɪ$\lambda\lambda$4634 − 4640 − 4642, N ɪɪɪ$\lambda\lambda$4510 − 4514 − 4518 and N ɪᴠλ6380 for the cooler solution, or N ɪᴠλ6380 and N ᴠ$\lambda\lambda$4603-4619 for the hotter one.

Mas09, restricted to He ɪλ4471 as a primary temperature indicator, derived $T_{\rm eff}$ = 49.5 kK and $\log g$ = 3.9, which would agree with our cool solution, but is insufficient for the N ɪᴠ/N ᴠ lines. The hotter solution is in better agreement with results from Bouret et al. (2003) and Walborn et al. (2004), who found $T_{\rm eff}$ = 52.5 kK and $\log g$ = 4.0 fitting the N ɪᴠ/N ᴠ lines by means of cmfgen. In particular, we achieved a similar fit quality as Bouret et al. (2003), for a similar nitrogen content. Bouret et al. stated that at $T_{\rm eff}$ ∼ 55 kK (identical with our hotter solution) their fit for He ɪɪλ4686 would improve. Such an increase in temperature would also improve their fit of N ᴠ, which we are able to fit accurately. The same stellar parameters as determined by Bouret et al. (2003) and Walborn et al. (2004) were derived by Heap et al. (2006) using tlusty, mostly based on lines from highly ionized species, in particular N ᴠ and N ɪᴠ. Unfortunately, they did not comment on He ɪ and N ɪɪɪ, but reassuringly they derived a nitrogen abundance very similar to ours, [N] = 7.92.
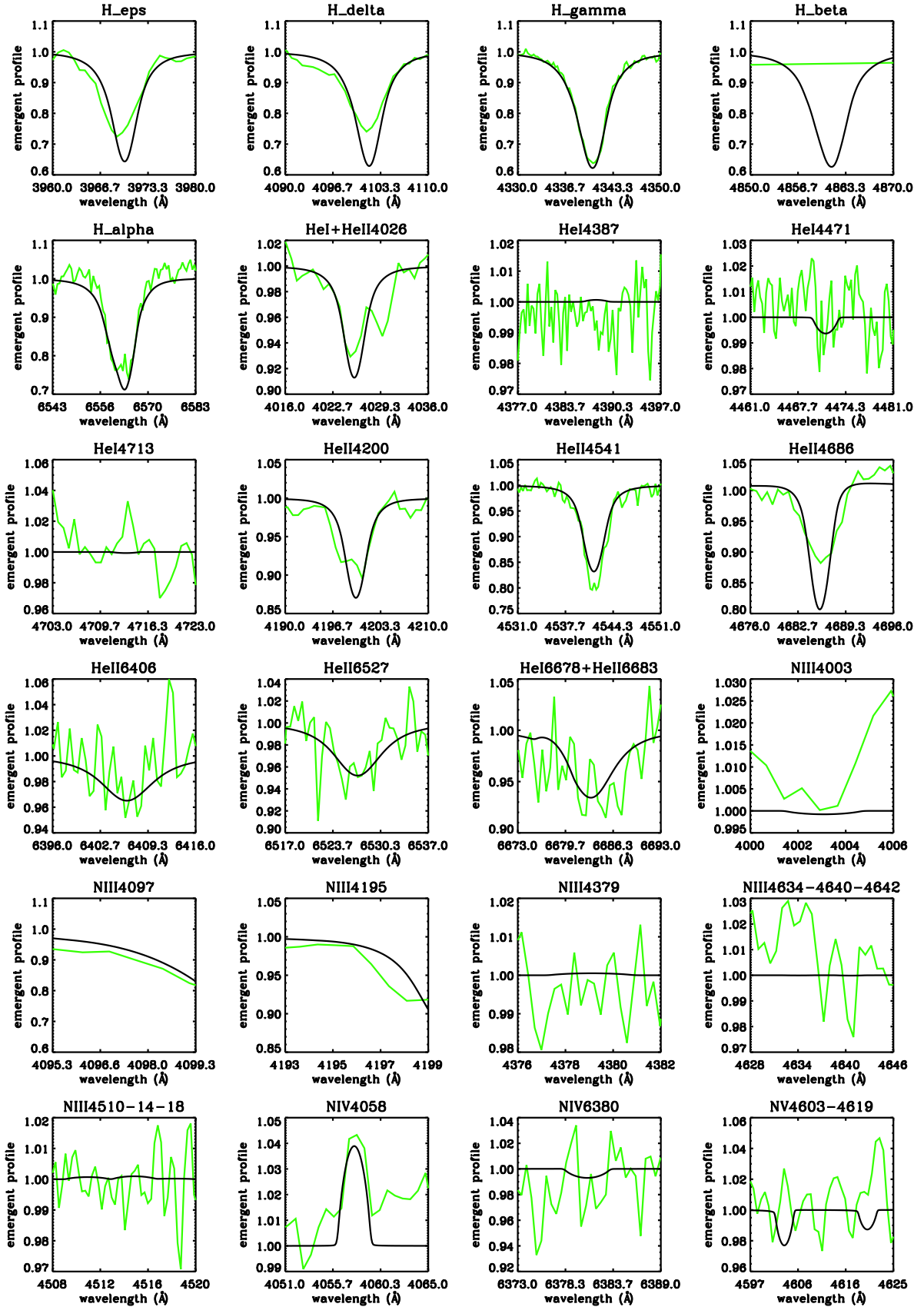
Fig. B.1. R136-040 - O2-3.5 V. Observed (green) and best fitting optical H/He and N spectrum. For the R136 O-stars, observed spectra for H_α, H_γ, He I$\lambda\lambda$4387, 4471, 6678, He IIλ4541, 6406, 6527, 6683, N III$\lambda\lambda$4510 − 4514 − 4518, and N IVλ6380 taken from the STIS/CCD dataset. Remaining, lower quality spectra collected by FOS. H_β was not observed for this star.
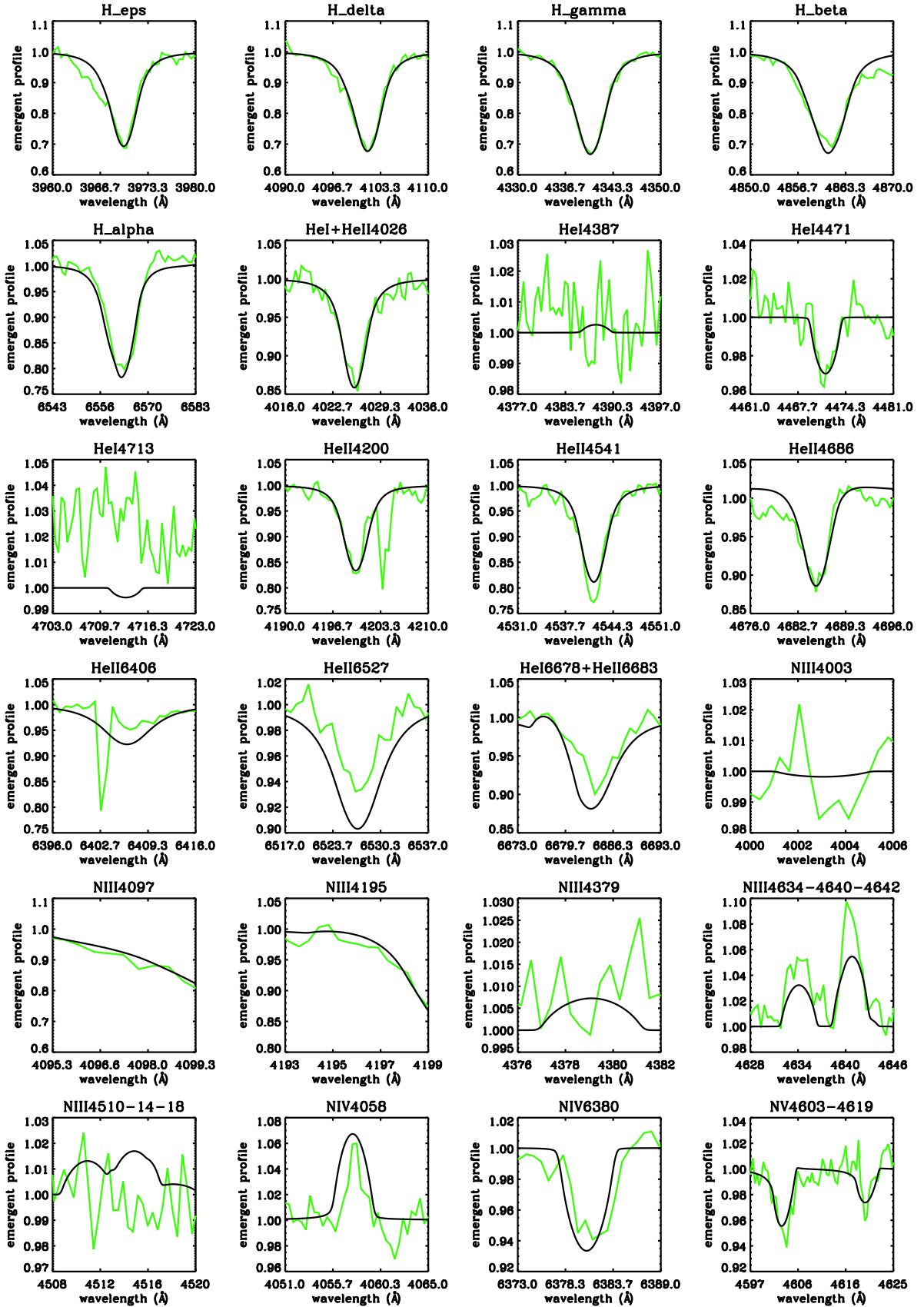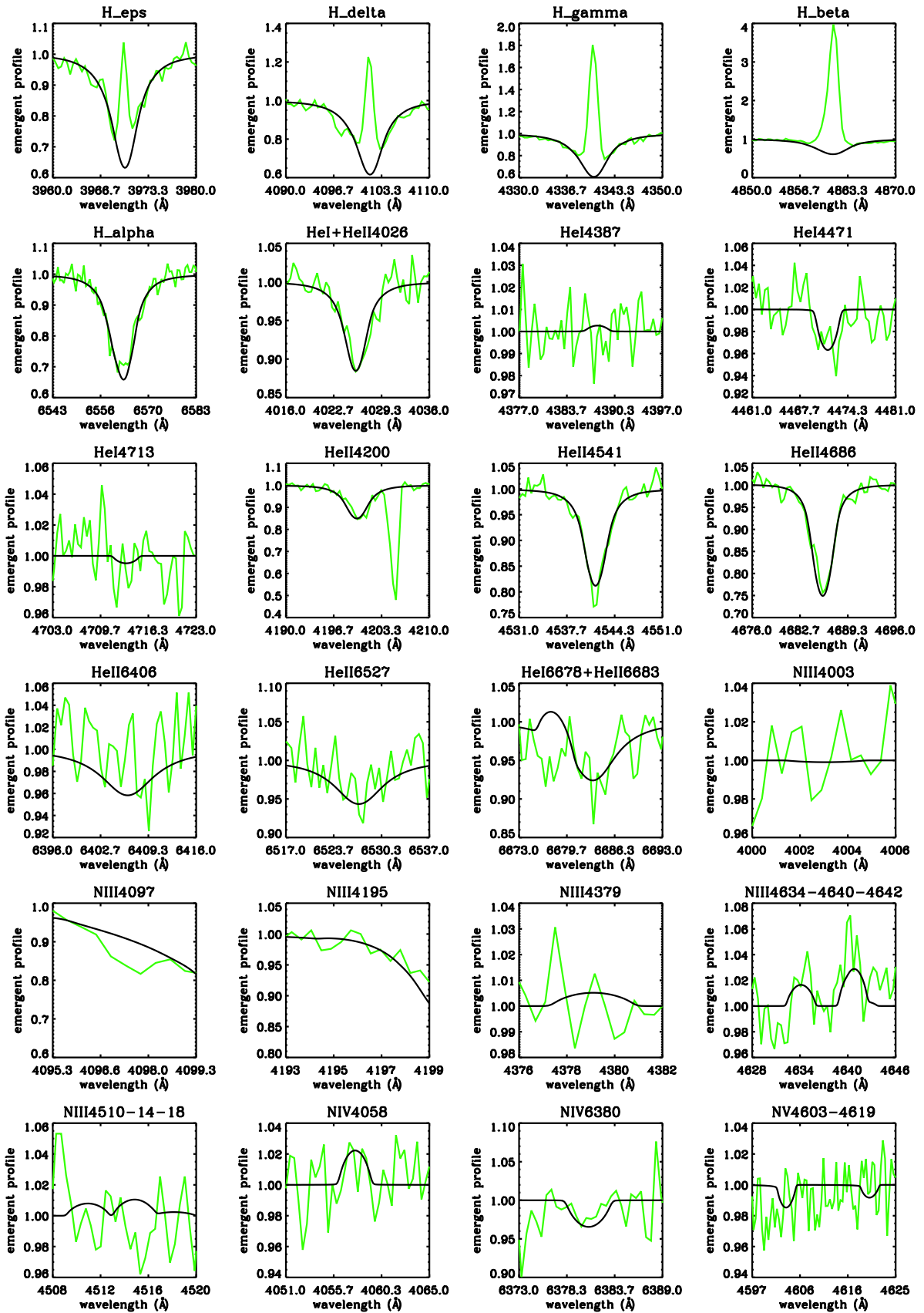
Fig. B.2. LH 81:W28-23 - O3.5 V((f+)).

Fig. B.3. LH 101:W3-24 - O3.5 V((f+)).
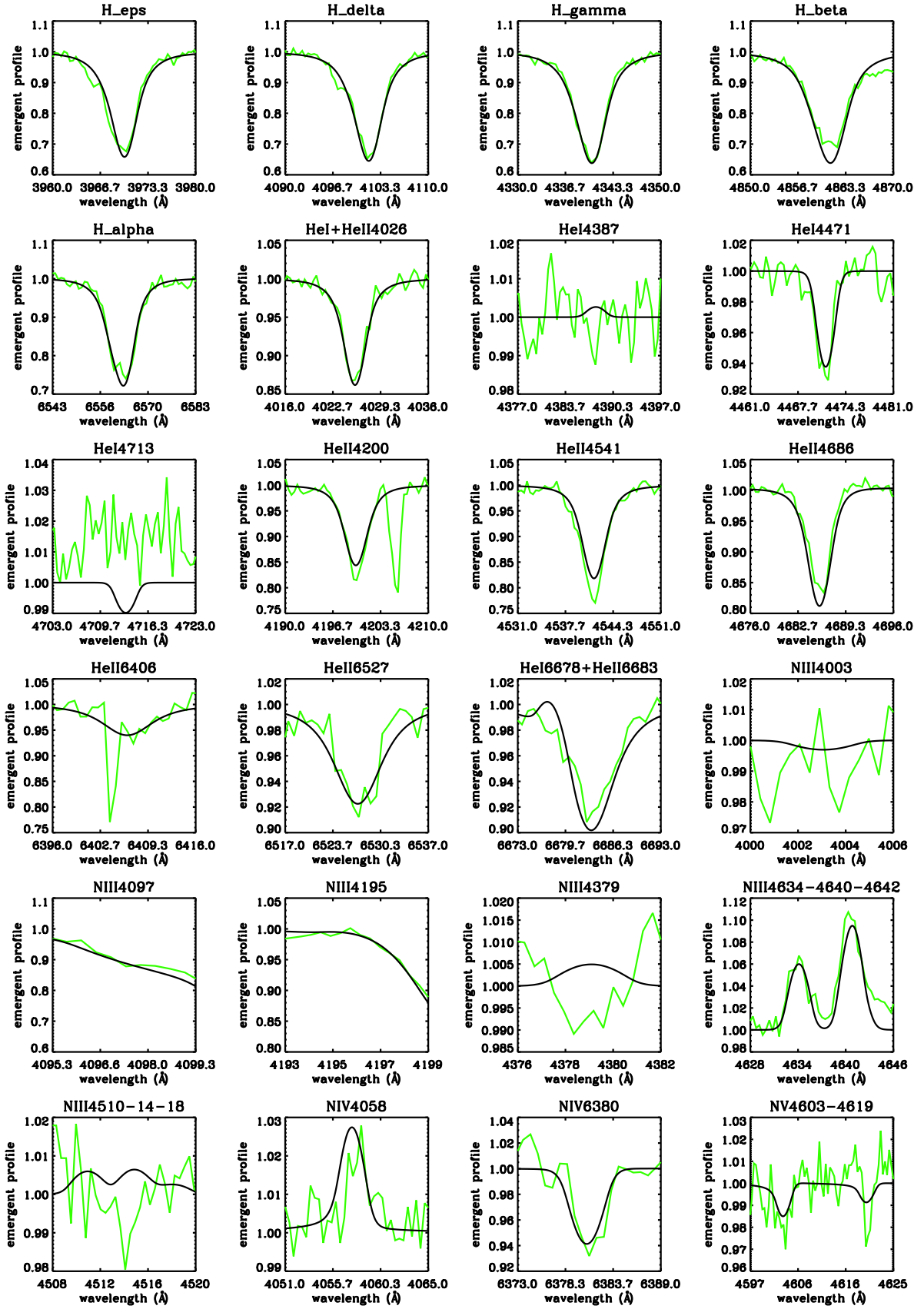
Fig. B.4. LH 81:W28-5 - O4 V((f+)).
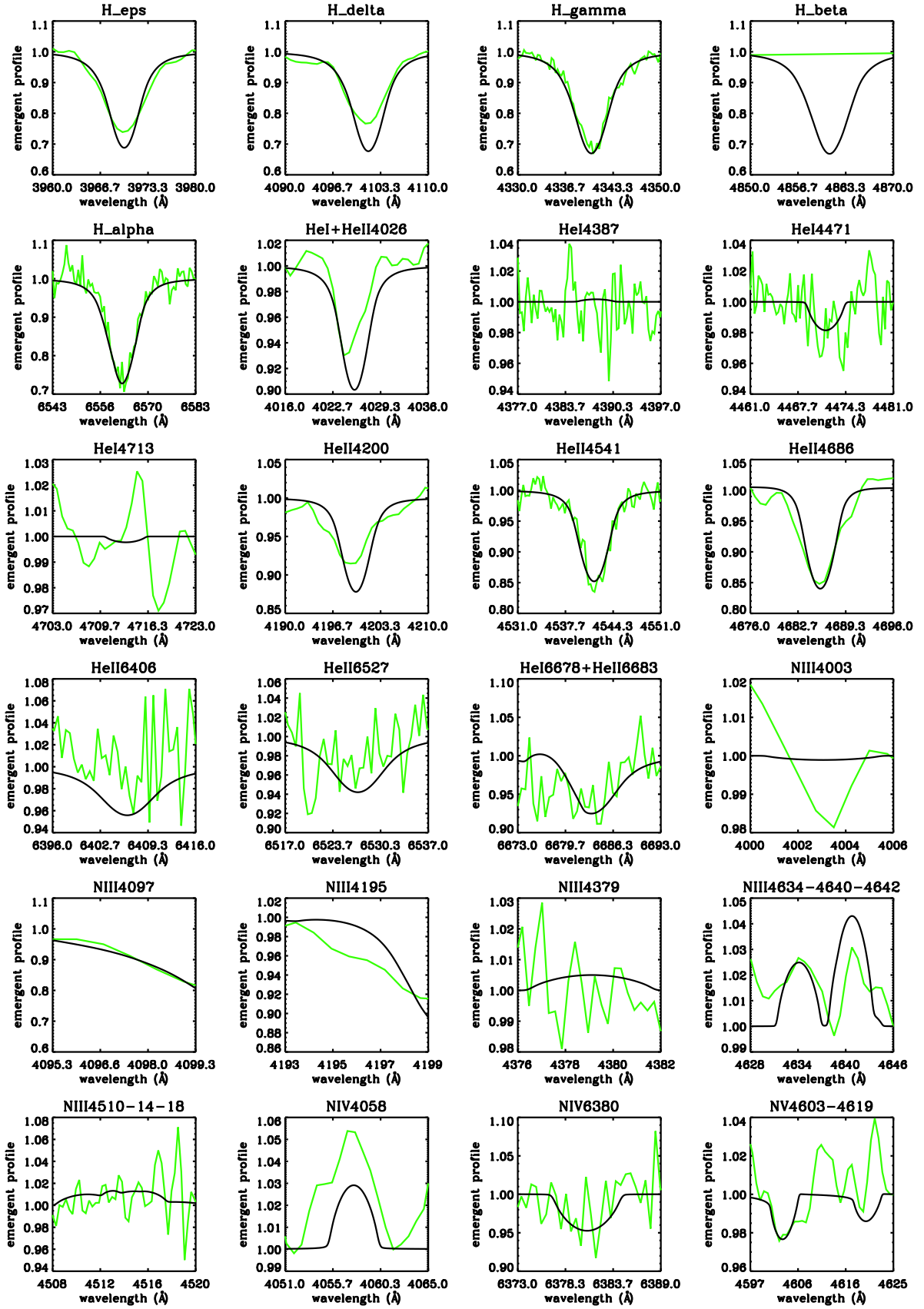
Fig. B.5. R136-018 - O3 III(f*). Observations as for R136-040 (Fig. B.1).
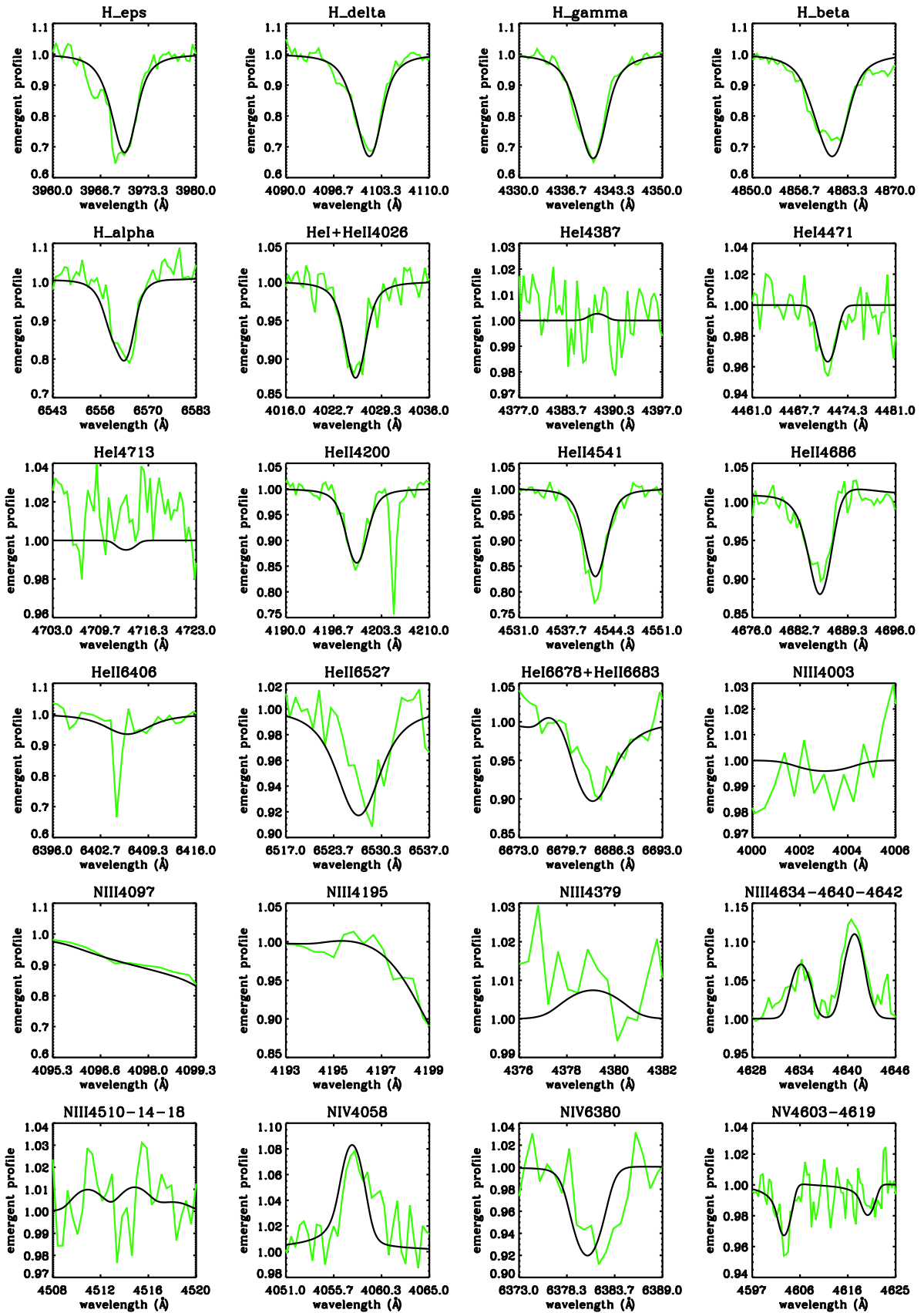
Fig. B.6. LH 90:ST 2-22 - O3.5 III(f+).
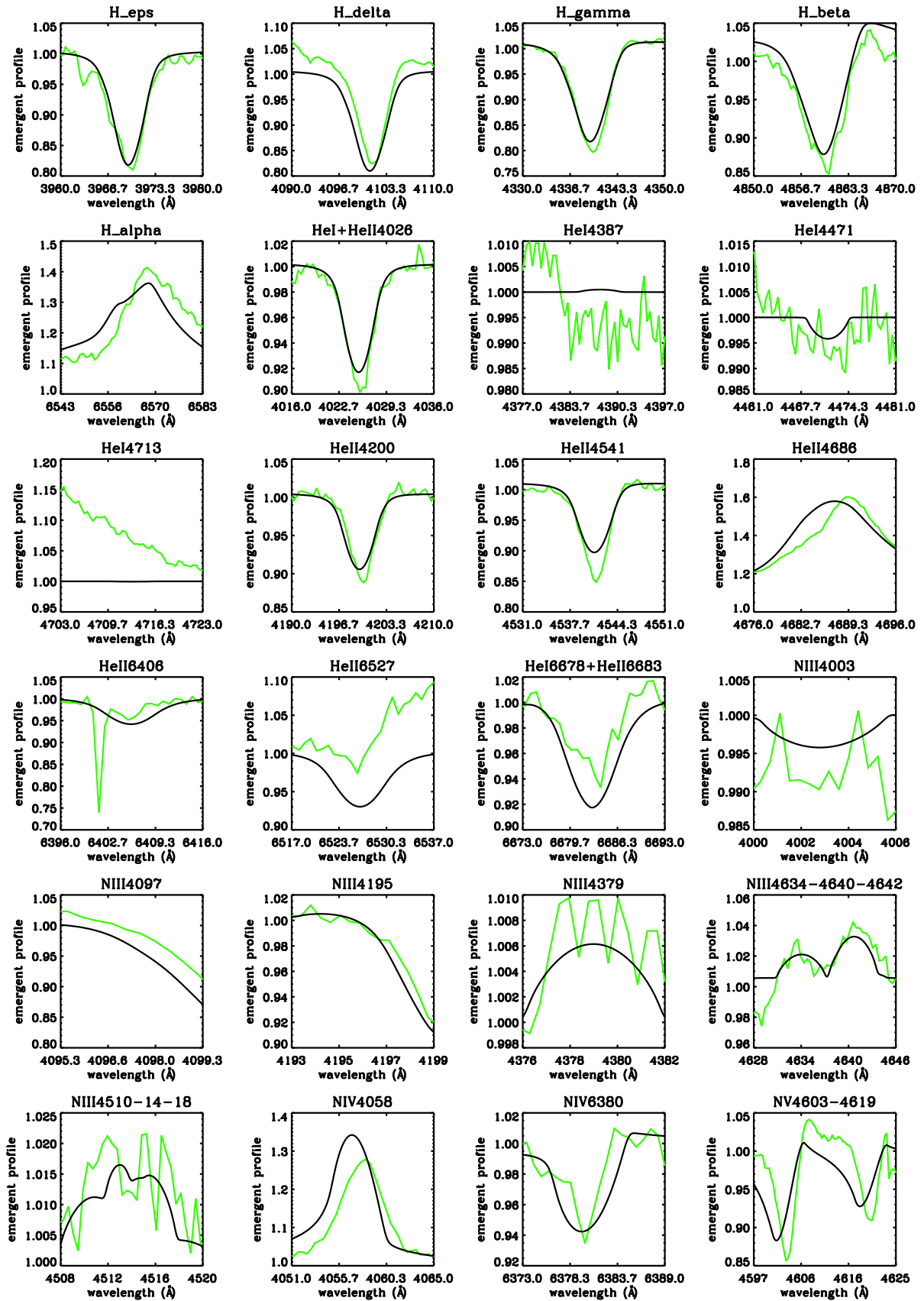
Fig. B.7. Sk–67° 22 - O2 If*/WN5.
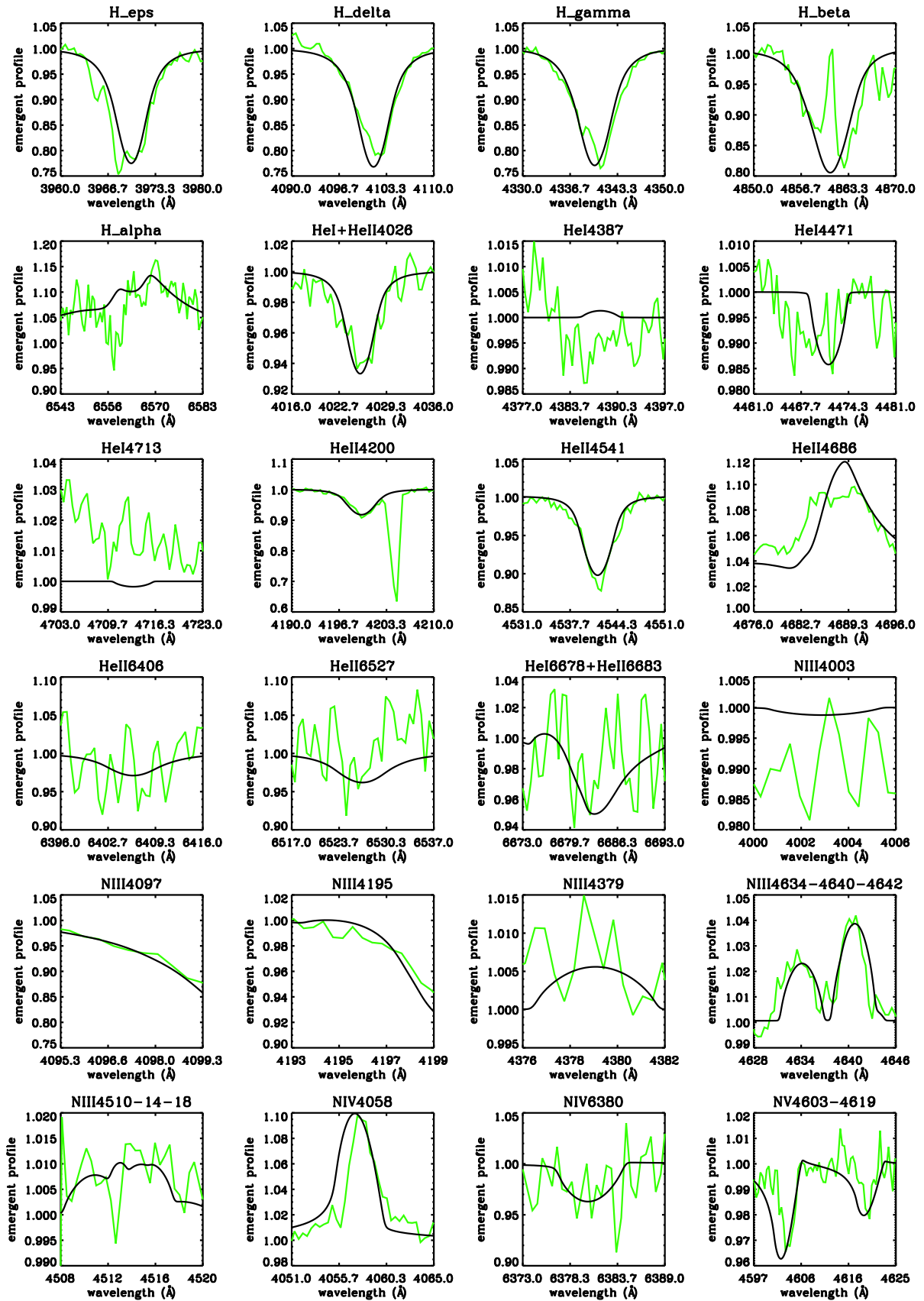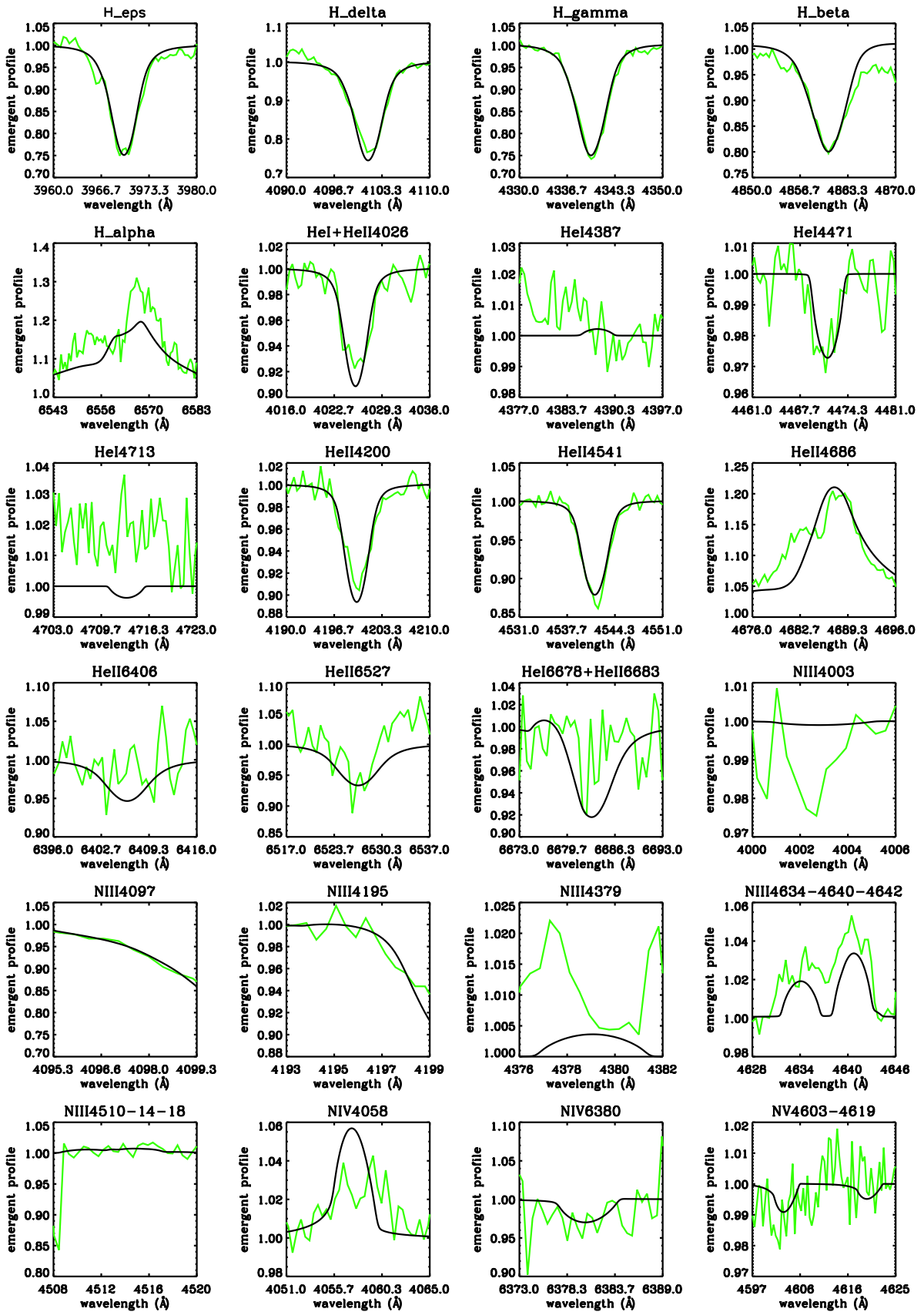
Fig. B.8. LH 101:W3-19 - O2 If*.

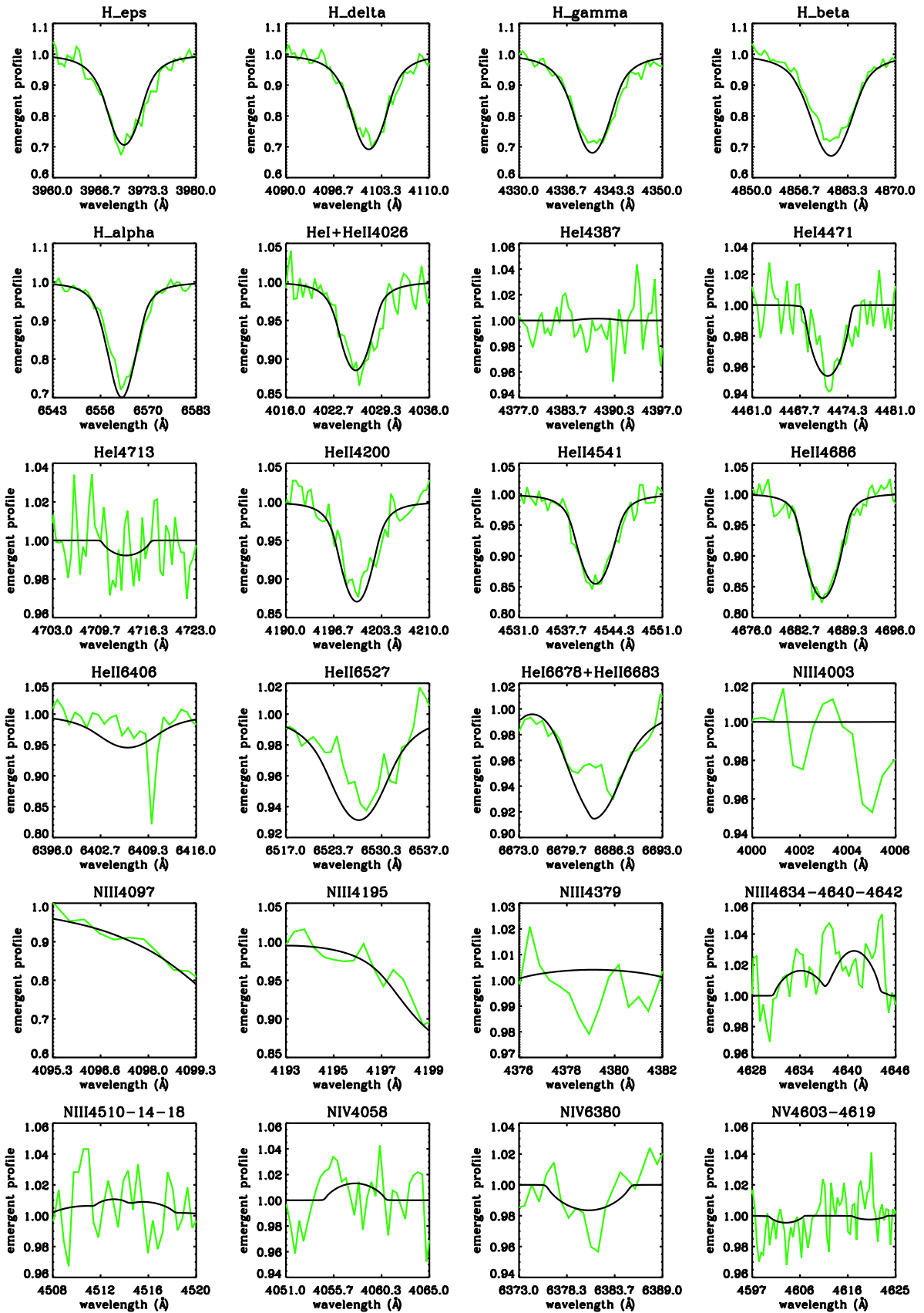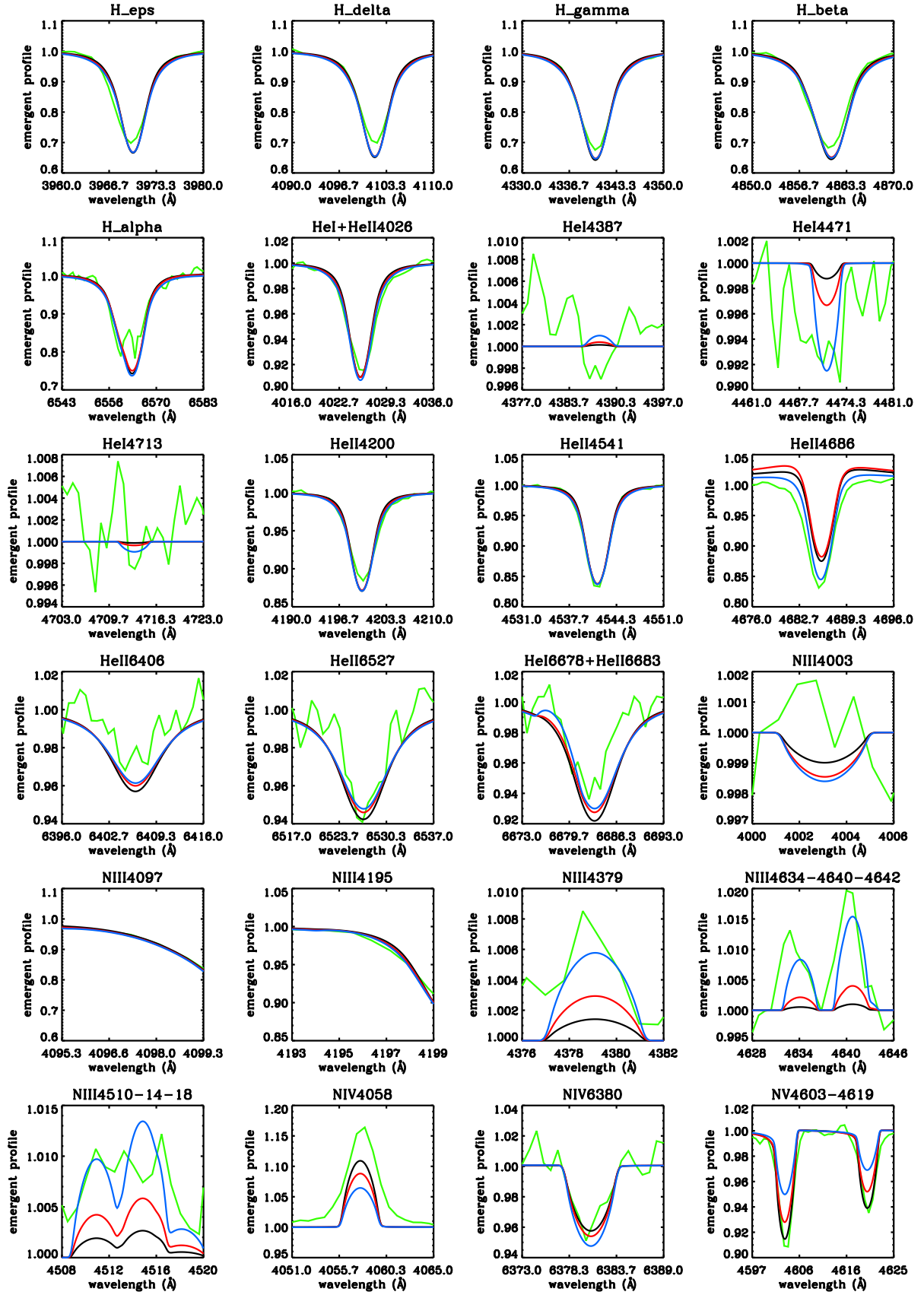**Fig. B.9.** Sk–65° 47 - O4 If.
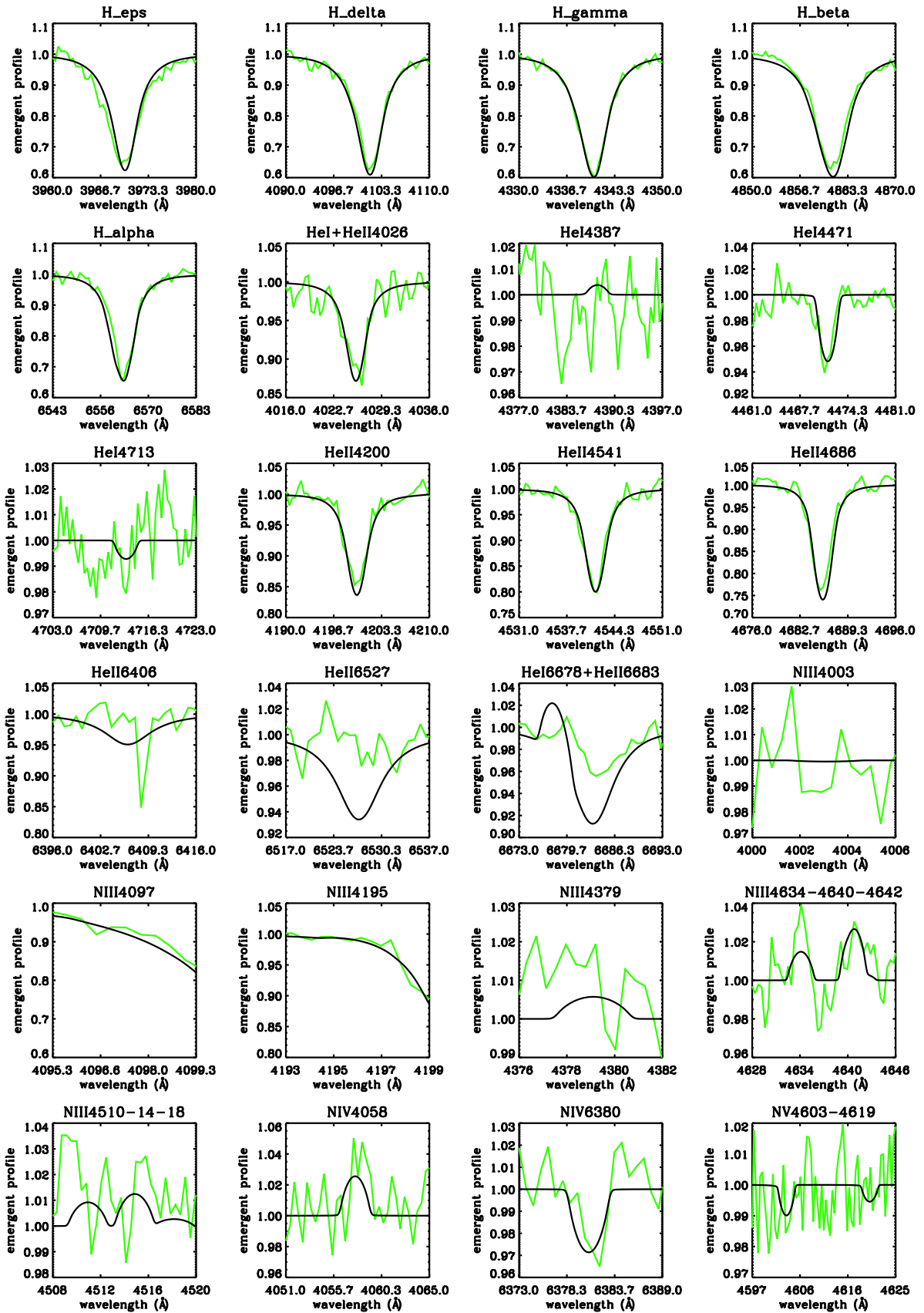
Fig. B.10. AV 435 - O3 V((f*)).

Fig. B.11. AV 177 - O4 V((f)).

Fig. B.12. NGC 346-355 - ON2 III(f*). Black: hotter solution ($T_{\rm eff}$ = 55 kK), supported by N ɪv/N v lines. Blue: cooler solution ($T_{\rm eff}$ = 51 kK), mostly supported by N ɪɪɪ (together with N ɪvλ6380). Red: 'average' solution ($T_{\rm eff}$ = 53 kK) used in Sect. 7.